Université de Liège

UNIVERSITÉ DE LIÈGE

Robustness of building structures

Experimental study and contribution to the development of analytical solutions

Travail de fin d'études réalisé en vue de l'obtention du grade de Master Ingénieur Civil des Constructions par Ieven Liesbeth

Année académique 2013 - 2014

Members of the jury:
L. Duchêne
J.-F. Demonceau
J.-P. Jaspart
M. Hijiaj

ACKNOWLEDGES

First of all, I would like to thank my supervisor, Mr. L. Duchêne, for his availability and guidance throughout this master thesis. I also would like to thank my 2nd supervisor, Mr. J.-F. Demonceau, for his advice and helpful questions.

Furthermore I thank the other members of the jury, Mr. J.-P. Jaspart and Mr. M. Hijiaj, for the attention they have brought to my work.

Finally I would like to thank my close relatives for their support during my studies. I also would like to thank them for their time spent on proofreading my master thesis.

OBJECTIVES

In this master thesis, the exceptional event “loss of a column” will be studied. Several complex models, able to reproduce the response of a frame during this event, exist. However, different parameters must be defined. One of the parameters we need to determine for these models is the elongation of the plastic hinges subjected to bending and to axial forces. At the University of Liège, an analytical model, able to predict this parameter, is developed. The main objective of this master thesis will be to validate this analytical model.

Later this year, experimental tests of different frames will be conducted at the University of Liège. These tests will allow us to study the behaviour of the frame under exceptional loads and to investigate in particular the deformations in the plastic zones.

The objective of the master thesis is to simulate these experiments numerically in the finite element code Lagamine. The responses of the different frames will be used to validate the analytical model. The influence of several parameters will be examined. Also by comparison with the numerical model, hypothesis of the analytical model will be investigated.

MEMBERS OF THE JURY:

L. Duchêne J.-F. Demonceau

J.-P. Jaspart M. Hijiaj

SUMMARY

TITLE: Robustness of building structures.
Experimental study and contribution to the development of analytical solutions.

AUTHOR: Liesbeth Ieven, Master Ingénieur Civil des Constructions

ACADEMIC YEAR: 2013 - 2014

Several catastrophes, like the partial collapse of Ronan point or the terrorist attacks in September 2001, have highlighted the importance of structural integrity of building structures. Indeed, under exceptional events we don't want that a localized damage causes the collapse of the global structure.

In the Eurocodes some guidelines are given on this subject. However, these guidelines are not concrete. In order to be able to master this phenomena better, many studies are conducted. The main goal is to predict the behaviour of a frame under exceptional events.

In this master thesis, the exceptional event "loss of a column" will be studied. Several complex models, able to reproduce the response of a frame during this event, exist. However, different parameters must be defined. One of the parameters we need to determine for these models is the elongation of the plastic hinges subjected to bending and to axial forces. At the University of Liège, an analytical model, able to predict this parameter, is developed. This elongation is characterized by the K_N parameter, i.e. axial stiffness of the plastic hinges under M and N. This parameter is complex to determine as it is influenced by many factors. That is why still many studies concerning this subject are conducted.

In this light, experimental tests of different frames will be conducted at the University of Liège later this year. These tests will allow us to study the behaviour of the frame under exceptional loads and to investigate in particular the deformations in the plastic zones.

In this master thesis, numerical simulations of those experimental tests will be performed. On the one hand, this allows us to predict the response of the different frames On the other hand, the results of the numerical simulations are used to validate the analytical model. Furthermore, the influence of several parameters is tested.

RÉSUMÉ

TITRE: Robustesse des structures de bâtiments.
Étude expérimentale et contribution au développement de solutions analytiques.

AUTEUR: Liesbeth Ieven, Master Ingénieur Civil des Constructions

ANNÉE ACADÉMIQUE: 2013 – 2014

Plusieurs catastrophes, comme l'effondrement partiel de Ronan Point ou les attaques terroristes de septembre 2001, ont souligné l'importance de l'intégrité structurale d'un bâtiment. En effet, sous événements exceptionnels on ne veut pas que des dommages localisées causent l'effondrement de la structure globale.

Dans les Eurocodes, des recommandations sur ce sujet sont données. Cependant, ces recommandations ne sont pas très concrètes. Dans le but de mieux comprendre ce phénomène, plusieurs études sont menées. Le but principal est de ces études est de prédire le comportement d'une portique sous événements exceptionnels.

Dans ce travail de fin d'études, l'événement exceptionnel « perte d'un poteau « est étudié. Plusieurs modèles complexe, capable de prédire le comportement d'une portique pendant cet événement, existent. Néanmoins, différents paramètres doivent être définis. Un de ces paramètres est l'allongement des rotules plastiques sous flexion et forces axiales. À l'Université de Liège, un modèle, capable de déterminer ce paramètre, a été développé. L'allongement est caractérisée par le paramètre K_N, la raideur des rotules plastiques sous M et N. Ce paramètre est complexe à déterminer car il est influencé par beaucoup de différents facteurs. C'est cette raison qu'encore maintenant beaucoup d'études concernant ce sujet sont menées.

À ce sujet, des études expérimentales seront menés à l'université de Liège. Ces essais nous permettront d'étudier le comportement d'une portique sous charges exceptionnelles et d'examiner en particulier les déformations dans les zones plastifiées.

Dans ce travail de fin d'études, des simulations numériques de ces essais seront mis en œuvre. D'un côté, ceci nous permettra de prédire la réponse de différentes portiques. De l'autre côté, ces résultats numériques sont utilisées pour valider le modèle analytique, développé à l'Université de Liège. De plus, l'influence de plusieurs paramètres est testée.

CONTENTS

LIST OF FIGURES

LIST OF TABLES

I. INTRODUCTION

In 1968 the apartment building Ronan Point partially collapsed due to a gas explosion. After this event, it became clear that structural integrity of a building is very important. From this point on, studies on this subject, as well as on the robustness of buildings were conducted. More recent catastrophes, like the terrorist attacks in September 2001, have once again highlighted the importance of these studies.

Figure 1: Ronan point (source [1])

The Eurocodes include some rules on how to incorporate structural integrity and robustness in the design of structures. The global idea is that a localized damage may not cause the collapse of the global structure. Nevertheless, there are no concrete guidelines given. In order to form some more practical guidelines and rules, many studies are conducted. Over the years, different complex analytical models are developed that aim to predict the behaviour of a frame under exceptional events.

In this master thesis, the model, developed at the University of Liège, for the exceptional event "loss of a column" will be studied. For this model different parameters must be defined. One of the parameters is the elongation of the plastic hinges subjected to bending and to axial forces. Until now, this parameter was needed to be determined experimentally. However, this analytical model is able to predict the elongation of the plastic hinges under M and N. In order to validate this model, numerical simulations will be conducted in this master thesis.

Before I present the work that I did on the numerical simulations and the results, I am going to discuss the literature about subject. Firstly, some important notions in the domain of robustness and in particular the exceptional event "loss of a column" will be explained. Also the concept of substructure modelling will be briefly described. Furthermore, the analytical model, developed at the university of Liège, will be detailed. This model is able to predict the stiffness K_N of the plastic hinges, subjected to bending and to axial forces. Lastly, the finite element code Lagamine, which I used for the numerical simulations, will be briefly described. Its principle and possibilities, in terms of elements and constitutional laws, will be presented.

Secondly, the experiments that will be conducted at the University of Liege later this year will be detailed. The different frames and experimental set-up will be explained in more detail. Also the pre-design of the different frame will be presented.

Furthermore, the approach followed for the numerical simulations in the finite element code Lagamine will be detailed. The meshing and the adopted model will be presented. Also hypothesis and assumptions will be explained as they can have a rather big influence on the results. Special attention will contributed to explanations of the symmetry, as they play an important role for the numerical simulations.

Finally, the results will be presented. After a brief discussion of the analytical results, the results of the numerical model will be showed. The outcome of the numerical simulations for different constitutional laws will be presented. Furthermore, encountered problems will be explained. Lastly, some parameters will be tested and some hypothesis, of the analytical model or of the numerical simulations, will be detailed.

II. STATE OF THE ART

II.1. BUILDINGS SUBJECTED TO EXCEPTIONAL EVENTS

II.1.1. INTRODUCTION

In this master thesis the exceptional event "loss of a column" is investigated. In this paragraph, we will first explain what we understand under exceptional events and we will explain some important notions in the domain of robustness.

As we are particularly interested in the event "loss of a column", this will be explained afterwards. Firstly some important notions and the approach adopted by the university of Liège will be detailed. Also the notion of substructure modelling is explained.

The main ideas presented below are based on [1], [2] and [3].

II.1.2. EXCEPTIONAL EVENTS

Exceptional events are events with a very small probability of occurrence. This probability is so small that it is not justified to take these loads into account in the traditional design of structures. These events can be of a natural type or a human type. In the category natural uncertainties we can find: excessive snow load, excessive wind load (e.g. hurricanes, tornados, etc.), excessive seismic actions, etc. In the category human uncertainties we can consider: impacts (by a vehicle for example), explosions, terrorism, etc.

Buildings are designed according to the traditional design methods. In these methods we verify if the structure has a sufficient resistance and a proper behaviour under service loads (SLS) and under design factored loads (ULS). These rules are predefined in the Eurocodes. Under exceptional events on the other hand, we demand structural integrity, i.e. we want the global structure to be stable even when one of its parts is destroyed. Progressive collapse, an event where local damage causes the collapse of a much greater part of the structure, has to be avoided.

One of the methods we can ensure structural integrity is by providing an certain robustness to the structure. This implies that the different elements can resist locally to the exceptional load and that structural integrity is ensured for a certain time. This time will be long enough to let the people inside the building evacuate safely.

II.1.3. THE EXCEPTIONAL EVENT "LOSS OF A COLUMN"

II.1.3.1. GENERAL CONCEPT

One particular exceptional event is the event "loss of a column". This loss can be caused by a number of different events: impact of a vehicle, explosion, etc. It is this exceptional event that will be investigated in this master thesis.

When losing a column, a structure can be divided in two parts (figure 2). Firstly, the directly affected part is the part of the building that is directly affected by the column loss (figure 2 in red). It includes the beams, the columns and the beam-column junctions located above the area where the column loss occurs. The second part is called the indirectly affected part (figure 2 in black). This part is influenced by development of loads in the directly affected part, but influences also the development of these loads.

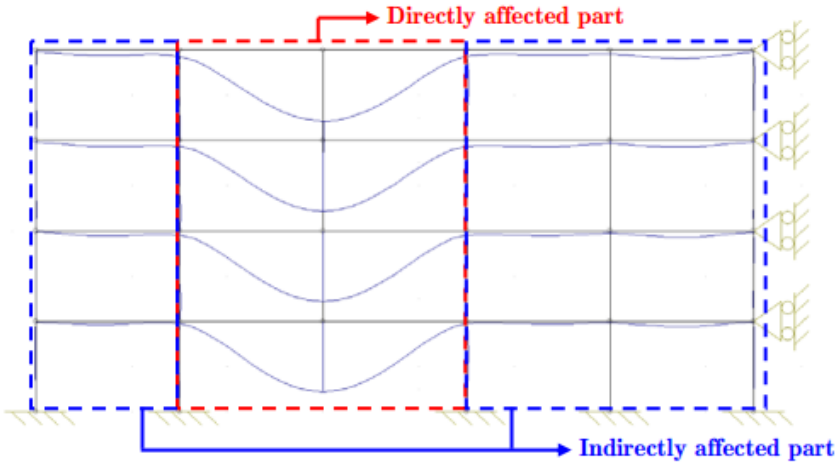

Figure 2: Directly and indirectly affected part (source: [2])

II.1.3.2. GLOBAL APPROACH

In [2] and [3], the approach adopted by the University of Liège is presented. We assume that a column is progressively removed. The loads vary from the "conventional" load, before removing of the column, to 0 when the column is completely removed. Note that we assume that the dynamic effects remain limited, thus we adopt a static approach.

The column that will be removed is indicated in red in figure 3. If we make a cut in the node A, we can determine the internal forces: the shear forces V_1 and V_2 in the extremities of the two beams, the axial load N_{up} in the column above A and the axial load N_{lo} is the failing column (figure 3).

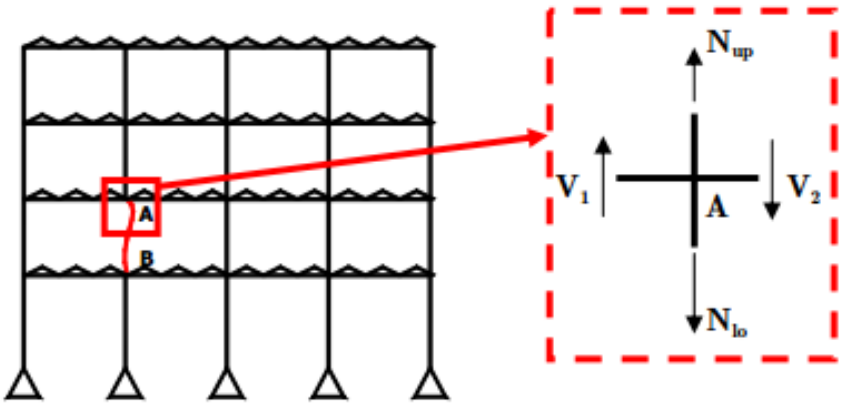

Figure 3: frame with failing column (source: [2])

We will investigate the response of the directly affected part while losing a column. As a result of studies performed at the university of Liège, the evolution of the axial load N_{lo} in function of the vertical displacement of the node A Δ_A can be predicted.

Figure 4 represents the evolution of the axial load in the column AB (in red in figure 3) according to the vertical displacement of the point A. Figures 5 till 8 present the frame during this evolution. We can observe different phases:

- Phase 1: From (1) to (2) the design loads are progressively applied. The axial load N_{lo} lowers while the vertical displacement Δ_A stays approximately 0. The column being compressed, N_{lo} is negative. We assume that de frame stays fully elastic, so no yielding appears.
  After point (2) the column will be progressively removed. The loads vary from the "conventional" load at point (2) to 0 when the column has completely failed.

- Phase 2: During this phase we can observe an elastic behaviour from point (2) to (3). At point (3) the first plastic hinges are formed in the directly affected part and at last at point (4) we reach a fully plastic mechanism.

- Phase 3: From point (4) to (5), we can observe high deformations in the directly affected part and secondary effects become important. Also, the catenary action play an important role.

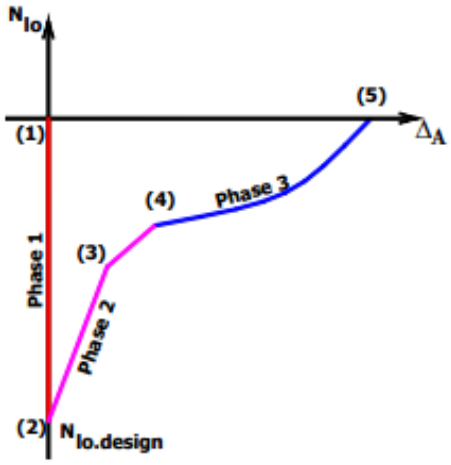

Figure 4: Evolution of N_{lo} according to Δ_A (source: [2])

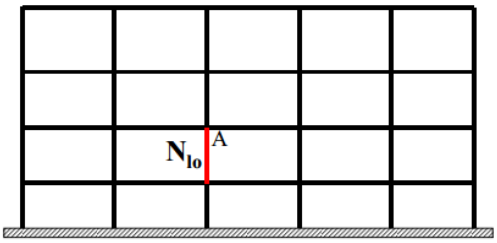

Figure 5: Frame at (2) (source: [1])

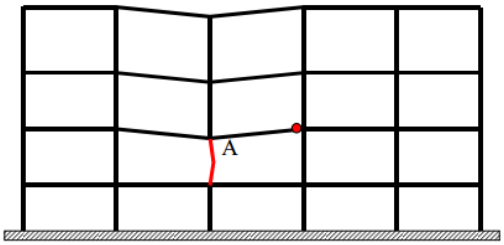

Figure 6: Frame at (3) (source: [1])

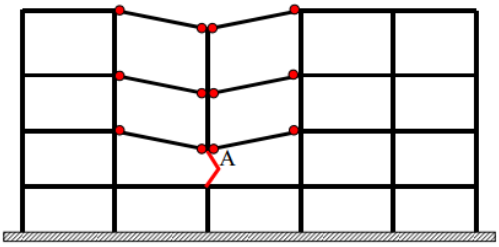

Figure 7: Frame at (4) (source: [1])

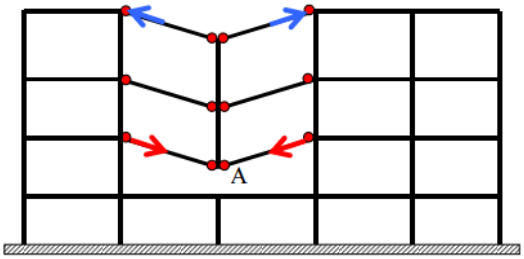

Figure 8: Frame at (5) (source: [1])

Note that we can only reach the point (5) if:

- The loads that are transferred from the directly affected part to the indirectly affected part don't cause other structural elements to collapse (e.g. instability of column or beams or formation of plastic mechanisms).
- The different constitutional elements are ductile enough to reach the vertical displacement corresponding to point (5).

II.1.4. SUBSTRUCTURE MODELLING

During phase 3, a plastic mechanism is formed and the membrane forces become very significant in the beams just above the failing column. The membrane forces in the beams above these, on the other hand, are limited. With exception of the top beams that are compressed because of the arch effect (blue arrows in figure 8).

In [2], it is investigated if it is possible to extract and study only the storey just above the failing column as it is there that the membrane forces are the most important. By numerical simulations, it was shown that the response of a frame during phase 3 can be reproduced by a simplified substructure.

The simplified substructure is represented in figure 9. In order to define this substructure, several parameters have to be detailed:

- The lateral restraint K: This parameter stands for the lateral stiffness of the indirectly affected part when the membrane forces appear in the directly affected part.
- The resistance F_{Rd} of the indirectly affected part: This parameter represents the maximal horizontal load (coming from the directly affected part) that the indirectly affected part can support.
- The loads p and Q: The loads that are applied to the subsystem.

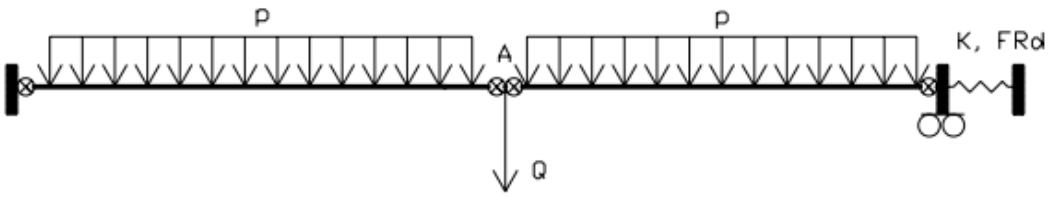

Figure 9: Simplified substructure (source: [2])

When considering this substructure model, 3 possible causes for its collapse can be noted:

- The resistance F_{Rd} of the indirectly affected part is reached.
- The deformation capacity of the beams of joints in reached.
- The axial resistance of the beams of joints is reached.

II.2. SIMPLIFIED EQUIVALENT STATIC APPROACH

II.2.1. INTRODUCTION

In [2], an analytical model, that can predict the response of a 2D frame during the loss of a column, has been introduced. Over the years, this model has been more developed at the university of Liège.

In this paragraph, the two analytical models will be presented. The information concerning these models is found in [2], [4] and [5].

II.2.2. DEMONCEAU'S MODEL

During phase 3, the structure can be represented by the substructure shown in figure 9. This substructure can predict the response of a 2D frame during this phase, as validated in [2]. Membrane forces play an important role and the lateral stiffness of the indirectly affected part K is activated. This value is assumed to stay constant during the exceptional event, as we assume that the indirectly affected part remains in the elastic domain.

To be able to use the analytical model, another parameter has to be defined. The response of the plastic hinges, that are subjected to bending and axial forces during phase 3, needs to be determined. Therefore we define K_N, i.e. the stiffness of the plastic hinges. By means of this parameter we can link the catenary actions N to the elongation of the plastic hinge δ_N.

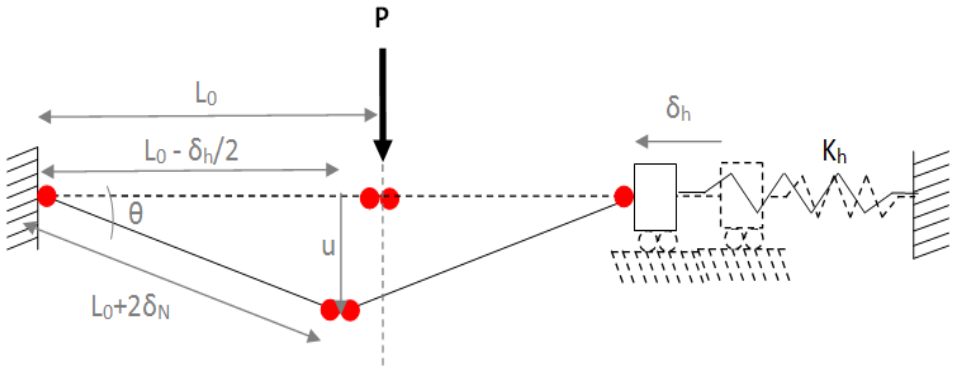

Figure 10: Substructure used for the analytical model (source: [5])

The parameters needed in order to define this model are:

- L_0: the initial length of the beam.
- K_H: the lateral stiffness of the indirectly affected part, represented by a spring. This value is assumed to stay constant during the exceptional event, as we assume that the indirectly affected part remains elastic.
- K_N: the stiffness of the plastic hinge while being subjected to bending and to axial forces. With this parameter and the catenary action N, we can determine the elongation of the plastic hinge δ_N.

– The M-N interaction curves at the section where the plastic hinges will be formed.

The unknowns and equations of the model are given in table 1.

Unknowns	Equations
u	u = input data
θ	$\sin(\theta) = \frac{u}{L_0 + 2\,\delta_N}$
δ_h	$\cos(\theta) = \frac{L_0 - \frac{\delta_H}{2}}{L_0 + 2\,\delta_N}$
δ_N	$\delta_H = \frac{F_H}{K_H}$
P	$\delta_N = \frac{N}{K_N}$
N	M = f(N)
M	$-0.25\,P\,(L_0 - 0.5\,\delta_H)0.5\,F_H\,u + 2\,M = 0$
F_h	$N = F_H \cos(\theta) + 0.5P \sin(\theta)$

Table 1: Unknowns and equations of Demonceau's model (source: [5])

II.2.3. ANALYTICAL METHOD

The analytical method is based on the method developed by Demonceau, explained just above. Only in this method, coupling effects are taken into account. This model is presented in [4] and [5].

II.2.3.1. COUPLING EFFECTS

The Demonceau model extracts one floor from the whole frame, and studies the response of this floor. In this case, one spring acts as the rest of the structure. Nevertheless, this substructure model is only valid if the compression force in the top beam remains constant which is not always the case. When comparing the two frames in figure 11, we can observe differences in this compression force. In the frame on the left, the compression forces in the top beams can increase or remain constant. On the other hand in the frame at the right, there is no horizontal displacement allowed. The upper beams can thus even be go in tension.

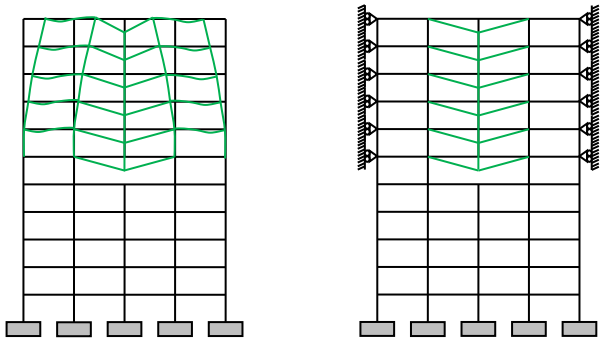

Figure 11 (source: [5])

The analytical model takes into account the coupling effects between the directly and indirectly affected part and as well between the different stories of the directly affected part. This is shown in figure 12. We can see that the stories above the failing column are taken into account and that the indirectly affected part is represented by horizontal springs.

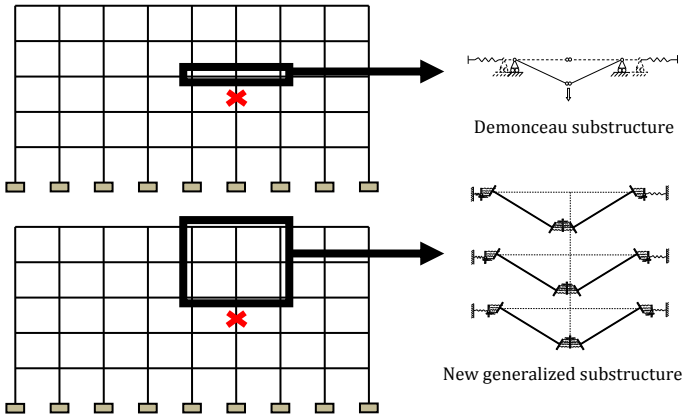

Figure 12: New substructure (source: [4])

II.2.3.2. SPRINGS REPRESENTING THE PLASTIC HINGES

As can be seen in figure 12, there are not only springs that represent the indirectly affected part, but also springs to act like the plastic hinges. This way, the response of these plastic hinges subjected to bending and to tension forces, as well as its elongation during phase 3 can be predicted. In order to determine the elongation and rotation of the plastic hinges a simple model has been developed.

The length of the plastic hinge is determined according to [6]. This is shown in figure 13. Also, the plastic hinges subjected to M and N have to be represented. These plastic hinges can be formed in the cross section or in the joint.

In order to model the plastic hinges in the cross section, 6 springs are placed in parallel. As is represented in figure 14, one spring per flange and 4 springs on the web are considered. Basing on the Bernoulli assumption, it is assumed that the section remains straight.

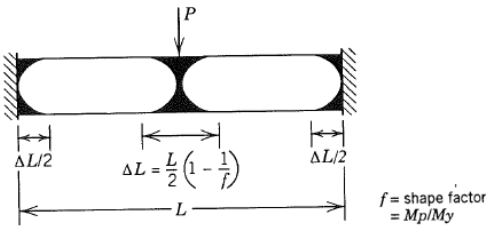

Figure 13: Plastic hinge length (source: [4])

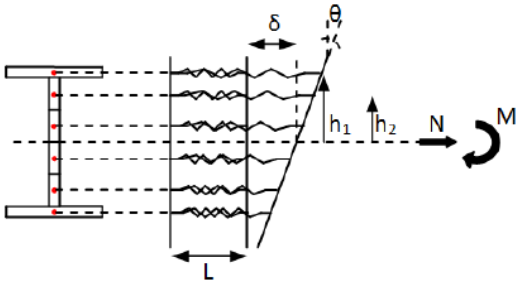

Figure 14: Springs simulating the pastic hinge in the beam cross-section (source: [4])

The same approach is followed when the hinges appear in the partially resistant joint. However, the hinge length is considered equal to zero. The yielded zone is assumed to be very small in comparison to the beam and the yielding cannot spread on further. In this case, we consider one spring per joint row and its characteristics, as its stiffness and resistance, are determined with the component method.

In both cases, the spring is considered to be elastic-perfectly plastic and to have an unlimited ductility.

II.2.3.3. ANALYTICAL MODEL

The analytical model is shown in figure 15. The entry data is given in table 4. The unkwons and equations are showed in table 5.

Hinge in the beam cross section	**Hinge in the partially resisting joint**
Cross section characteristics of the beams and columns of the frame	Localisation of each row of the joint (h_i)
Material information E, f_y	Resistance and stiffness of each component row the joint (→ component method)
Frame dimension: – L_0: span of the beams – H_0: Height of the beams Lost column localisation: – n_{st}: number of stories of the directly affected part (i.e. number of beams above the lost column) – n: number of stories under the lost column – c: number of columns in the indirectly affected part (left and right if not symmetrical)	

Table 2: Entry date for the analytical model(source: [4])

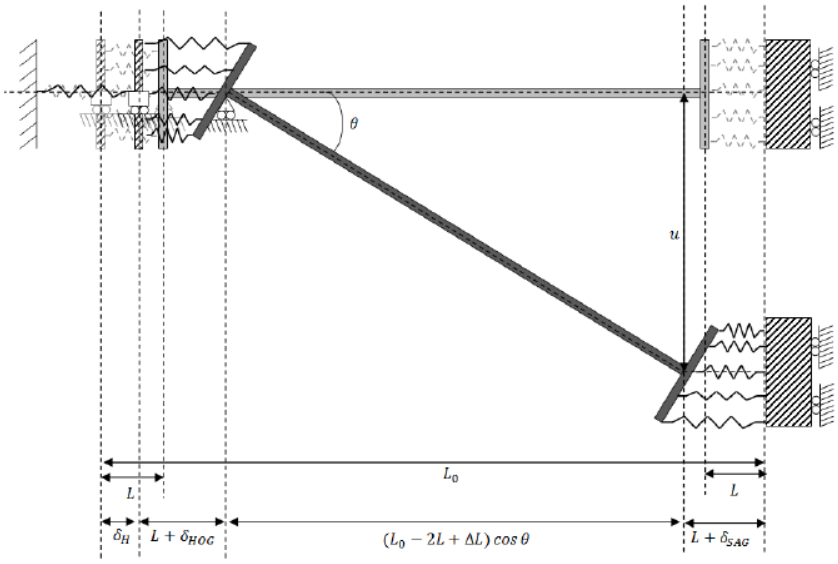

Figure 15: Half the substructure (source: [4])

Unknowns	Number	Equations	Number
u	1	u = input data	1
θ	n_{st}	$\sin(\theta) = \frac{u}{L_0 - 2\,L + \Delta_L}$	n_{st}
δ	n_{st}	$\cos(\theta) = \frac{L_0 - 2\,L - \delta_H - 2\,\delta}{L_0 - 2\,L + \Delta_L}$	n_{st}
$\delta_{H,g}$	n_{st}	$\delta_{H,g}(n_{st}x1) = S_g(n_{st}x, n_{st}) \times F_H(n_{st}x1)$	n_{st}
$\delta_{H,d}$	n_{st}	$\delta_{H,d}(n_{st}x1) = S_d(n_{st}x, n_{st}) \times F_H(n_{st}x1)$	n_{st}
Δ_L	n_{st}	$\Delta_L = \frac{F_H\,(L_0 - 2\,L)}{EA}$	n_{st}
M	n_{st}	$M = \sum F_i\,h_i$	n_{st}
F_H	n_{st}	$F_H = \sum F_i$	n_{st}
F_i (i=[1:6])	$6\,n_{st}$	$F_i = f(\delta_i)$	$6\,n_{st}$
δ_i (i=[1:6])	$6\,n_{st}$	$\delta_i = \delta + h_i$	$6\,n_{st}$
P	n_{st}	$-0.5\,P\,\left(L_0 - 0.5\left(\delta_{H,g} + \delta_{H,d}\right)\right) + F_H\,u + 2\,M = 0$	n_{st}
P_{tot}	1	$P_{tot} = \sum P$	1

Table 3: Unknows and equations of the analytical model(source: [4])

With:

P Force simulating the loss of a column
u Vertical displacement at the top of the lost column
K_H Stiffness of the horizontal spring simulating the lateral restraint of the indirectly affected part
F_H Horizontal force acting on the spring
δ_H Horizontal elongation of the spring
N Axial force in the beams of the directly affected part
M Bending moment at the extremities of the beams of the directly affected part
K_N Axial stiffness of the plastic hinges submitter to M and N
δ_N Axial elongation of the plastic hinges submitted to M and N
θ Rotation at the extremities of the beams of the directly affected part
Δ_L Elastic elongation of the beams of the directly affected part

II.3. LAGAMINE

II.3.1. GENERAL

For the numerical simulations in this master thesis, Lagamine code is used. Lagamine is a finite element code developed at the University of Liège. This code is non-linear and has a Lagrangian formulation. It is as well fitted for large strains and large deformations. The principle of this non-linear code will be discussed in this paragraph.

Also, many different elements and constitutive laws are implemented in Lagamine. Most finite elements used in the numerical simulations in this master thesis are BWD3D elements. These elements and the constitutive laws used in this master thesis are presented further in this paragraph.

II.3.2. PRINCIPLE

In [7] and [8], I found more information about the finite element principle.

II.3.2.1. VIRTUAL WORK PRINCIPLE

Physical phenomena are managed by equations with partial derivatives. In order to find a solution for these equations, we have to minimize the total energy of the system. Doing this is the equivalent of verifying the virtual work principle. The virtual work principle in presented in the next equation (source: [7]):

$$\int_V \underline{\sigma}^T \, \underline{\delta\varepsilon} \, dV = \int_V \rho \, \underline{b}^T \, \underline{\delta u} \, dV + \int_S \rho \, \underline{t}^T \, \underline{\delta u} \, dS$$

Virtual internal power Virtual external power

Avec:
- $\underline{\sigma}$ Cauchy stress tensor
- $\underline{\delta\varepsilon}$ Virtual deformation
- $\underline{\delta u}$ Virtual displacement
- V Volume
- S Surface
- ρ Density
- $\underline{b}$ Volume loads
- $\underline{t}^T$ Surface loads

II.3.2.2. TEMPORAL DISCRETIZATION

We look to resolve a problem that varies in time. As it is impossible to define the equilibrium in every instant, we introduce the notion of time step. We look for a solution in a defined number of instants. This temporal discretization is linear, as in most finite element codes.

II.3.2.3. FORCE NORM

In order to obtain an equilibrium, the internal forces $\underline{F}^{int}$, i.e. the equivalent of the stresses, have to be equal to the external forces $\underline{F}^{ext}$, i.e the equivalent of the applied loads. However, these forces are not always equal, so there exist out-of-balance forces:

$$F_{HE} = \underline{F}^{int} - \underline{F}^{ext}$$

Because it isn't always possible to obtain this perfect equality, we approximate the equilibrium with a certain precision. In order to classify a solution as acceptable, we use an out-of-balance force criterion. To satisfy this criterion, a norm has to be inferior to a certain value, often 10^{-3} or 10^{-4}. In Lagamine code, there exist different options for the calculation of this norm (source [9]):

- Average of the squares:

$$\sqrt{\frac{\sum_{Dimensions} \frac{\sum_{Equations} \frac{F_{HE}^2}{N_{Equations}}}{\sum_{Reactions} \frac{Reactions^2}{N_{Reactions}}}}{N_{Dimensions}}}$$

– Average of the absolute values:

$$\frac{\sum_{Dimensions} \frac{\sum_{Equations} \frac{|F_{HE}|}{N_{Equations}}}{\sum_{Reactions} \frac{|Reactions|}{N_{Reactions}}}}{N_{Dimensions}}$$

– Average of the maximum values:

$$\frac{\sum_{Dimensions} \frac{Max\,(F_{HE})}{Max\,(Reactions)}}{N_{Dimensions}}$$

When the equilibrium is not verified, with other words when the norm is greater than the imposed precision (10^{-3} or 10^{-4}), the solution has to be improved. In order to find a solution, the out-of-balance forces have to be decreased and we do this by modifying the imposed displacements.

II.3.2.4. TEMPORAL INTEGRATION

For temporal integration, an incremental method is used. We apply the imposed force P step by step, so that the force varies from 0 to P. By means of the Newton-Raphson method, we can find the new equilibrium for that force.

The Newton-Raphson method is represented in figure 16. We linearize the problem in order to find the real solution. So the iteration matrix is calculated, this matrix represents the tangent to the curve in a certain point. This way the out-of balance forces are reduced and we get closer to the solution. This operation has to be repeated a number of times, just until the out-of-balance forces become small enough.

The calculation of this matrix can be done in every point, as is represented in figure 16. However, we can also indicate in Lagamine to only calculate the matrix every x times. This is interesting because it allows to reduce the duration of the simulation. The calculation of the matrix can be very complex and can take a lot of time.

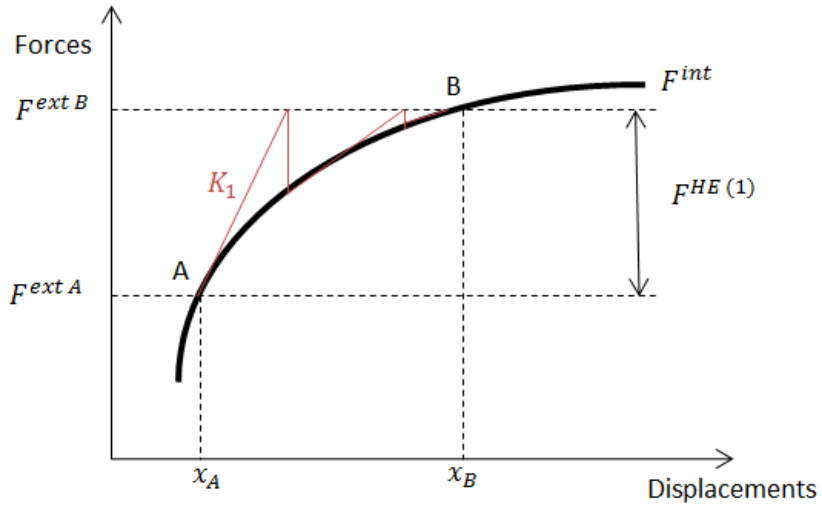

Figure 16: Newton-Raphson method

II.3.2.5. GENERAL ALGORITHM

In figure 17, the general algorithm of the non-linear code is showed. Two files have to be introduced: a data file and a strategy file. In the data file we can find parameters of constitutive laws, a list of the nodes, types of elements, etc. This file will be processed by the pre-processor PREPRO. The other file, the strategy file, contains the strategy of the simulation, e.g. which force criterion is used, the precision of the simulation, etc. Afterwards, the Lagamine calculations can start with the methods explained above.

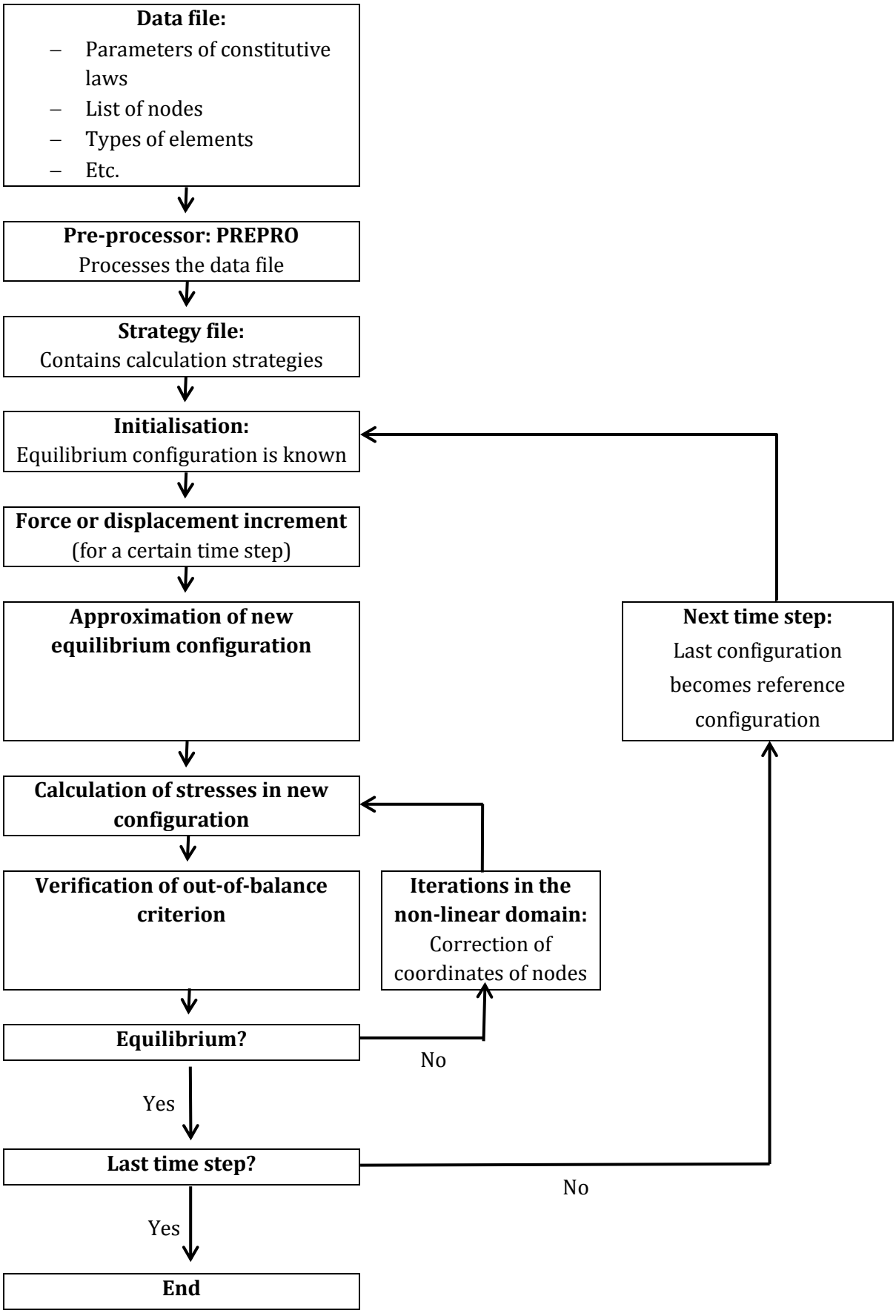

Figure 17: General algorithm (based on [7] and [8])

II.3.3. FINITE ELEMENT BWD3D

The BWD3D element is a simple block element with 8 nodes (figure 18). These elements are presented in [10] and [11]. These elements are fitted for large strains and large deformations. Integration is done with only one integration point and controls for hourglass modes. The BWD3D elements are an improvement of the elder BLZ3D element in several ways.

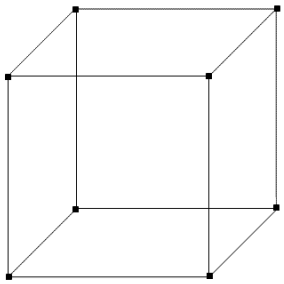

Figure 18: 8-node element (source: https://cubit.sandia.gov/public/14.0/help_manual/WebHelp/mesh_generation/mesh_modification/create_elements.htm)

Firstly, a novel shear locking treatment is used for the BWD3D elements. This treatment is based on the Wang and Wagoner method. The hour glasses modes, that are responsible for shear locking, are singled out and removed with this method.

A second novelty of these BWD3D elements is that they operate with a corotational reference system. This is necessary to be able to single out the hourglass modes.

Another feature of these elements is that the local reference axes are determined with a new method. This method is based on the *Constant symmetric local velocity gradient* method developed by Cescotto and Munhoven. These axes are needed for the objectivity of stress integration, but also for material modelling.

II.3.4. MATERIAL LAWS

Many materials laws are implemented in Lagamine. The two laws that I made use of, EP-ARB and LSTIFF, will be detailed in this paragraph.

II.3.4.1. EP-ARB

The first constitutive law is EP-ARB. This is an elasto-plastic law that is suited for solid elements at constant temperature. We can describe this law by different graphs, that will be represented just after.

The first type of law is showed in figure 19. This law is characterized by the Young's modulus E that represents the slope of the elastic part. We can also enter σ_{y1} and σ_{y2}, the lower and upper yield limit. These two stresses define the parabola. If we desire a bilinear law, we can .. the same value for σ_{y1} and σ_{y2}, this way the parabolic segment is inexistent. Another

important parameter is the elasto-plastic tangent modulus E_t. If this parameter equals zero, the material is elastic-perfectly plastic. If non, we allow some hardening to occur. We also have to indicate is the hardening is isotropic or kinetic. Other parameters that have to be entered are the Poisson's ratio and the upper yield strain ε_2.

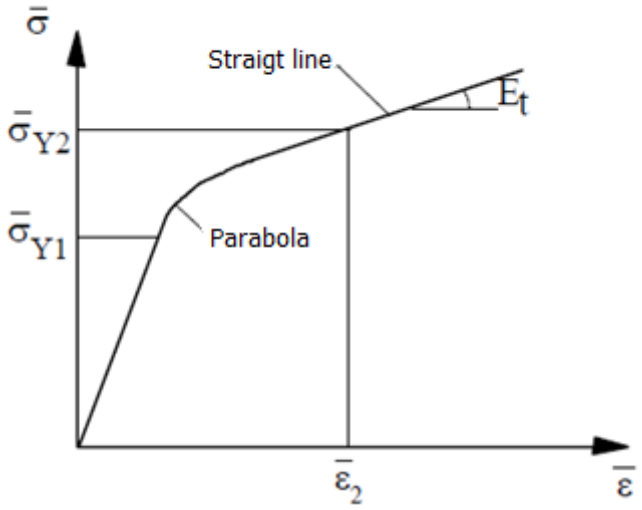

Figure 19: Bilinear law with or without parabola (source: [9])

Another type of law is represented in figure 20. This law can be entered by a number points, the number of points also being a choice. Furthermore, the Poisson's ratio and the type of hardening, isotropic or kinematic, have to be defined.

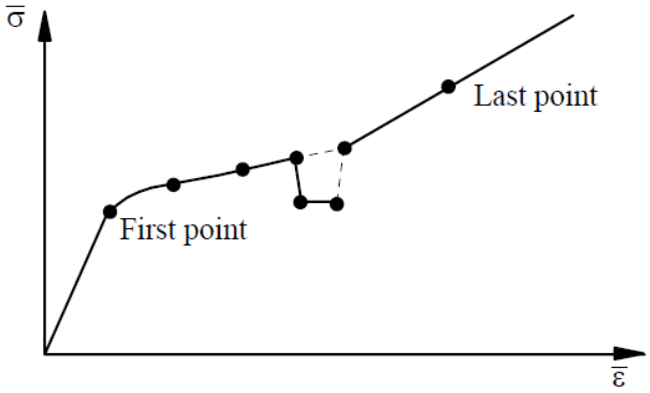

Figure 20: Law consituted of linear segments (source: [9])

Lastly, the material can be represented by an exponential law, as shown in figure 21. The law is of the type $\sigma = C\ \varepsilon^n$. So, the parameter C and n have to be entered in the program. And yet again, the Poisson's ratio and the type of hardening, isotropic or kinematic, have to be defined.

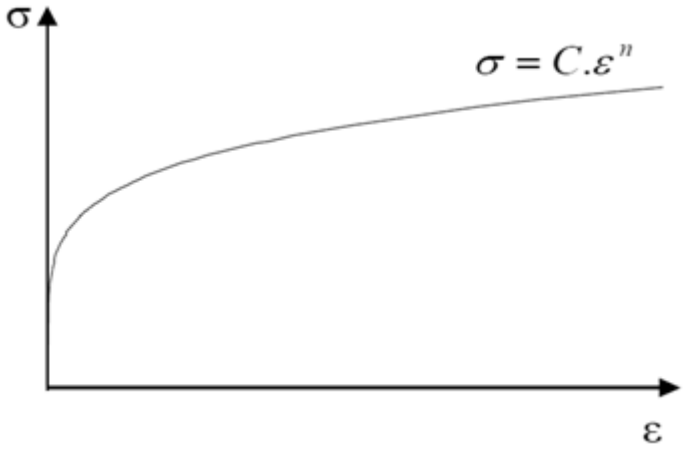

Figure 21: Exponentional law (source: [9])

II.3.4.2. LSTIFF

The LSTIFF constitutive law is used to define a concentrated stiffness at one particular node and this according to one degree of freedom.

Few parameters have to be defined for this constitutive law. We only have to enter the value of the concentrated stiffness. Furthermore, the spring can be placed at a certain angle. In this case the value of the angle has to be defined.

III. EXPERIMENTAL TESTS

III.1. INTRODUCTION

Later this year, experimental tests of different frames will be conducted at the University of Liège. In this paragraph more information about these tests and about the experimental set-up will be given.

Firstly, the main principle of the experimental tests, reproducing the exceptional event "loss of a column" will be reminded. Furthermore, the substructures that will be tested are presented and more details will be given about their configuration. Also will be explained how the experimental tests will be conducted. Finally, the pre-design of the substructures will be presented.

III.2. PRINCIPLE

III.2.1. EXCEPTIONAL EVENT "LOSS OF A COLUMN"

As explained in the state of the art, the exceptional event that will be studied in this master thesis is the event "loss of a column", by whichever cause.

We assume that a column is progressively removed and not all at once. The loads vary from the "conventional" load, before removing of the column, to 0 when the column is completely removed. Note that we assume that the dynamic effects remain limited, thus we adopt a static approach.

As detailed in the state of the art, the response of the directly affected part, while losing a column, will be investigated. As a reminder, the evolution of the axial load N_{lo} in function of the vertical displacement of the node A Δ_A as shown in figure 23.

In this master thesis, we are particularly interested in the response of the structure during phase 3. During this phase, we can observe high deformations in the directly affected part and secondary effects become important. Furthermore, the catenary actions in the beam play an important role.

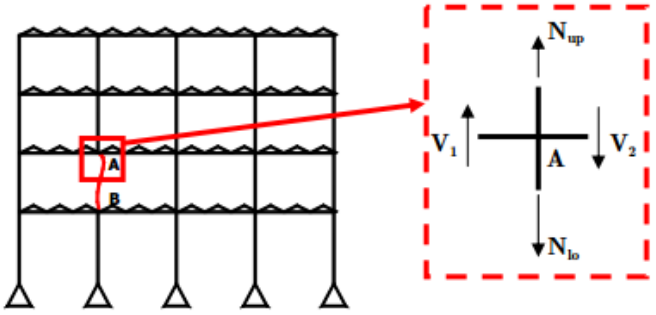

Figure 22: Frame with failing column (source [2])

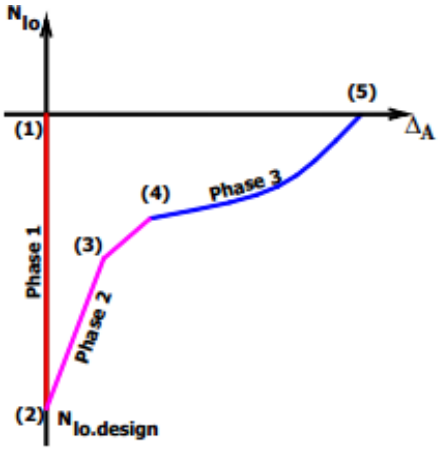

Figure 23: Evolution of N_{lo} according to Δ_A (source: [2])

III.2.2. SUBSTRUCTURE MODELLING

In order to obtain the response of the frame during phase 3, not the whole frame has to be modelled. As explained in the state of the art, a simplified substructure can recreate the response of the frame during phase 3.

The simplified substructure is represented in figure 24. In order to define this substructure, several parameters have to be detailed (source: [2]):

- The lateral restraint K: This parameter stands for the lateral stiffness of the indirectly affected part when the membrane forces appear in the directly affected part.
- The resistance F_{Rd} of the indirectly affected part: This parameter represents the maximal horizontal load (coming from the directly affected part) that the indirectly affected part can support.
- The loads p and Q: The loads that are applied to the subsystem.

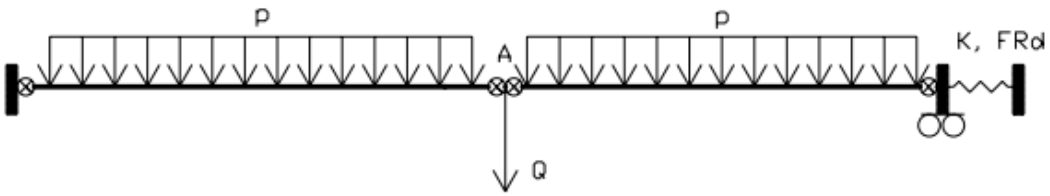

Figure 24: Simplified substructure (source: [2])

III.3. EXPERIMENTAL SET-UP

During the experimental tests that will be performed at the University of Liège, 4 different substructures will be tested. There are 2 main configurations (figures 25 and 26). Each of the two configurations is characterized by a different value of K_H, representing the lateral stiffness of the indirectly affected part.

Both configurations are tested for two different beams: an IPE100 and an IPE160 in S355.

III.3.1. CONFIGURATION LOW K_H

The first configuration is shown in figure 25. This configuration is known as configuration "low K_H,".

In this case, we impose a lateral stiffness of $25000\ {}^{kN}/_{m}$ on both extremities. To obtain this stiffness artificially, two horizontal jacks are placed at each side of the substructure. We assume that the restraint shows an elastic behaviour during the whole test. These jacks have a capacity of 100 ton and a maximal length of 300 mm. Once this maximal capacity is reached, the experimental test stops.

The jacks are placed symmetrically on both extremities, this way we will obtain a symmetric response of the substructure. The information obtained the experiments will so be easier to process.

III.3.2. CONFIGURATION HIGH K_H

The second configuration is shown in figure 26. This configuration is known as configuration "high K_H,".

For this configuration, the lateral restraint is obtained with the help of a superstructure. This way the artificial restraint is $300000\ {}^{kN}/_{m}$. We assume once again that the restraints show an elastic behaviour, thus the superstructure needs to remain elastic. Also in this case, the substructure is symmetrical, so we will obtain a symmetrical response.

III.3.3. SIMULATION OF THE COLUMN LOSS

During the experimental tests, the loss of a column will be represented by imposing a vertical displacement in the centre of the beam, where the column normally would be situated. In the beginning of the tests the imposed displacement is equal to zero and will be progressively increased during the experimental tests.

The displacement at the centre of the beam will be imposed by means of a jack. The position of this jack is showed in figure 25 and 26. Remark that the jacks are placed under the beam, the displacement thus will be upwards. However, during a real column loss, the displacements would be downwards. The reason for this are practical considerations: it is easier to place a jack on the ground below the beam.

The maximal vertical displacement of this jacks is equal to 0.4 m. That is why for the numerical simulations and analytical model, we only study vertical displacements u going from 0 to 0.4 m.

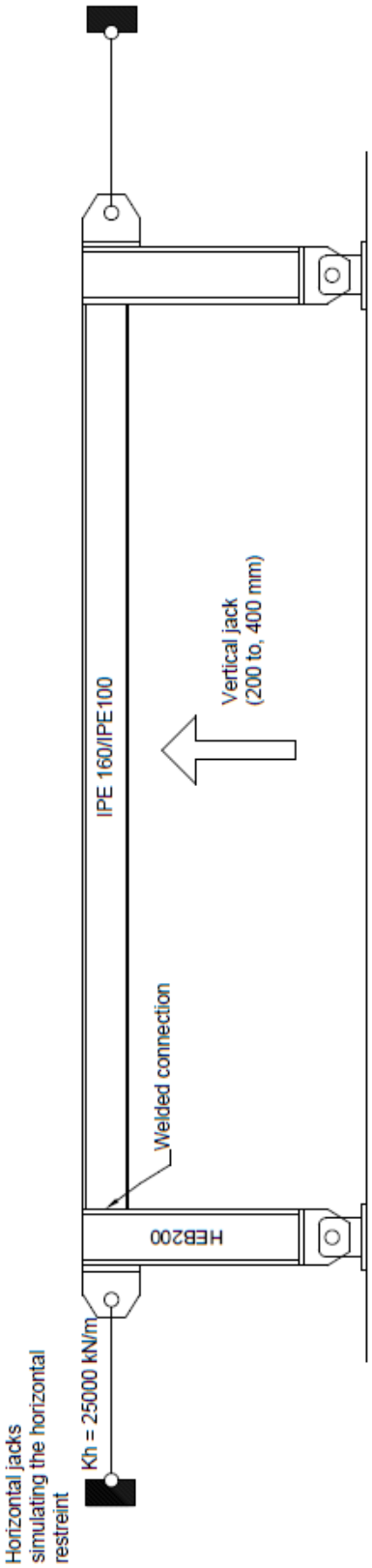

Figure 25: Configuration "low K_H" (figure by Clara Huvelle)

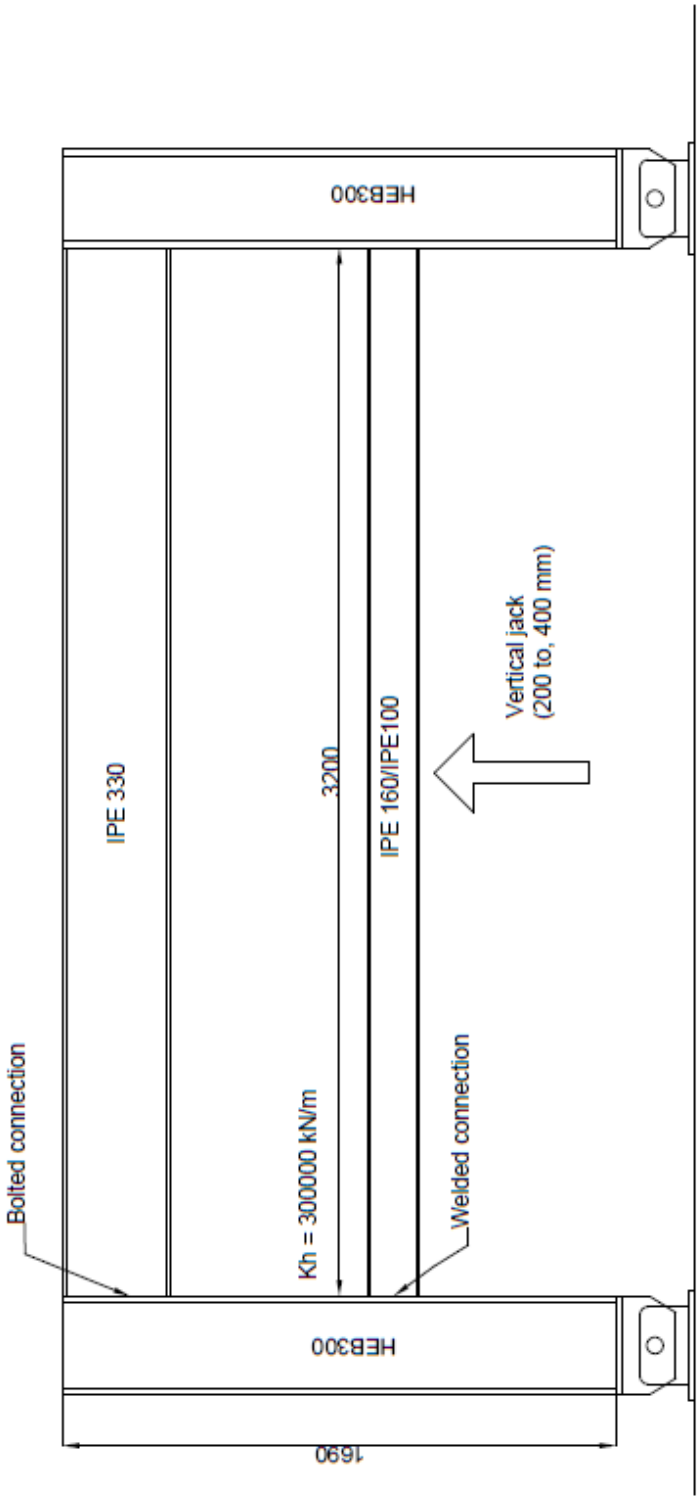

Figure 26: Configuration "high K_H" (figure by Clara Huvelle)

III.4. PRE-DESIGN OF THE SUBSTRUCTURE

One part of my work consisted in the pre-design of the substructure. I based this pre-design on calculations already directed by Clara Huvelle and I continued her work.

Note that this is not a detailed design of the substructure. The objective is to verify if the capacity of the jacks is big enough to reach phase 3. Also the rest of the substructure will be pre-designed. Here, the interest is to verify whether the rest of the structure (columns and beams) will sustain the loads and not collapse. It would not be very interesting if the experiment has to be stopped because of a failing column, as we are mostly interested in the development of the loads in the tested beam.

Firstly the pre-design of beams that will be tested is presented. Afterwards the pre-design, of the two different configurations, will be demonstrated.

III.4.1. BEAMS

Firstly, the plastic resistance to normal forces of the gross cross-section is calculated (table 4). A security coefficient of 2 is used. This is to take into account the overstrength phenomena that may occur. Indeed, the steel grade is S355, but the yield limit may in reality be higher than 355 MPa. We want to make sure that during the experimental tests that N_{pl} will be reached with the capacity of jacks.

	IPE 100	**IPE 160**
$\boldsymbol{N_{pl}}$	452.98 kN = 45.30 to	1427.10 kN = 142.71 to
$\boldsymbol{P_{pl}}$	37.31 kN = 3.73 to	117.39 kN = 11.74 to

Table 4: N_{pl} and P_{pl} for the IPE 100 and IPE 160 beams

As explained above, the jacks representing the indirectly affected part for the low K_H configuration have a limit of 100 to. For the IPE 100 beam, the plastic resistance is well under this value. However, the experimental test with the beam IPE 160 will probably not reach the plastic resistance of the section. The M-N interaction curve will thus not be completely followed. However for the high K_H configuration, this will not be a problem as the restraint representing the indirectly affected part is obtained with the superstructure and not by means of jacks.

In order to conduct a plastic analysis, the beam has to be classified class 1. In the catalogue of ArcelorMittal, the two beams, IPE 100 and IPE 160 in S355, are classified class 1. A plastic analysis may thus be conducted.

The assumed collapse mechanism is showed in figure 27. We can determine the vertical load P, for which this plastic mechanism will be formed. These values are given in table 4.

We observe that the capacity of the jacks, representing the force P, is high enough. The capacity of 200 to remains loosely above the values for P_{pl} (table 4).

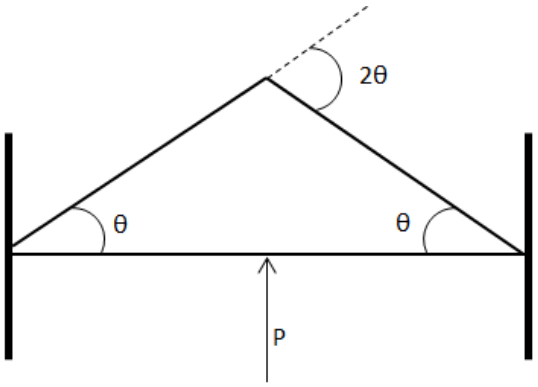

Figure 27: Plastic mechanism

The details of the calculations can be found in appendix 1.

III.4.2. CONFIGURATION LOW K_H

The model of configuration low K_H assumed for the pre-design is shown in figure 28. The two load cases that are considered are represented in figures 29 and 30. The first load case corresponds to the point when the bending moment in the tested beam has reached M_{pl}. Afterwards, the M-N interaction curve will be followed, the bending moment in the beam will decrease while the normal forces increase until we reach N_{pl}, which corresponds to load case 2.

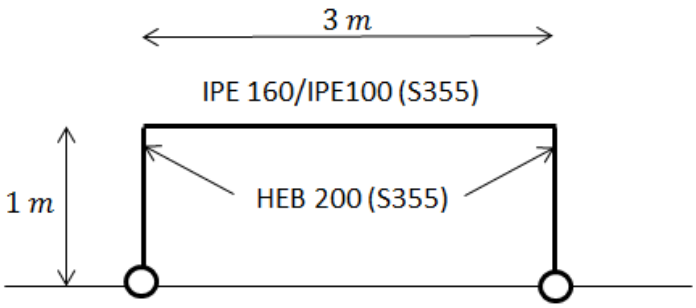

Figure 28: Model for pre-design (configuration low K_H)

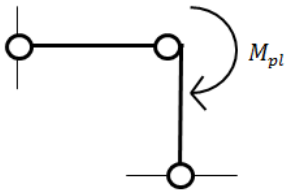

Figure 29: Load case 1

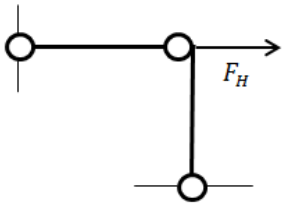

Figure 30: Load case 2

F_H	$N_{pl,IPE\ 160}$
M	$M_{pl,IPE\ 160}$

Table 5: Considered values for F_H and M

The considered loads are given in table 5. The columns are checked for both load cases in appendix 2. We can conclude that they can resist the applied loads.

III.4.3. CONFIGURATION HIGH K_H

The model of configuration high K_H assumed for the pre-design is shown in figure 31. The dashed line indicates the position of the tested beam. The two load cases that are considered are represented in figures 32 and 33. These are the same as for the configuration low K_H.

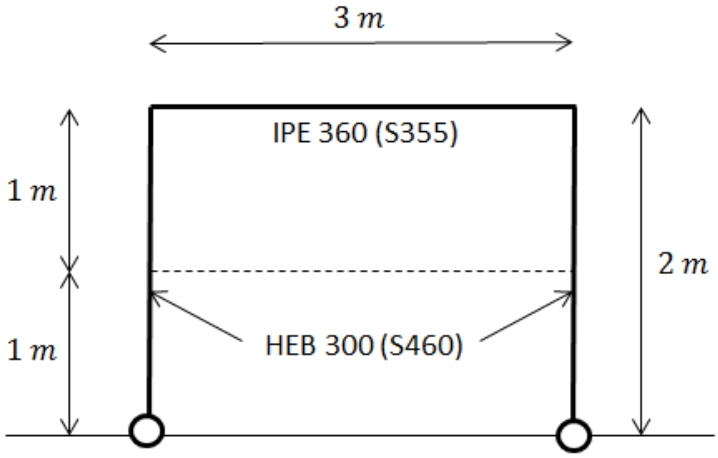

Figure 31: Model for pre-design (configuration high K_H)

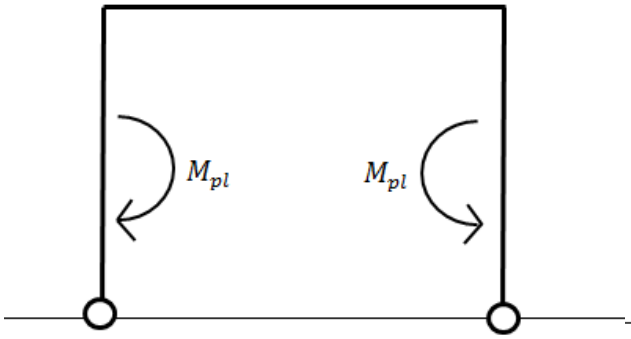

Figure 32: Load case 1

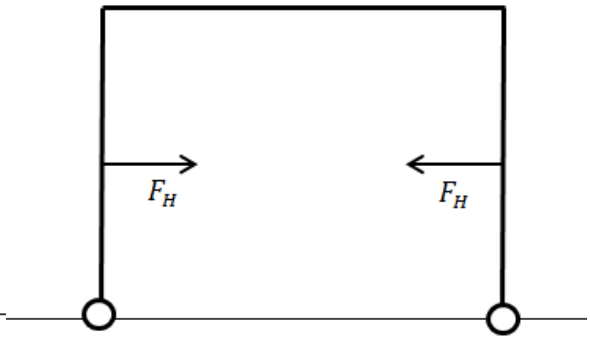

Figure 33: Load case 2

To begin, the magnitude of K_H has to be calculated. In order to calculate this stiffness we use load case 1 with F_H being equal to its maximal value, i.e. the ultimate resistance to normal forces of the gross cross-section N_U of the IPE 160 beam, no security coefficients being applied. The horizontal displacement δ_H is calculated with the structural design analysis program Diamonds.

$$K_H = \frac{N_{U,IPE160}}{\delta_H} = \frac{1427.1\ kN}{0.0043\ m} = 331883.73\ {}^{kN}/_{m}$$

This value corresponds well to the assumed value of $300000\ {}^{kN}/_{m}$.

Furthermore, the elastic resistance of the substructure has to be verified. We have to check if the different elements do not enter in plasticity as we assume that the indirectly affected part, which is represented by the superstructure, remains elastic throughout the whole test.

The considered values for F_H and M are given in table 6. Note that here partial security coefficients are applied as we have to make sure that the superstructure remains in the elastic domain.

F_H	$1.5\ N_{U,IPE\ 160}$
M	$2\ M_{pl,IPE\ 160}$

Table 6: Considered values for F_H and M

In appendix 3, the IPE 360 beam and the HEB 300 columns are checked. Their resistance is great enough to sustain the loads.

IV. NUMERICAL SIMULATIONS

IV.1. INTRODUCTION

In this paragraph, the approach followed for the numerical simulations will be detailed. Also hypothesis and assumptions will be explained.

Firstly, the choices for the meshing of the beam will be illustrated. Afterwards, the modelling of the cross section and the structure will be presented. Assumptions that are made will be demonstrated and justified too. This includes, among other things, explanations of the symmetry of the model and how this symmetry influences the parameters needed to impose. Furthermore, the modelling of the materials and some encountered problems will be detailed. Lastly, some more numerical aspects of the simulation will be demonstrated.

IV.2. MESHING

In order to limit the calculation time of the Lagamine program, we decided to only model one fourth of the beam-length, i.e. 750 mm. Also only half the cross section was modelled. This is shown in figures 34 and 35. We were able to do this because of the symmetry of the configuration. This will be detailed and justified in §IV.4.2.

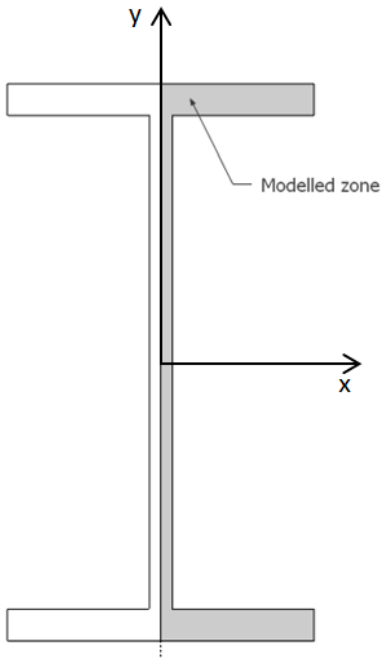

Figure 34: Modelled zone (cross section)

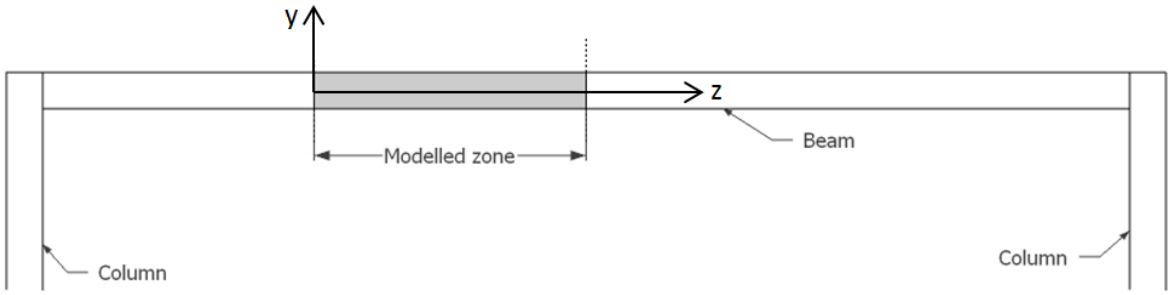

Figure 35: Modelled zone (length of the beam)

The substructure is modelled using 8-node block elements, named BWD3D in Lagamine. Furthermore, when needed to refine the meshing, there is made use of 3D- transition elements. The cross section of these transition elements is shown in figure 36.

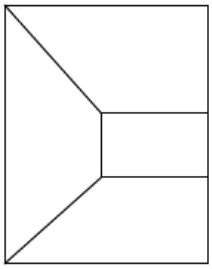

Figure 36: Transition element (source: [12])

The meshing of the beam was done using a 3D mesh generator developed by Cédric Lequesne. This mesh generator, named Mesh3D, was developed for Lagamine code.

We can differentiate three different zones in the meshing (figure 37). The first zone consists of larger elements (figure 38). We are not so much interested in the information we find in this area as we do not expect plastic hinges to form here. The elements are approximately cubic and measure roughly 5,7 x 3,8 x 18,0 mm. Next to this zone, we can find a transition area. Its purpose is to refine the meshing in the z direction. As shown in figure 39, transition elements are used to pass from one to three divisions. The last zone is densely meshed (figure 40). We are particularly interested in this zone, as this is where we expect a plastic hinge to form. The elements are cubic and measure roughly 1,9 x 3,8 x 5,0 mm.

Finally we obtain 6468 elements from which:

- 1260 in the coarsely meshed zone
- 168 in the transition zone
- 5040 in the densely meshed zone.

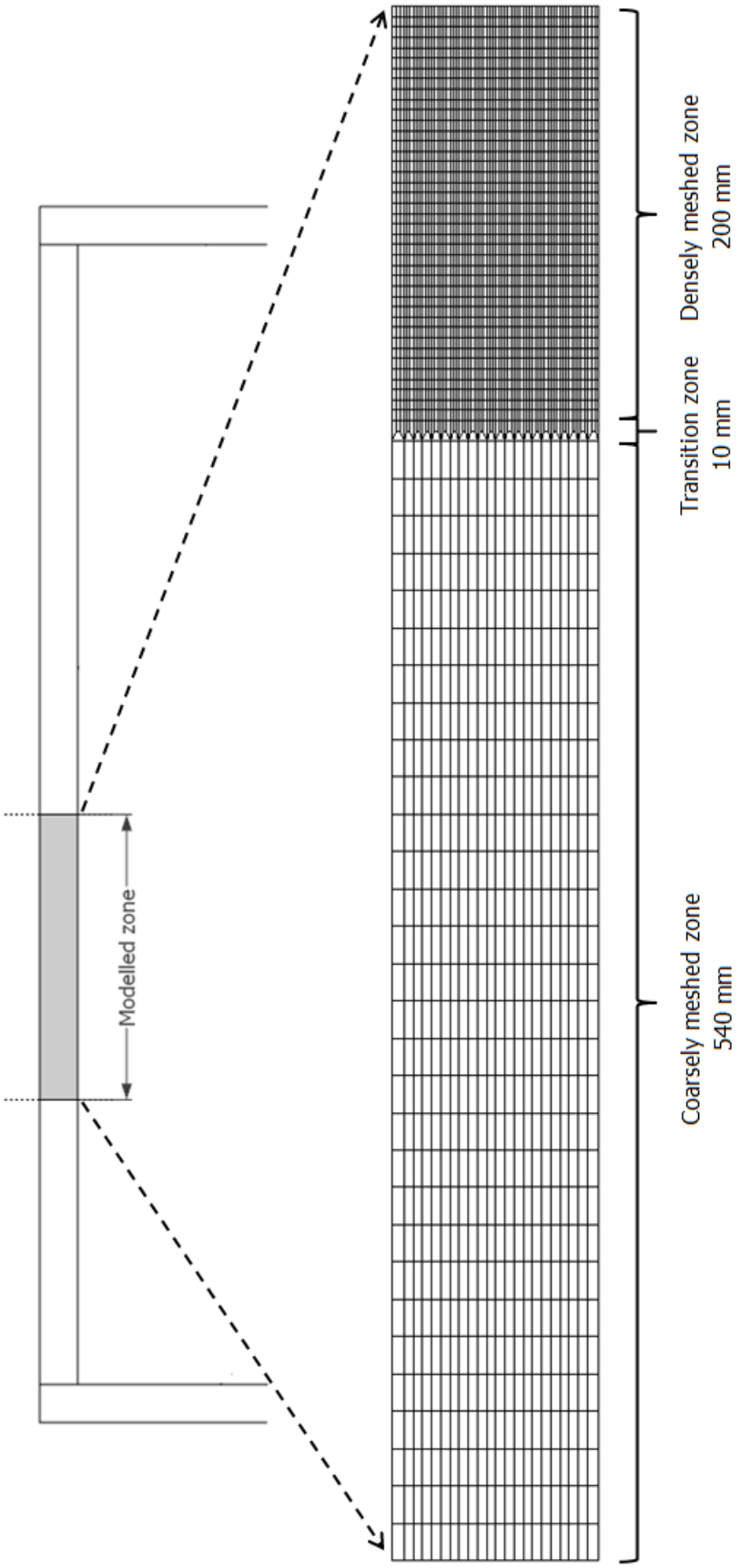

Figure 37: Meshing

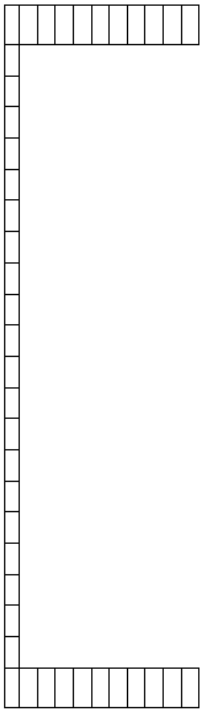

Figure 38: Cross section of the coarsely meshed zone

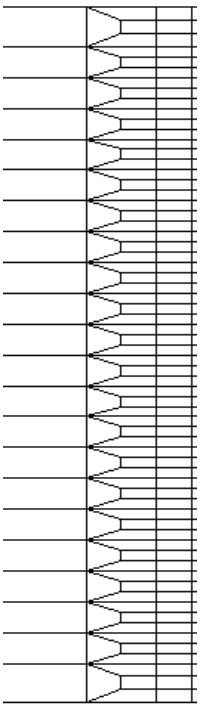

Figure 39: Transition zone

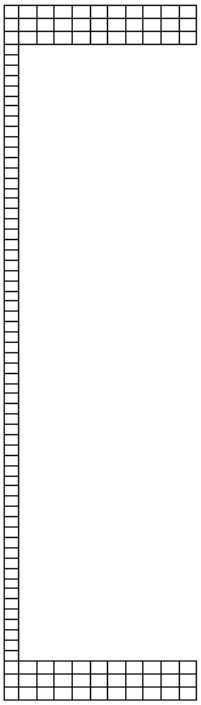

Figure 40: Cross section of the densely meshed zone

IV.3. MODELLING: CROSS SECTION

When modelling the cross section, we decided to separate it in 5 different parts, as can be seen in figure 41. It was made sure that every part had 2 nodes in common with an adjacent part. This way, detachment of the different parts could be avoided.

Figure 41: Cross section model

Note that the fillet radius does not appear in the model, even though it is well present in the real cross section.

IV.4. MODELLING: STRUCTURE

IV.4.1. GLOBAL MODEL

The global model is represented in figures 42 and 43.

In figure 42, the longitudinal view of the model is showed. At the symmetry plan of the beam, i.e. the right extremity of the model, the displacement of the nodes is blocked according to the z-direction. However, at its left extremity, the beam is free to undergo a displacement according to this direction. The displacement of the beam in this point is governed by the spring, representing the stiffness of the indirectly affected part. However, the vertical displacement is blocked at this point.

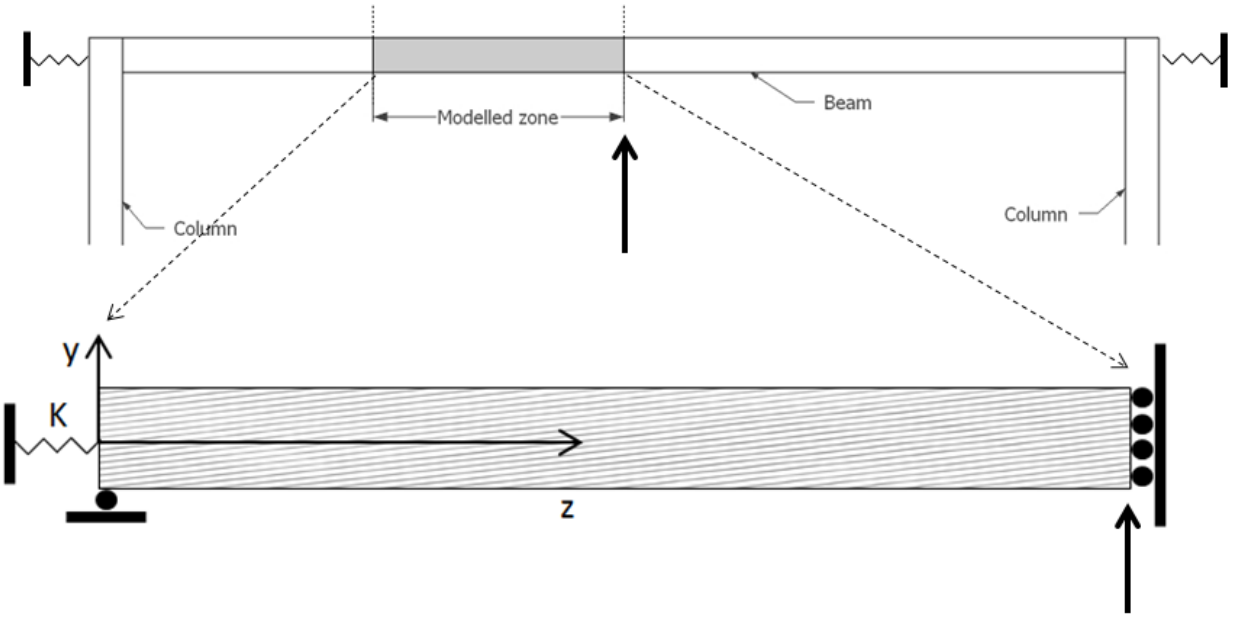

Figure 42: Longitudinal view of the global model

In figure 43, the model of the cross section is presented. As can be observed, the degrees of freedom in the symmetry plan are blocked according to the x-direction.

In the following paragraphs, the symmetry of the model will be justified and the blocked degrees of freedom will be detailed. Also the influence of the symmetry on the parameter K, representing the stiffness of the indirectly affected part, will be explained.

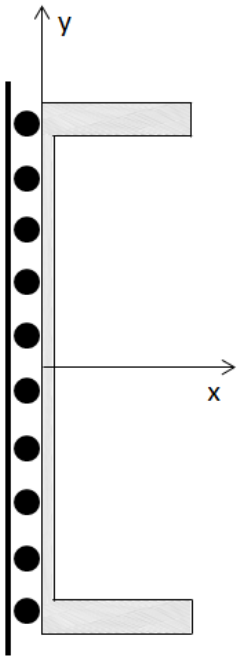

Figure 43: Model of beam cross section

IV.4.2. SYMMETRY

As explained above, only one fourth of the beam is modelled in the program. Also, thanks to the symmetric cross section, we only needed to model half this cross section.

The reasons why it is justified to only consider one fourth of the beam length are detailed below.

IV.4.2.1. SYMMETRIC MOMENT DIAGRAM

The beam is subjected to punctual load in its centre, which represents the jack, as is showed in figure 44. It is assumed that the beam is clamped at both its extremities. We can observe that the moment diagram, represented below, is symmetrical about the centre of the beam. Furthermore we note that every fourth part of the beam shows the same moment diagram, admittedly with an opposite sign.

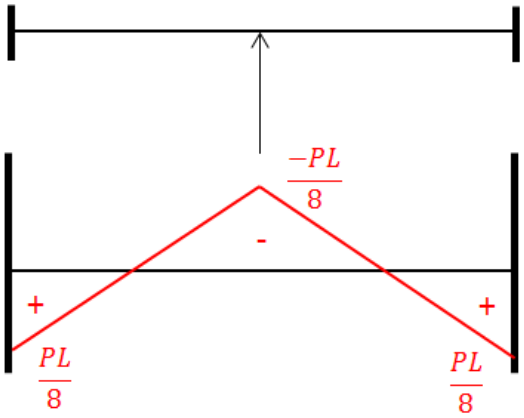

Figure 44: Moment diagram

In reality the force is not punctual but distributed over a limited surface. This is because during the experiments, the jack doesn't push the beam directly, but its force is distributed over a greater surface with the help of a metallic plate.

Nevertheless, we assume that its influence is little and it is justified to model only one fourth of the beam. As will be explained in §IV.4.5., tests will be performed to study if the dimensions of the plate have an influence on the results.

We can conclude that in terms of the moment diagram, it is justified to make use of the symmetry of the simulation and only model one fourth of the beam.

IV.4.2.2. ROTATION AT EXTREMITIES OF THE BEAM

The beam being symmetrical and continue about its centre, this section has to stay straight at all times. This will be imposed by blocking nodes in a particular direction as will be demonstrated in §IV.4.3.

The beam is supposed to be clamped at its extremities. This way the rotation at the beam-column joint is supposed to be equal to zero. However in reality a certain rotation may appear. As a result the problem would not be perfectly symmetric.

In order to check this, the 2 different configurations, each for a IPE 100 and IPE 160 beam, are tested in Diamonds, a structural design analysis program. The two configurations are showed in figures 45 and 46.

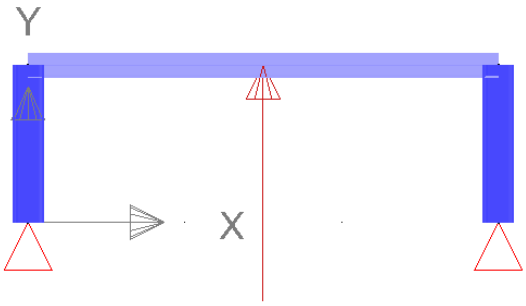

Figure 45: Configuration low K_H

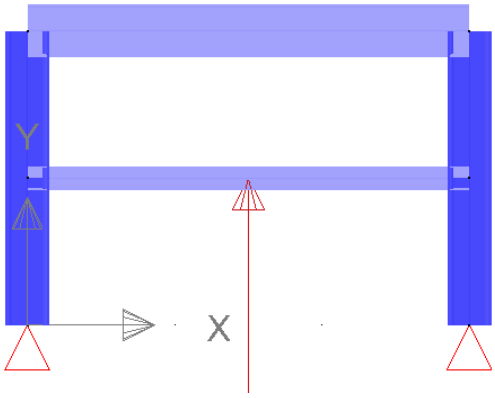

Figure 46: Configuration high K_H

For each test, the magnitude of the punctual load corresponds to the maximal value of the vertical force P, that has been determined with the analytical model. We obtain the following results (table 7):

Configuration low K_H: IPE 100	0.1 °
Configuration low K_H: IPE 160	0.3 °
Configuration high K_H: IPE 100	0.0 °
Configuration high K_H: IPE 160	0.0 °

Table 7: Rotation the extremity of the beam

As we can see in table 7, the rotations at the extremities of the beam remain very small. It is thus justified to consider the beam as clamped. By consequence, the assumed symmetry can be used.

IV.4.3. BLOCKED DEGREES OF FREEDOM

In order to obtain this symmetry, certain degrees of freedom have to be blocked. The blocked degrees of freedom are shown in figures 47, 48 and 49. The direction of the red lines indicates according to which axis the nodes are blocked.

First of all, the nodes at the right extremity of the beam are blocked according to the z-direction (figure 47 on the right). The beam being symmetrical and continuous in its middle point, this section has to stay straight at all times. The z-position of these nodes may thus not vary during the simulations.

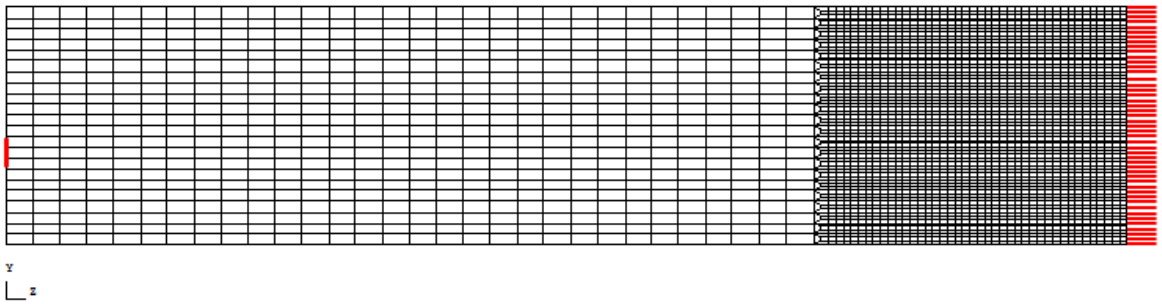

Figure 47: Longitudinal view: blocked degrees of freedom

The symmetry of the cross section also needs to be verified by blocking certain degrees of freedom. This cross section needs to remain straight at its axis of symmetry, i.e. the y-axis. That is why the at this axis the x-degree of freedom of the nodes is blocked as is represented in figures 48 and 49.

Lastly, two nodes are blocked according to the y-degree of freedom. This is showed in figures 47 and 48. These two nodes are situated in the centre, according to the y-direction, of the beam cross section. This way, the extreme left section can rotate without restraint about these supports. This is necessary because we assume that the bending moment in equal to zero in this point, as explained in §IV.4.2.1.

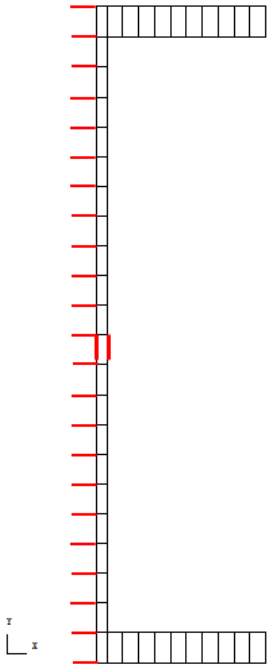

Figure 48: Extreme left cross section

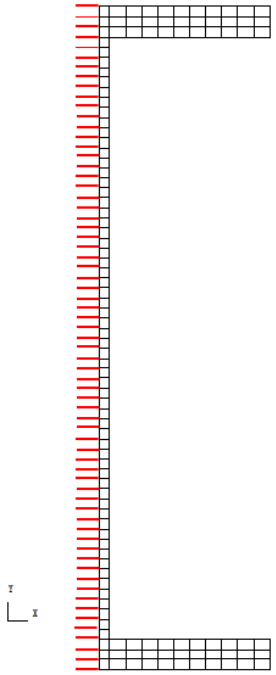

Figure 49: Extreme right cross section

IV.4.4. LATERAL RESTRAINT

IV.4.4.1. MODELLING

The lateral restraint coming from the indirectly affected part also has to be modelled. To model this, STIFF elements are used. These elements are applied to the left extremity of the beam as shown in figure 50. However, the spring-elements are not placed on all the nodes in this section. This section needs to be able to be subjected to a rotation without restraint, because the bending moment is supposed equal to zero in this section (figure 44). That is why, the STIFF elements are only applied to the two middle nodes (figure 51). These are the same nodes for which we blocked the y-degree of freedom (figure 48).

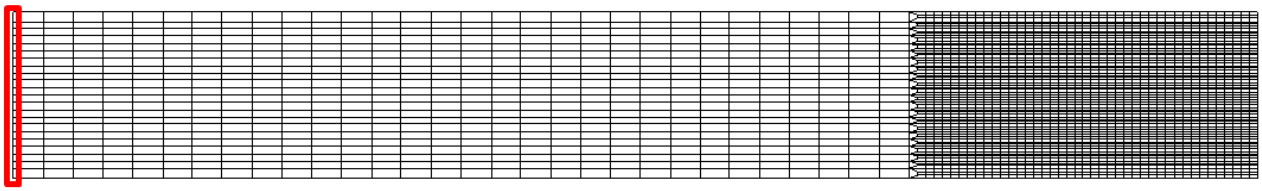

Figure 50: Section on which the STIFF elements are applied

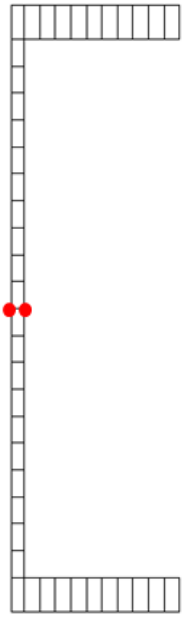

Figure 51: Nodes where the STIFF elements are applied

The lateral restraint K will be divided between the two elements. Every element will thus have a lateral restraint $K/_2$.

IV.4.4.2. VALUE OF THE LATERAL RESTRAINT

The value of the lateral restraint K that has to be imposed in the program. As we only model one fourth of beam length and only half the cross section, the value of K needed to impose in the simulation may change.

Firstly, we will investigate how modelling only one fourth of the beam influences the K-value. When looking at figure 52, we can see half the beam in its initial configuration (in black) and its deformed configuration (in red). As shown in figure 52, when point 1 is subjected to a displacement δ_H, point 2, situated in the middle, will undergo a displacement $\frac{\delta_H}{2}$. This is assuming that the elongation of the plastic hinges, with a stiffness valuing K_N, is equal in point 1 and 3. So for the same force P applied in point 3, the displacement in point 2 is only the half of point 1. Thus we find:

$$K^* = \frac{P}{\delta_H/_2} = 2\,\frac{P}{\delta_H} = 2\,K$$

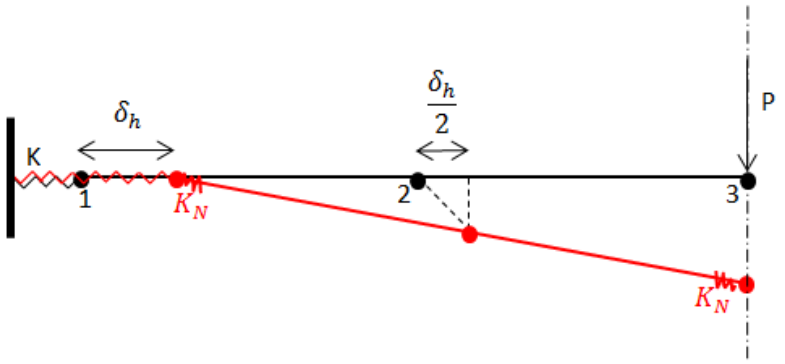

Figure 52: Half the beam in initial and deformed configuration

So for the simulations of one fourth beam, we need to double the value of the lateral restraint (figure 53).

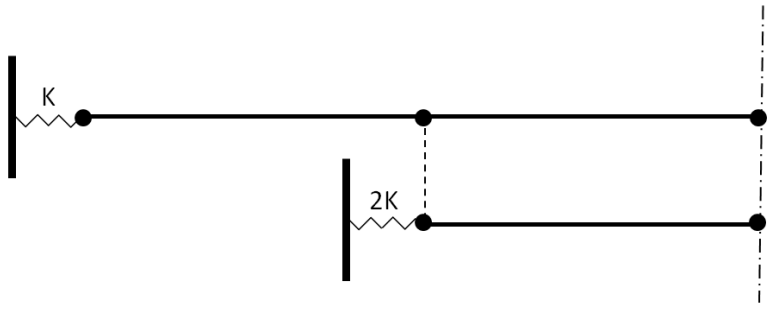

Figure 53: Lateral restraint of the whole beam and of the modelled part

On the other hand, modelling only half the cross section will also has an influence on the K-value needed to impose. The beam being symmetrical, we assume that both half cross section are subjected each half the K-value. Thus, we must divide the lateral restraint by 2.

In conclusion, the value of the lateral restraint K, has to be multiplied by 2, because of the longitudinal symmetry and divided by 2, because of the cross section symmetry. As a result, the lateral restraint, that needs to be imposed for the simulations, stays equal to the values defined for the experimental tests.

IV.4.5. DISPLACEMENT

As explained in an earlier paragraph, during the experimental tests the column loss will be simulated by imposing a displacement, varying from 0 to 0.4 m, by means of a jack.

In the Lagamine model, the column loss will also be simulated by imposing a displacement. The relation displacement – time is defined to be linear. The time varies from 0 (start of the simulation) to 1 (end of the simulation) and the displacement from 0 to 0.2 m. Note that the time in this case doesn't correspond to the real calculation time. The displacement in function of the time is represented in figure 54.

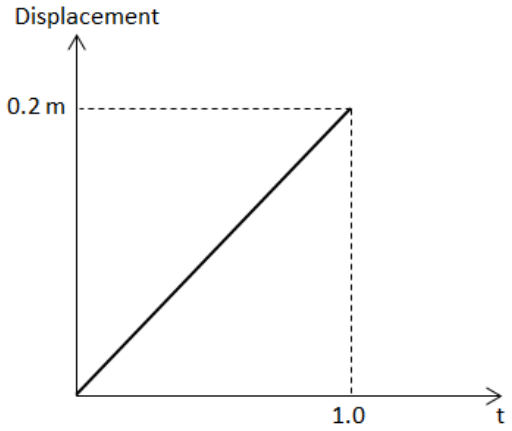

Figure 54: Imposed displacement in function of the time

During the simulation, the displacement varies from 0 to 0.2 m and not 0.4 m as it is for the experimental tests. This is because we only model one fourth of the whole beam. As can be seen in figure 55, when the beam is submitted to a displacement of 0.4 m, the one fourth that we modelled is only displaced 0.2 m.

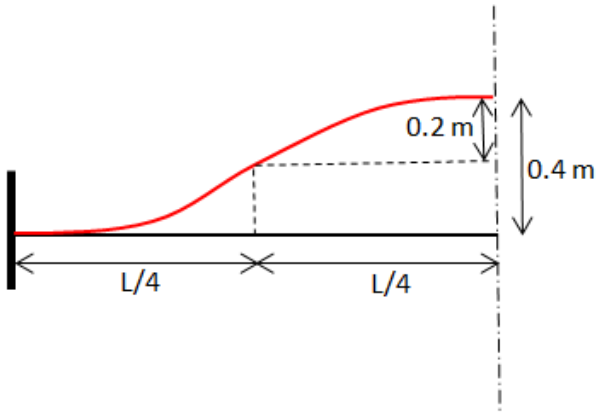

Figure 55: Initial (in black) and deformed configuration (in red)

During the execution of the experiments, the jack won't be applied directly on the beam. A metallic plate will be used to distribute the forces on a larger surface. For the numerical model, the imposed displacement is also considered to be applied to a certain zone. There are

two reasons for this. Firstly, this in conformity with the experimental tests. In addition, there is a numerical reason. Applying the displacement only to few nodes, could cause great local deformations and stresses. These great stresses could influence the results and if the deformations become very great, this could cause difficulties for the program to converge towards a solution.

Initially, the metallic plate was assumed to be applied to the whole width of the flange and to have a length of 60 mm. As only one fourth of the beam is modelled, the length of the plate to be considered in the model is 30 mm. The surface where the displacement is applied is supposed to remain straight in this model, as can be seen in figure 56 (especially on the deformed structure). However, in reality, this surface may not stay straight. It would thus be interesting aspect to consider in future simulations.

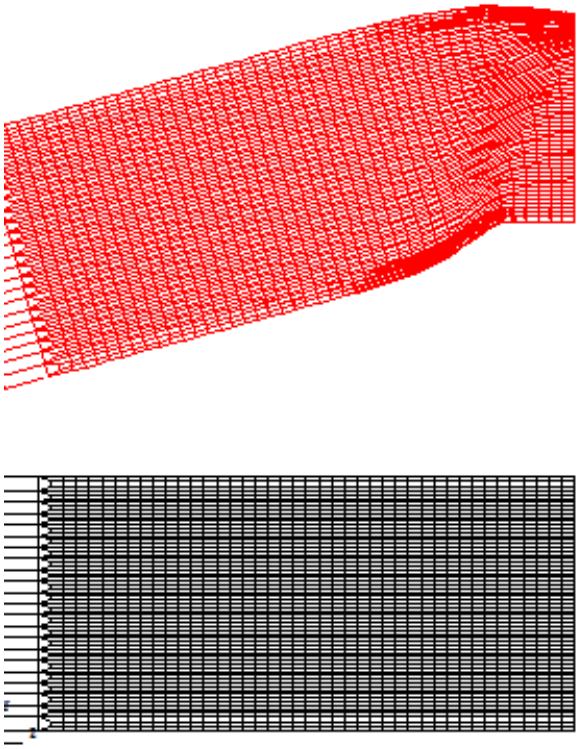

Figure 56: Initial structure (in black) and deformed structure (in red)

As illustrated in paragraph IV.4.2.1, we assume that the influence of the width of the plate on the symmetry of the simulation remains little. To investigate this assumption, tests with a 120 mm long metallic plate will be performed, i.e. a 60 mm long plateau in the Lagamine simulation. This way, we will be able to study its influence on the results.

IV.5.MODELLING: MATERIAL LAWS

IV.5.1. BEAM: EP-ARB

For the elements representing the beam, the elasto-plastic law EP-ARB is used. This constitutional law and its different options are presented in the state of the art. In this substructure model, I made use of 3 different options: an elastic-perfectly plastic law, a bilinear law and a quad-linear law.

IV.5.1.1. ELASTIC-PERFECTLY PLASTIC LAW

The first law that is used in the model is an elastic-perfectly plastic law. This law doesn't take into account the strain hardening of the material. The parameters necessary to define this law can be found in table 8 and the constitutional law is shown in figure 57.

E	210000 MPa
f_y	355 MPa

Table 8: Parameters for the elastic-perfectly plastic law

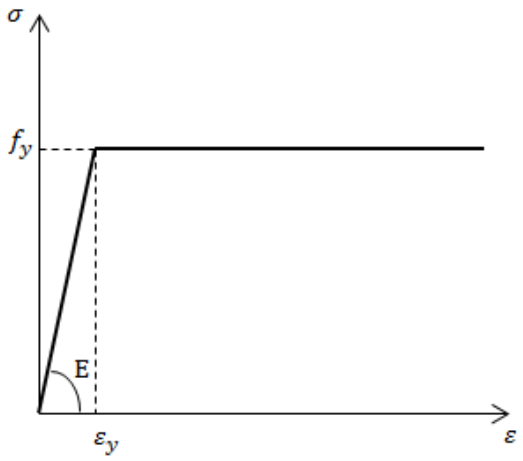

Figure 57: Elastic-perfectly plastic law

It is this model that is used in the analytical solution developed at the University of Liège. The simulations based on this law can be thus compared with this analytical solution.

IV.5.1.2. BILINEAR LAW

A second law that is used in simulations is a bilinear law. After the elastic domain, we introduce the tangent modulus. This way we can take into account the strain hardening and the model reproduces better the real behaviour of the material. The parameters needed to define this law are given in table 9 and the law is represented in figure 58.

E	210000 MPa
f_y	355 MPa
E_t	0.01 E

Table 9: Parameters for the bilinear law

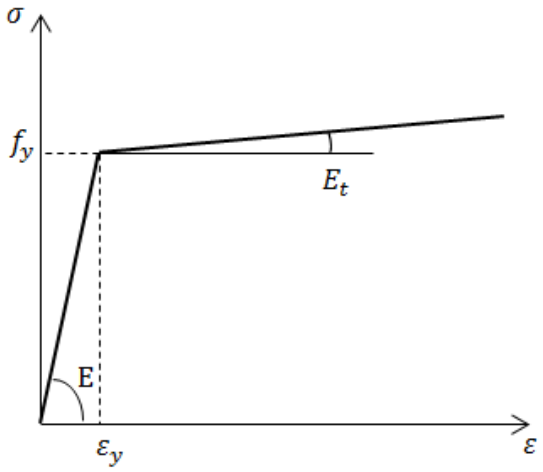

Figure 58: Bilinear law

Based on [13], I considered a value of 0.01E for the tangent modulus. Nevertheless, other values of the tangent modulus will be tested in order to study its influence on the results.

Note that we cannot predict the value of the tangent modulus beforehand. In order to obtain a good estimation of E_t, experimental tests should be conducted on a small sample of the constitutional material of the beams.

IV.5.1.3. QUAD-LINEAR LAW

Lastly, a quad-linear law will be used for the simulations. In this model, we introduce a yield plateau. Also we assume that after having reached the ultimate stress, the material loses all its bearing power and the experiment stops.

E	210000 MPa
f_y	355 MPa
E_t	0.01 E
f_u	510 MPa

Table 10: Parameters for the quad-linear law

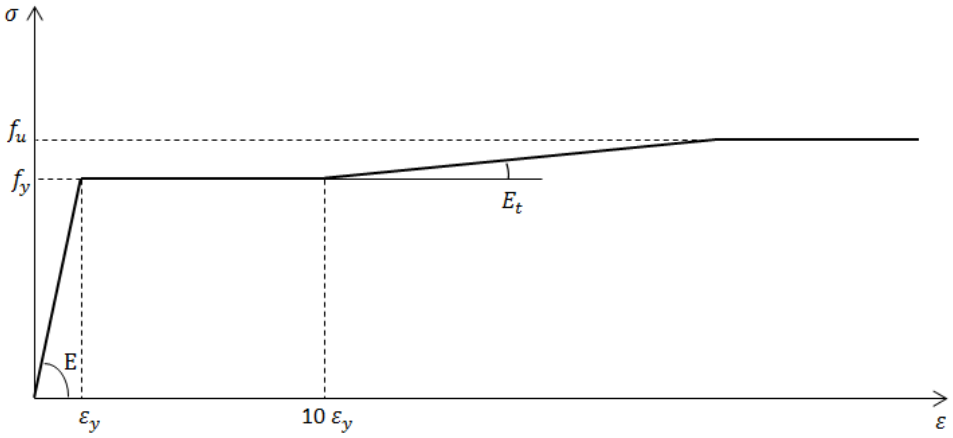

Figure 59: Quad-linear law

Once again, the form and values of this constitutional law are based on [13].

IV.5.2. RIGID ZONE

Initially we considered the same material for the all the elements of the beam. Looking at the deformed structure, we observed very big local deformations where the springs were placed (figure 60). This influenced the results so it was needed to avoid these big local deformations and to keep the extremity of the beam straight. In order to achieve this, the two element rows at the left extremity of the beam where replaced by very rigid elements. These elements are shown in figure 62. The imposed law is elastic-perfectly plastic and its characteristics can be found in table 11.

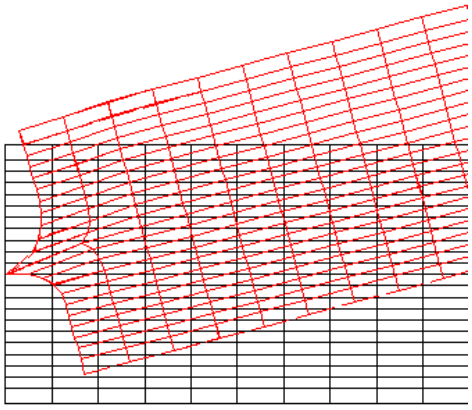

Figure 60: Initial configuration

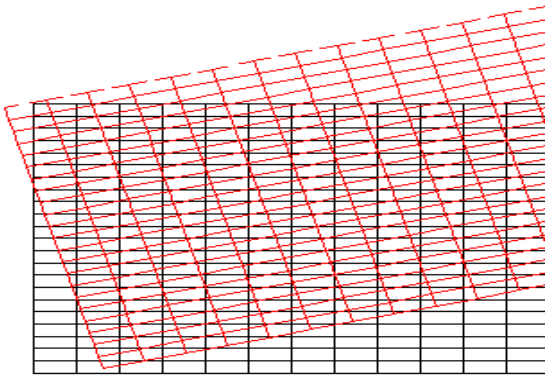

Figure 61: Configuration with rigid zone

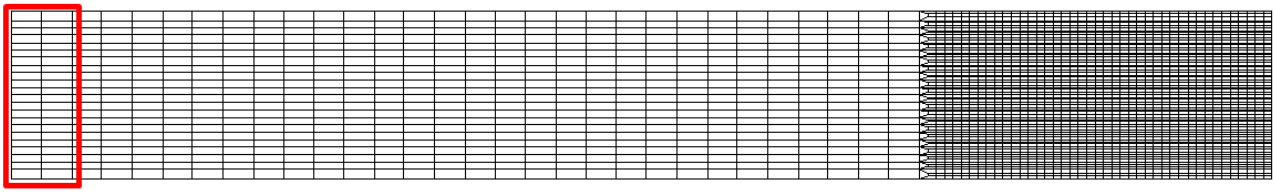

Figure 62: Longitudinal view of the beam (very rigid elements indicated in red)

E	2100000000 MPa
f_y	355000000 MPa

Table 11: Parameters for the elastic-perfectly plastic law

As these elements deform less than the other elements due to their high rigidity, the results may be slightly influenced. However, these elements are not placed in the zone of interest, i.e. in the centre of the beam where we expect a plastic hinge to form. On the contrary they are even situated at the other extremity of the beam. The assumption is thus made that the influence on the results stays minor.

IV.6. PARAMETERS OF THE SIMULATION

As mentioned in the state of the art, we use an out-of-balance force criterion to determine is a solution is acceptable. To satisfy this criterion, a norm has to be inferior to a certain value. For the simulations in this master thesis, the norm is calculated with the average of squares method. This formula is showed just below:

$$\sqrt{\frac{\sum_{Dimensions} \frac{\sum_{Equations} \frac{F_{HE}^2}{N_{Equations}}}{\sum_{Reactions} \frac{Reactions^2}{N_{Reactions}}}}{N_{Dimensions}}} \leq 10^{-3}$$

The precision, chosen for these simulations, is 10^{-3}. This criterion is precise enough to converge to a solution, but on the other hand not too precise so that the program takes a long time to finish.

As explained above, the displacement varies linearly with the time. When the program has converged to a solution (according to the criterion explained just above), we pass on to the next time step. The time increment is in the beginning equal to 10^{-4}. When the simulation shows good convergence, this increment is multiplied by 2. We assume that the convergence is good when multiple consecutive steps converge to a solution. For these simulations, 4 steps are considered. When the simulation doesn't converge for a particular time step, we decrease the time increment and look to find a solution once again.

Note also, that we didn't impose a maximum number of steps, so the program can take as many time steps as it needs. However we imposed a minimum and maximum time increment. The minimum time increment is equal to 10^{-6}. When the program wants to go beneath this value (because the time increment decreases when no solution is found), the simulation stops. On the other hand, we also imposed a maximum value of 10^{-1}. When this value is reached, we maintain the same value (if the converge stays good). We do not want to go over this value in order to keep a certain precision.

Finally, in order to give an idea about the duration of the simulation, some numbers:

- Number of steps: approximately 140 steps
- Duration: approximately 3 hours

V. RESULTS

V.1. INTRODUCTION

In this paragraph the results will be discussed and then compared to the analytical model.

To begin, the analytical results will be briefly commented. Thereafter, the results of the numerical model for the elastic-perfectly plastic constitutional law will be presented, as well as some encountered problems. Furthermore, the results for the bilinear constitutional law will be presented and compared with the analytical model. The results for the quad-linear constitutional law will also be presented. Lastly, some parameters will be tested and some hypothesis, of the analytical model or of the numerical simulations, will be detailed.

V.2. NOTATIONS

In the following graphs, many notations are used. As a reminder the main notations are presented below (source [4]):

P Force simulating the loss of a column

u Vertical displacement at the top of the lost column

K_H Stiffness of the horizontal spring simulating the lateral restraint of the indirectly affected part

F_H Horizontal force acting on the spring

δ_H Horizontal elongation of the spring

N Axial force in the beams of the directly affected part

M Bending moment at the extremities of the beams of the directly affected part

K_N Axial stiffness of the plastic hinges submitter to M and N

δ_N Axial elongation of the plastic hinges submitted to M and N

V.3. RESULTS: ANALYTICAL MODEL

To begin, the results of the analytical model will be presented. As a reminder, the main assumptions and hypothesis of the analytical model are:

- The constitutional law is elastic-perfectly plastic.
- The fillet radius is not modelled.
- The cross section remains constant.
- The springs representing the plastic hinges are elastic-perfectly plastic and have an unlimited ductility.
- The shear force is considered negligible, so its influence on the resistant bending moment are not taken into account.

In the following paragraphs, the different results are demonstrated.

V.3.1. U –P CURVES

In figure 63, the vertical force P according to the vertical displacement u is presented.

Firstly, we observe a linear fragment for the different curves. This corresponds to the elastic domain. Afterwards, the rigidity of the beam, represented by the slope of the curve, decreases drastically. This is where the plastic mechanism is formed. When pre-deigning the frame (§III.4.), we determined the vertical load P, for which this plastic mechanism will be formed (table12). As can been seen in figure 63, these values correspond well to the end of the plastic domain.

	IPE 100	**IPE 160**
$\boldsymbol{P_{pl}}$	37.31 kN	117.39 kN

Table 12: P_{pl} for the IPE 100 and IPE 160 beam

Remark that during the elastic phase, the curves of the low K_H configuration and the high K_H configuration are practically superposed for both beams. The stiffness of the indirectly affected part does not yet play a big role in the development of forces.

Thereafter, we note that the slope of the curve becomes greater, the rigidity increases. It is here that the membrane forces become significant. The more the system deforms, the more the membrane forces N will oppose the vertical force P. That's why the rigidity increases the more the system deforms.

It is during this phase that the stiffness of the indirectly affected part becomes important. This can be observed on the graph: the curves do not superpose any more. The greater the stiffness of the indirectly affected part, the greater the membrane forces have to be to deform the structure. This explains why for the high K_H configuration, the vertical force P is higher than for the low K_H configuration for a same displacement u.

Next we can observe, for all the tests except the IPE 160 beam with $K_H = 25000\ {}^{kN}/_{m}$, that the curves become linear once again. This is when yielding of the beam occurs again, but this time because N_{pl} , the plastic resistance in tension of the gross cross-section, is reached. Note that the low and high K_H configuration superpose. However, the curves of the high K_H configuration become linear before the other configuration. As the membrane forces are greater in the high K_H configuration, N_{pl} will be sooner reached for that configuration.

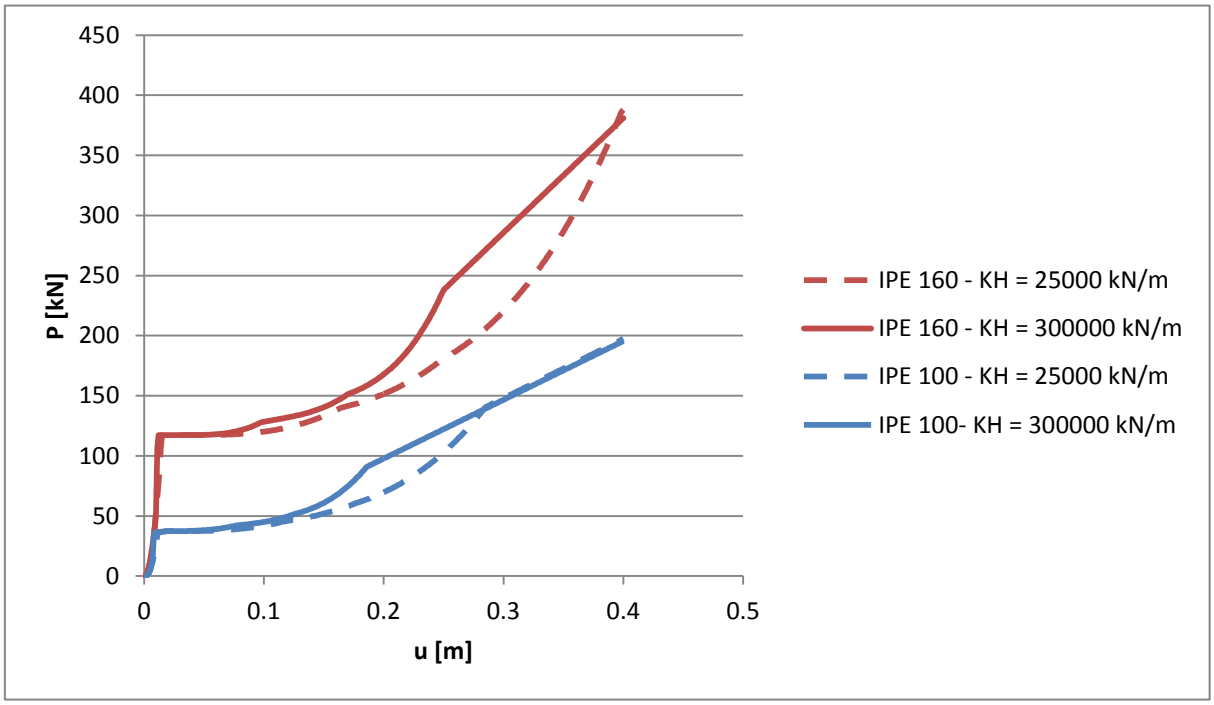

Figure 63: u – P curve of the analytical results

V.3.2. F_H –P CURVES

In figure 64, the evolution of the vertical force P in function of the horizontal load in the spring is shown for the different simulations.

We observe once again the elastic domain. The curves are linear and the force in the spring remains almost equal to zero. The indirectly affected part does not play a big role during in this phase, the spring is thus almost not activated.

When the plastic mechanism is formed we enter phase 3. This is where the stiffness of the indirectly affected part becomes important. The slope of the curve changes abruptly. We observe that the configuration with the same K_H show approximately the same slope.

Finally, the force in the spring F_H remains constant. This corresponds to the linear segment in the end of the curve in figure 63. Yielding occurs because N_{pl} in tension is reached. We notice once again that this happens earlier for the high K_H configuration than for the low K_H configuration.

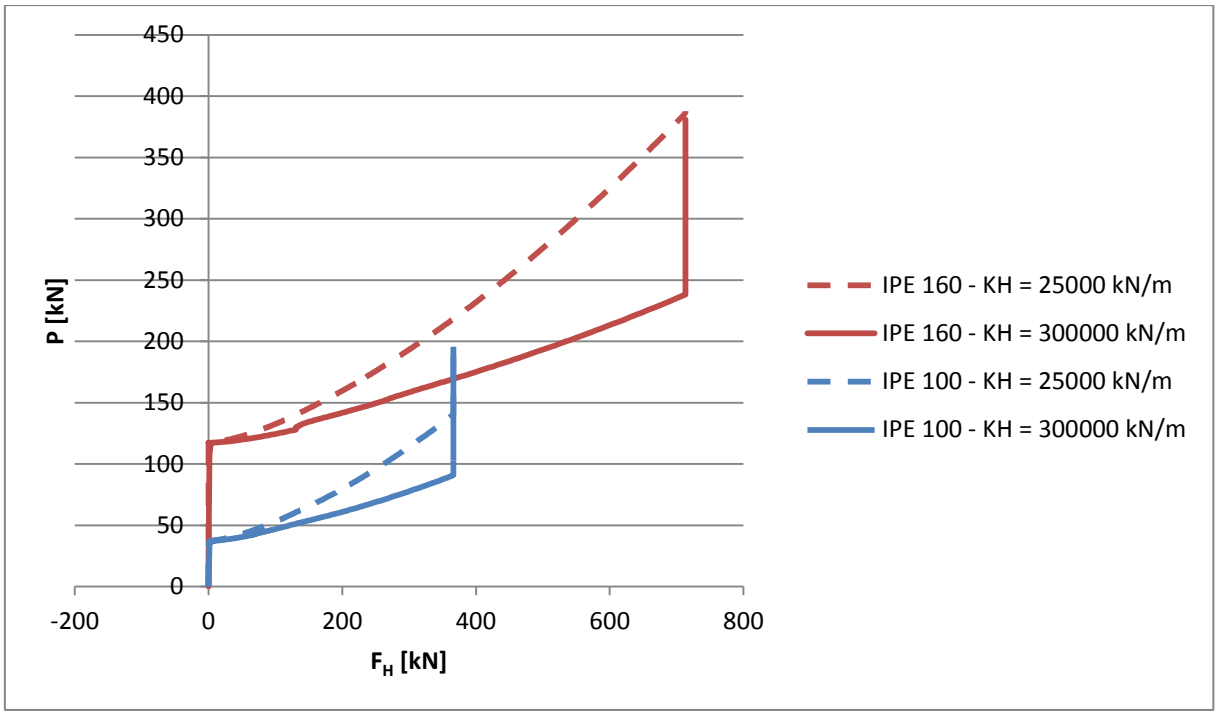

Figure 64: F_H – P curve of the analytical results

V.3.3. DELTA N-N CURVES

In figure 65, the axial forces in the beams according to the axial elongations of the plastic hinges is shown. The parameter that we are most interested in to determine is the K_N value, the axial stiffness of the plastic hinges under M and N. This parameter is represented by the slope of the δ_N –N curve.

One observation we can make is that, in contrast to the results presented above, not the identical beams show the same solutions, but the configurations with the same K_H value give similar results. With Excel, the slopes of the different curves is calculated. These results are represented in table 13. This confirms what we have observed in the graph. For the same configurations, we find approximately the same K_N value.

It can also be observed that the K_N parameter is for both configurations slightly lower for the IPE 100 beam. The height of the section may thus also influence this parameter.

This corresponds to what has been concluded in [5]. The K_N value is influenced by parameters as Young's modulus, the yield limit f_y and the type and height of the section, but the K_H parameter has the most important influence.

Configuration low K_H – IPE 100	39622 kN/m
Configuration low K_H – IPE 160	42086 kN/m
Configuration high K_H – IPE 100	52980 kN/m
Configuration high K_H – IPE 160	57907 kN/m

Table 13: K_N value for the different configurations

Furthermore, we notice that a plateau appears. This plateau corresponds to the moment when the plastic resistance in tension of the gross cross-section is reached. We observe that N_{pl} is earlier reached for the high K_H configurations than for the low K_H configurations. This is because of the greater membrane forces in the high K_H configurations.

Lastly, we notice that the curves are not always straight, indeed little peaks appear in the graph. These correspond to the activation of one of the springs that represent the plastic hinges. As a reminder, the analytical model considers 6 parallel springs to represent a plastic hinge. These springs are not all activated at once, so every time a spring or several springs are activated, we observe a little peak in the graph.

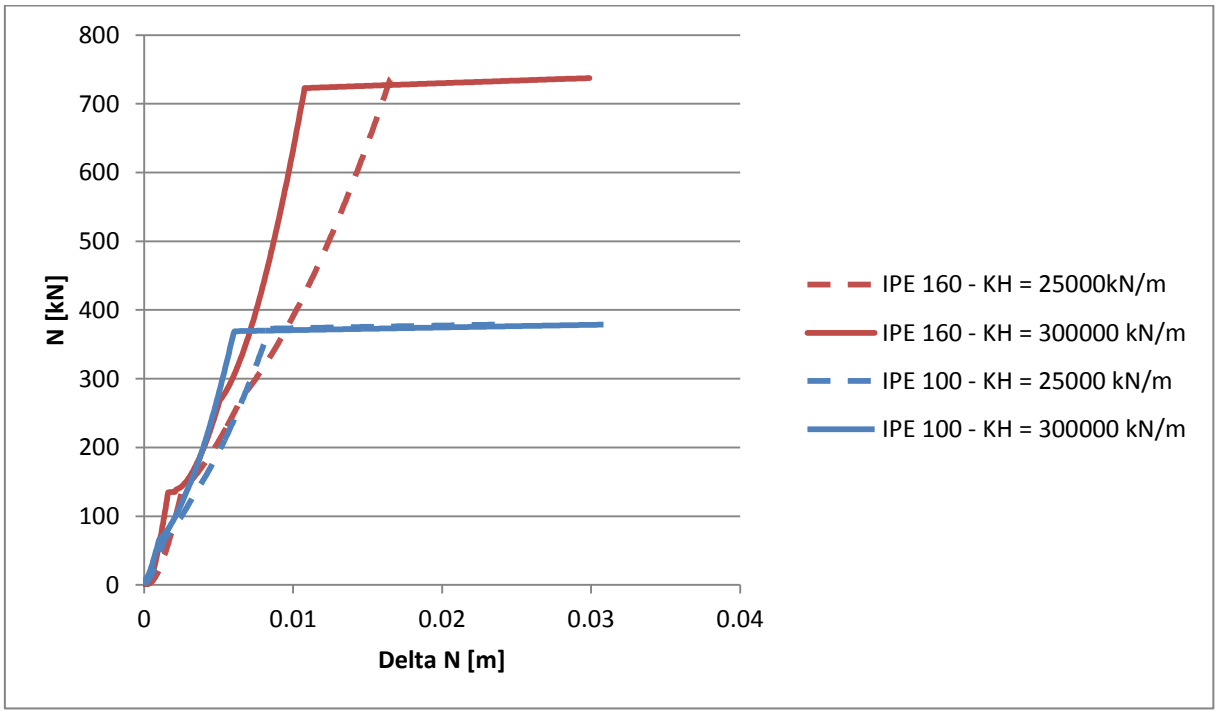

Figure 65: δ_N –N curves of the analytical solution

V.3.4. M-N CURVES

Lastly the M-N curves are shown (figure 66). We observe that these superpose for the same beam section. The values of N_{pl} and M_{pl} for the two beam cross sections are given in table 14.

To begin the beam is submitted to a bending moment. We see that the moment varies from 0 to M_{pl}, when the plastic hinge appears. Thereafter, plastic hinges are subjected to bending and axial forces. The bending moment decreases, but the axial forces increase. The curve will be followed until the bending moment reaches zero and the axial force is equal to the plastic resistance to axial forces of the gross section.

The resistance of the IPE 100 beam being lower than the IPE 160 beam, its M-N interaction curve is smaller than the IPE 160 beam.

We observe that the graph corresponds well to the values given in table 14.

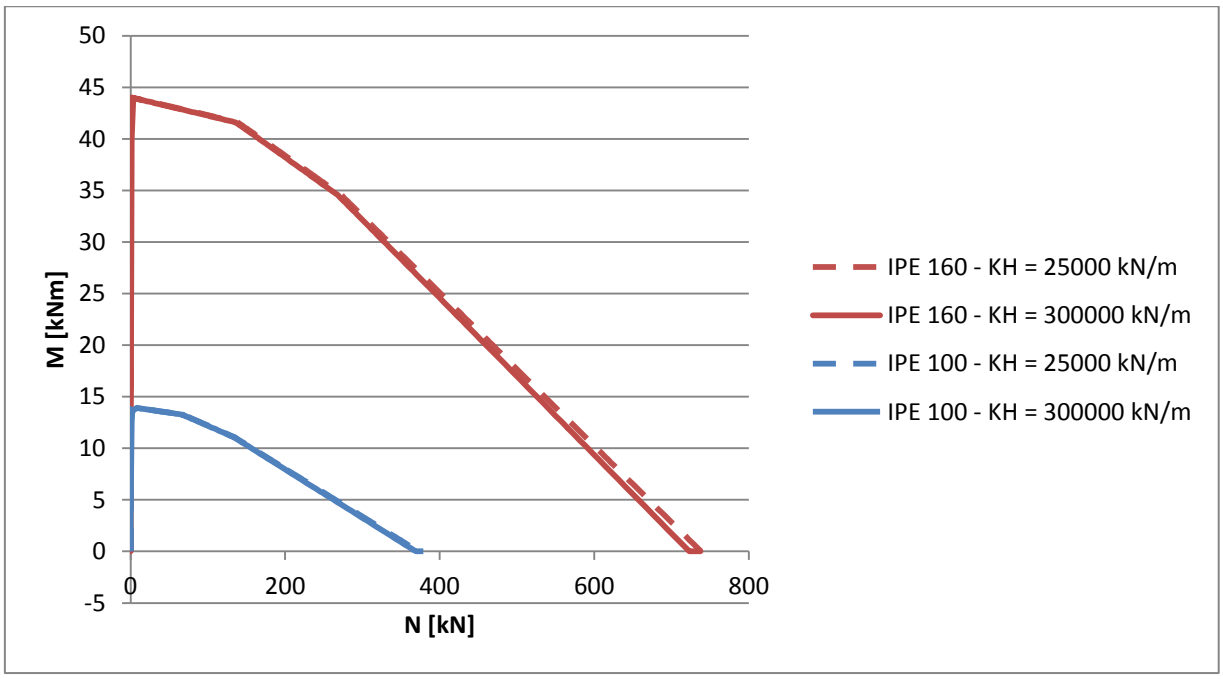

Figure 66: M – N curves of the analytical solution

	N_{pl}	M_{pl}
IPE 100	365.7 kN	14.0 kNm
IPE 160	713.6 kN	44.0 kNm

Table 14: plastic resistance of the different beam sections

V.4. RESULTS: ELASTIC-PERFECTLY PLASTIC LAW

Firstly, the results of the simulations with an elastic-perfectly plastic law will be presented. This is the same law as used in the analytical model, so initially we would use these results to compare the analytical model with the numerical simulations. However, very large deformations occur and these influence the results.

V.4.1. DEFORMATIONS

The deformation of the substructure at the end of the test (vertical displacement u equal to 0.4 m) is shown in figure 77. This global model is according to our expectations. However when we look more in detail, we observe large deformations at the right extremity of the beam (figure 78). Note that in this paragraph the results for the beam IPE 160 in the low K_H configuration are showed, because these deformations are the most significant.

When investigating more in detail the extreme right cross section, we observe that the top flange reduces drastically according the displacement. The evolution of the deformation of the cross section is given in figures 67-76. We observe that for vertical displacements lower

than 0.12 m the deformations of the cross section remain small. However, for greater vertical displacements, the cross section deforms significantly. Nevertheless, even for the first 3 figures (67, 68 and 69), the surface area of the cross section reduces. Table 15 shows the surface area of the cross section for some values of u. Calculating the surface area for greater values of the vertical displacement becomes more difficult because of the great deformations of the cross section. Note also that this is the surface of half the cross section, as it is this that is modelled during the numerical simulations. When looking at table 15, we remark that the surface area of the cross section even increases for small values of the vertical displacement u.

u	**A**
0 m	1005 mm^2
0.04 m	957.32 mm^2
0.08 m	915.50 mm^2
0.12 m	828.85 mm^2

Table 15: Surface area of the cross section

In reality, the cross section will also deform, but not this significantly. The results of the numerical simulations will thus not be a good representation of the real results. The main reason for this is that the reduction of the cross section has an influence on the resistance of the beam. In fact, the resistance of the cross section depends on its surface area. Looking at the reduced cross sections, it is clear that the plastic resistance in tension of the gross cross-section, as found in ArcelorMital catalogue, can never be reached.

Two factors can explain why the deformation are so important. To begin, the filet radius are not modelled. This element contributes to the rigidity in the angle of the beam. Without the filet radius, the junction flange - web can deform more easily. This is also noticeable when looking at the deformed structure (figure 67-76). We observe that the deformations are the most significant in the upper flange – web joint. Secondly, the necking phenomena appears. By consequence the deformation increase fast. As the imposed law is elastic – perfectly plastic, no strain hardening is considered. This could avoid the early apparition of the necking phenomena and by consequence the excessive deformations. In figure 67-76, representing the evolution of the cross section, we can also observe the influence of the Poisson's ratio. When the section decreases in one direction, it increases in the other.

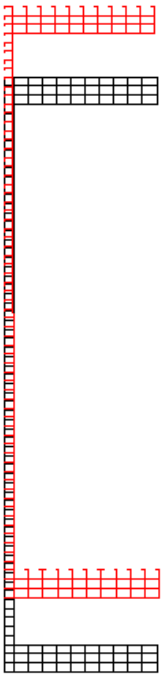

Figure 67: Deformation of the beam at u = 0.04 m

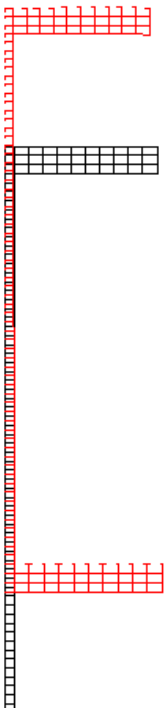

Figure 68: Deformation of the beam at u = 0.08 m

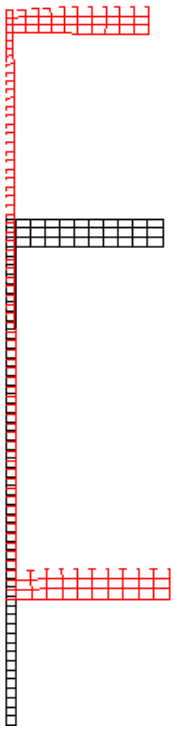

Figure 69: Deformation of the beam at u = 0.12 m

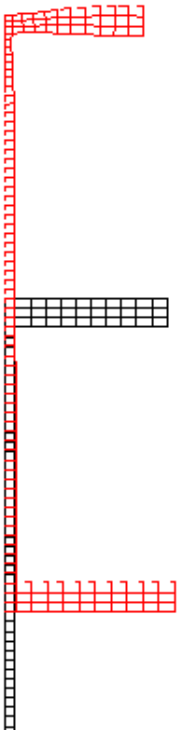

Figure 70: Deformation of the beam at u = 0.16 m

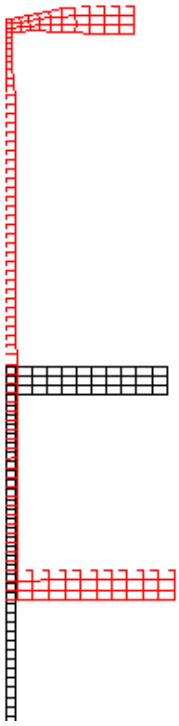

Figure 71: Deformation of the beam at u = 0.20 m

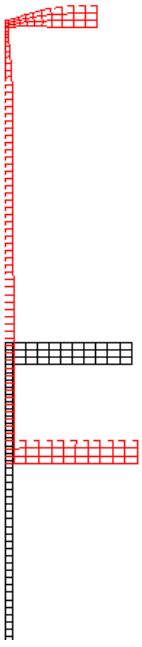

Figure 72: Deformation of the beam at u = 0.24 m

Figure 73: Deformation of the beam at u = 0.28 m

Figure 74: Deformation of the beam at u = 0.32 m

Figure 75: Deformation of the beam at u = 0.36 m

Figure 76: Deformation of the beam at u = 0.40 m

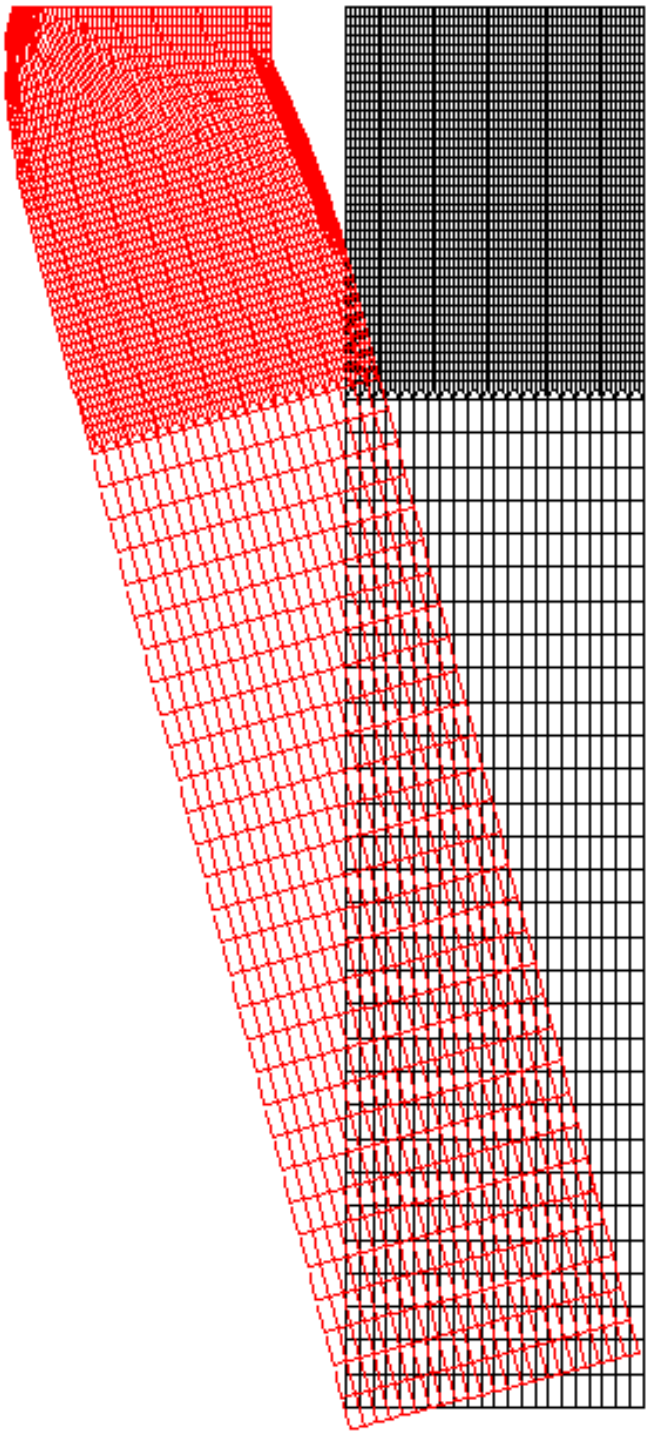

Figure 77: Deformation of the beam at u = 0.4 m

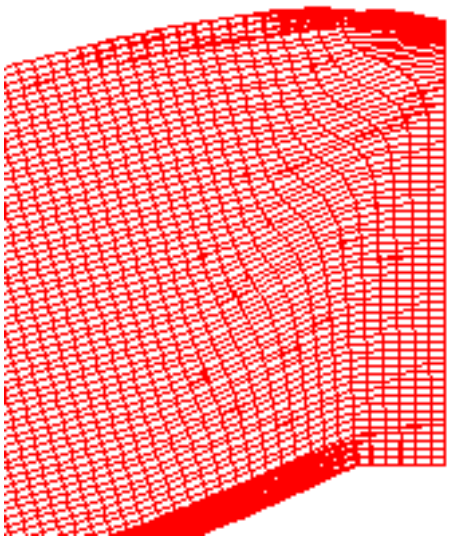

Figure 78: Zoom of figure 77

V.4.2. RESULTS

The results of both configurations are presented in this paragraph. Even though we concluded that the this constitutional law does not reflect well the real experimental tests, it is still interesting to observe its influence on the results.

When looking at the u-P curves (figure 79), we observe that the numerical solution differs from the analytical solution, but globally the curves show the same allure. Before formation of a plastic mechanism, the curves are similar, the reduction of the section being still small. Hereafter the curves start to differ. We notice that the numerical curves are below the analytical curves. For the IPE 160 beam we notice even a decrease of the vertical force P. This is a results of the deformations that become important and the necking phenomena that appears. When comparing figures 80 and 81, we observe that the deformations of the IPE 160 beam are already more noticeable than those of the IPE 100 beam. The IPE 160 having a greater height than the IPE 100 beam, the deformations become faster important. For the high K_H simulations, we obtain the same results (figure 83).

As the deformations become significant after a vertical displacement of 0.12 m, the results hereafter are not very reliable. It is thus difficult to draw conclusions for the points from here on.

When studying the F_H – P curve (figure 82), we can draw almost the same conclusions. The global allure of the curves is similar. The IPE 160 beam decreases in the beginning of phase 3 as for the u – P curve.

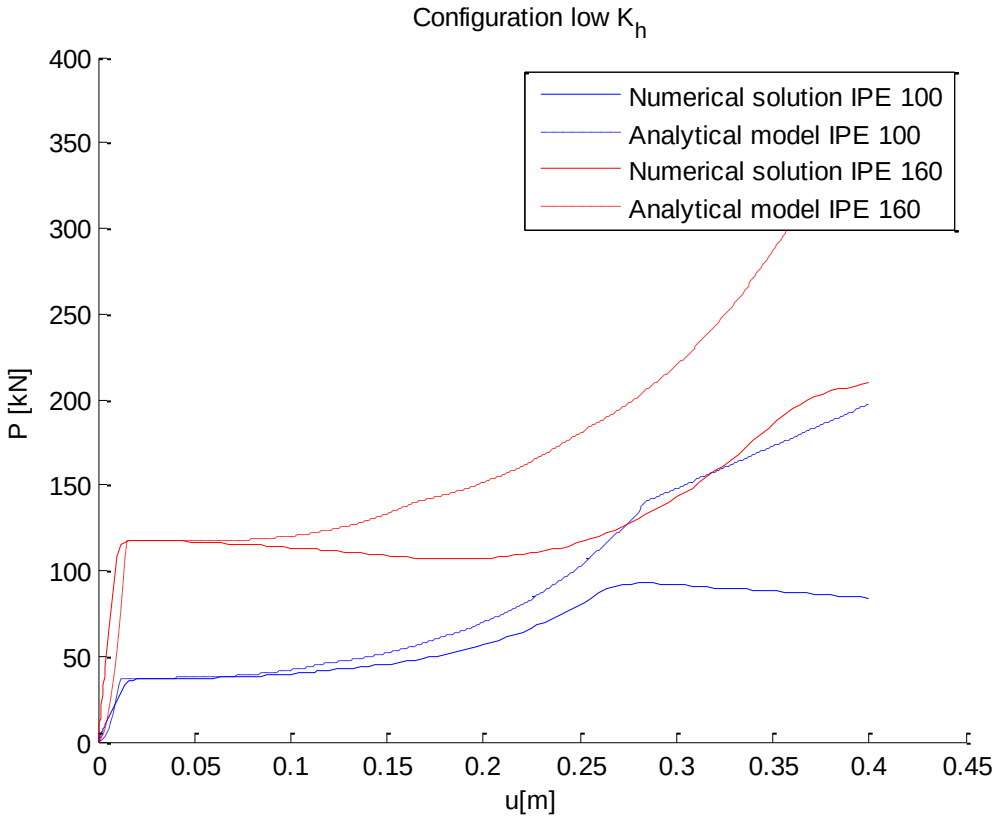

Figure 79: u – P curve for configuration low K_H

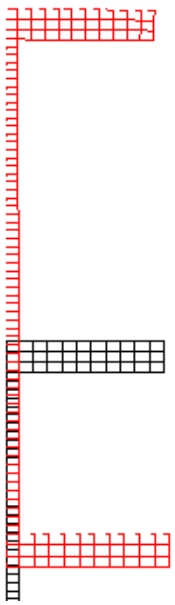

Figure 80: Deformation of the IPE 100 beam at u = 0.12 m

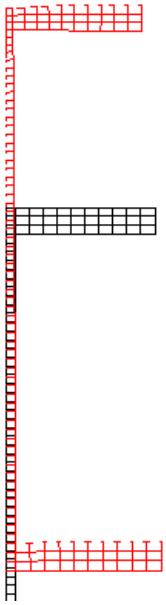

Figure 81: Deformation of the IPE 160 beam at u = 0.12 m

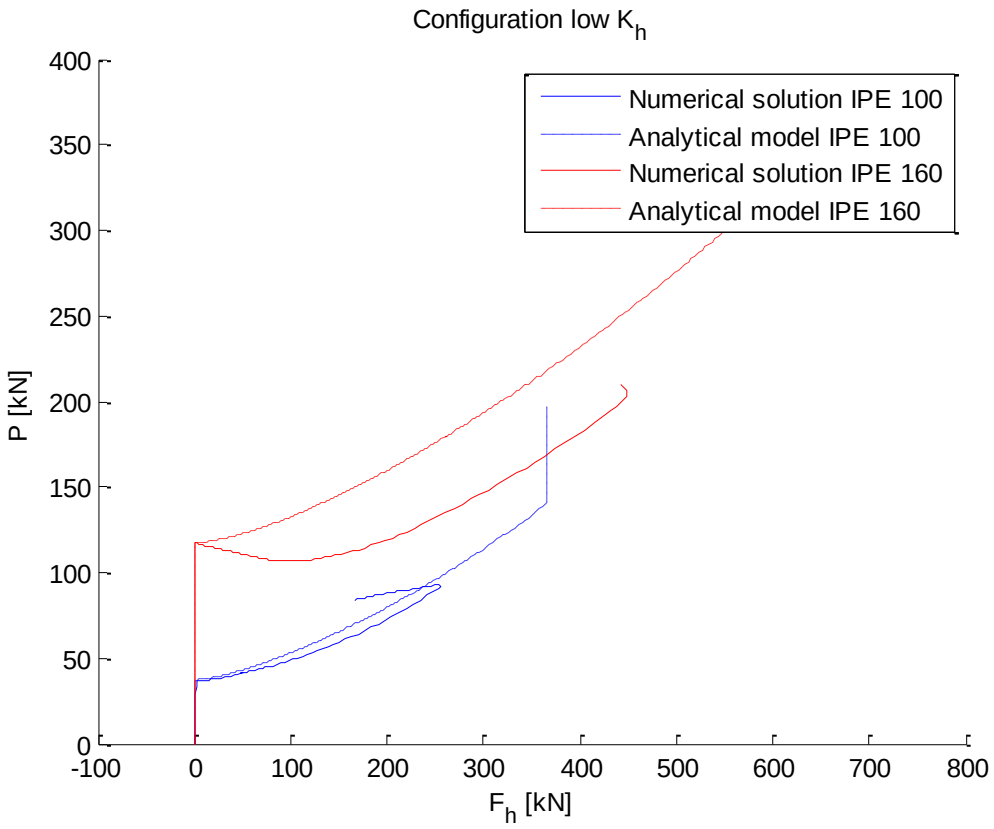

Figure 82: F_H – P curve for configuration low K_H

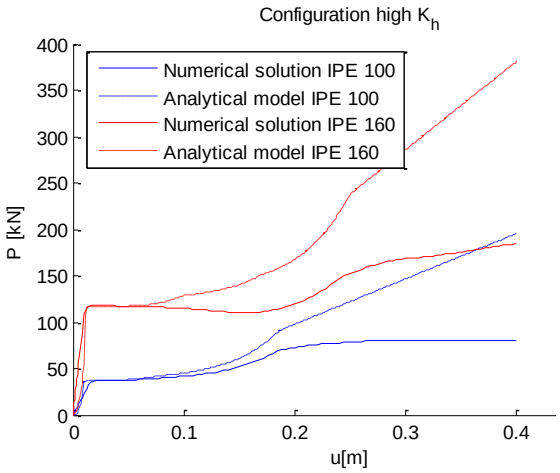

Figure 83: u – P curve for configuration high K_H

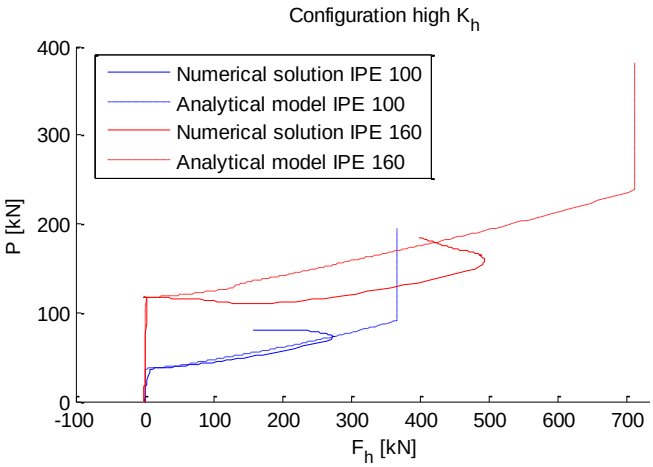

Figure 84: F_H – P curve for configuration high K_H

V.5. RESULTS: BI-LINEAR LAW

As we have concluded in the previous paragraph, the elastic perfectly plastic law does not give a good representation of the experimental tests. That's why we will use a bilinear law with a tangent modulus of E/100 for the comparison with the analytic model. Even though the hypothesis for the constitutional laws are not the same, this will give a more realistic view of the experimental tests. The constitutional law is detailed in §IV.5.1.2. The results for this law will be presented hereafter.

V.5.1. U – P AND F_H – P CURVES

In figure 85, the force simulating the column loss in function of the vertical displacement at the top of the lost column is represented. When studying this graph, we observe that the numerical model and the analytical solution fit well for both the IPE 100 and IPE 160 beam. This can also be observed for the high K_H configuration (figure 95).

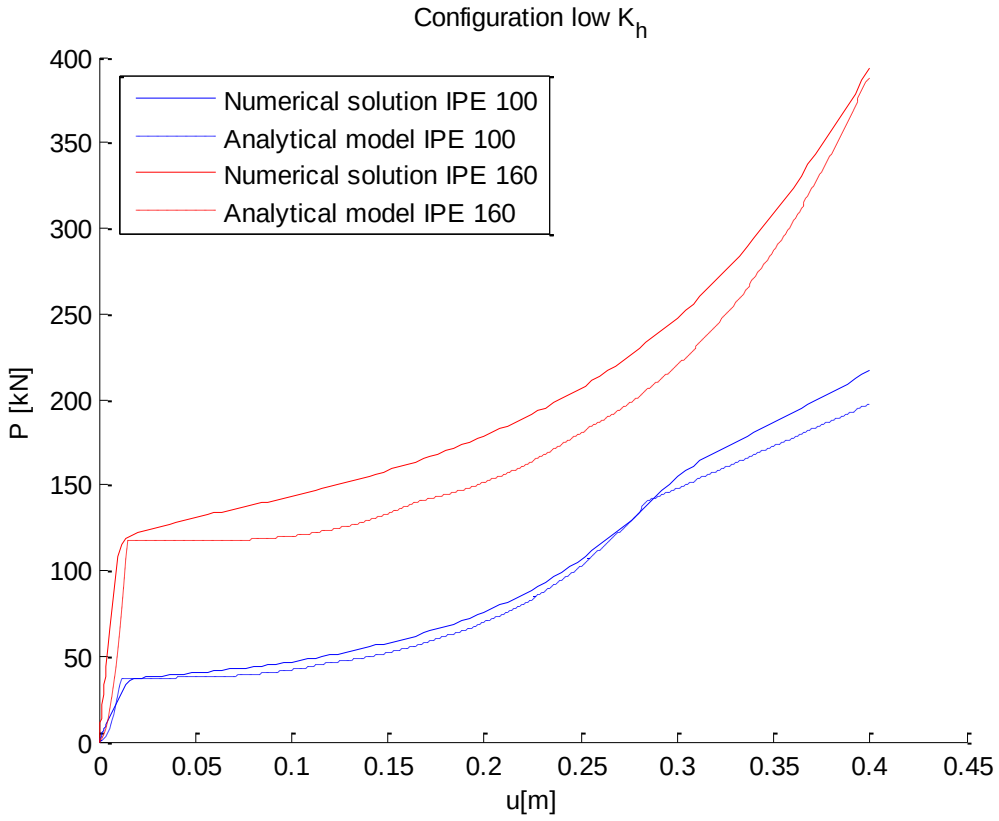

Figure 85: u – P curve for configuration low K_H

We observe that during phase 1, when the material remains elastic, the numerical and analytical curves are rather close. Tough we observe that the transition from phase 1 to phase 3, when a plastic mechanism is formed and the membrane forces start to play an important role, is rather abrupt for the analytical model. For the analytical model, the global section is considered. However, for the numerical model the transition is more rounded. This is because

the Lagamine program calculates the stresses for every element for every time step. As a consequence, the yielding influence starts to be noticeable from the point when the extreme fibre reaches the yield strength f_y. This situation is represented in figure 86 (nr. 1). The vertical force P, corresponding to this moment, can be calculated as followed:

$$\sigma = \frac{M\,y}{I_y} = \frac{PL/_8\; y}{I_y}$$

$$\Rightarrow P = \frac{8\,\sigma\,I_y}{L\,y}$$

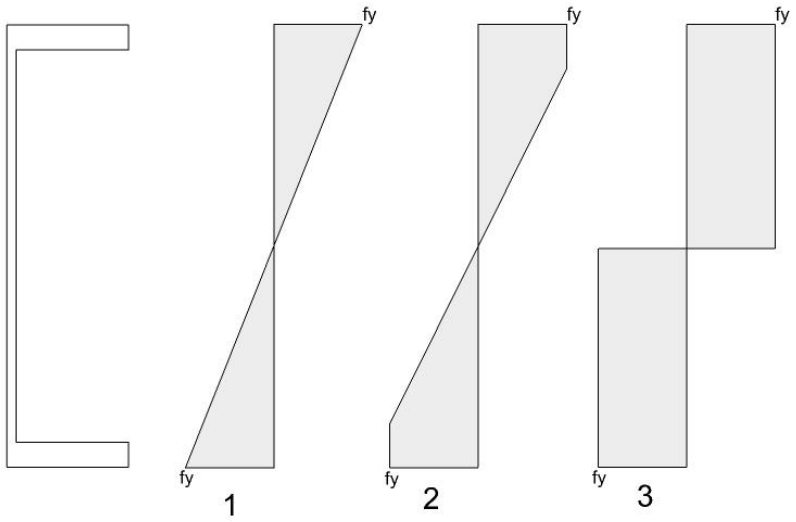

Figure 86: stresses in the cross section

The results, i.e. the vertical force P for which the extreme fibre reaches f_y, are given in table 16. Also as a reminder the values of the vertical force P for which a plastic mechanism is formed are noted (P_{pl}). Note that the stress distribution passes from point 1 to point 3 (figure 86). In figure 87, these two P-values are plotted, with a dotted line for $P_{yielding,extreme\ fibre}$ and a dashed line for P_{pl}, for both the IPE 100 and IPE 160 beams. We observe clearly that it is between these two lines that the slope of the u-P curves starts to decrease.

	IPE 100	**IPE 160**
L	3000 mm	3000 mm
$\boldsymbol{\sigma}$	355 MPa	355 MPa
$\boldsymbol{I_y}$	1710000 mm^4	8690000 mm^4
y	50 mm	80 mm
$\mathbf{P_{yielding,extreme\ fibre}}$	32.4 kN	102.8 kN
$\mathbf{P_{pl}}$	37.31 kN	117.39 kN

Table 16: Results

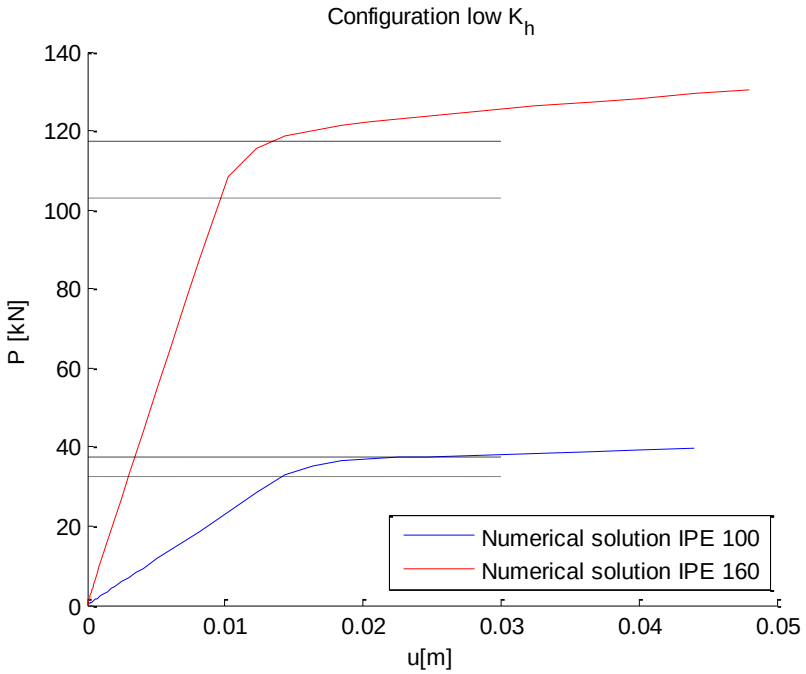

Figure 87: Zoom of figure 85

Continuing the discussion of figure 85, we observe that the numerical simulations fit the analytical solutions rather well. For the IPE 100 beam, they almost superpose during phase 3. The cross section still reduces, but less than for the simulations with an elastic-perfectly plastic law. Thanks to the strain hardening the necking phenomena does not appear in the beginning of the simulation. The analytical model however considers that the cross section remains constant, but does not take into account the strain hardening of the material.

For the IPE 160 beam, we notice a greater difference between the two curves, though they show the same allure. As already mentioned for the elastic-perfectly plastic law, the height of the IPE 160 being greater than these of the IPE 100, by consequence the IPE 160 beam is subjected to higher deformations. The influence of the strain hardening is thus faster noticeable in this case. The gap between the numerical and analytical curve firstly increases, but more toward the end of phase 3, the gap decreases. As we compare figure 88 and 89, we see that at a displacement u of 0.16 the cross section is only slightly deformed for the bilinear law. Due to the small deformations in combination with the strain hardening, the beam is more resistant for the numerical simulations than for the analytical model. However, as we can see in figure 90 and 91, the deformations are more noticeable for a displacement u of 0.24 m. We note that it is from this u-value on that the numerical curve starts to tend to the analytical curve.

In general the deformations remains much smaller for the bilinear law than for the elastic-perfectly plastic law. This can be observed in figures 92 and 93. Where the elements almost become strings in figure 92, the elements remain approximately cubic in figure 93.

For the last segment of the curve (IPE 100), we observe a linear part. This is when yielding of the beam occurs once again, but this time because N_{pl} , the plastic resistance in tension of the gross cross-section, is reached. The slope of the numerical curve is greater than those of the analytical curve. The increase of f_y due to the strain hardening may explain this phenomena.

The curves of the simulation high K_H (figure 95 and 96) show the same behaviour.

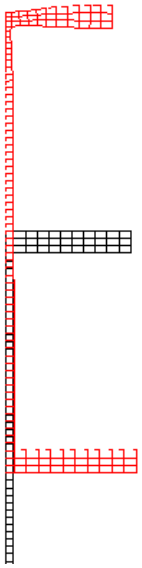

Figure 88: Deformation of the cross section at u = 0.16 m (elastic-perfectly plastic law)

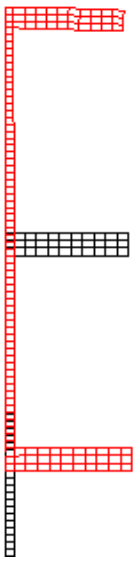

Figure 89: Deformation of the cross section at u = 0.16m (biinear law)

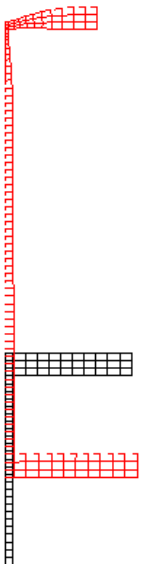

Figure 90: Deformation of the cross section at u = 0.24 m (elastic-perfectly plastic law)

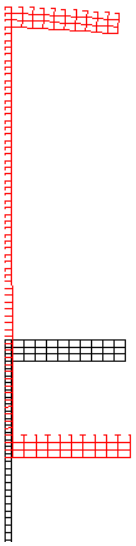

Figure 91: Deformation of the cross section at u = 0.24 m (bilinear law)

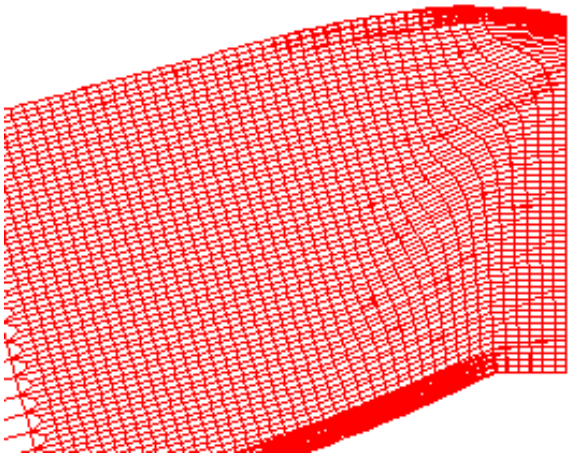

Figure 92: Deformation of the beam at u = 0.40 m (elastic-perfectly plastic law)

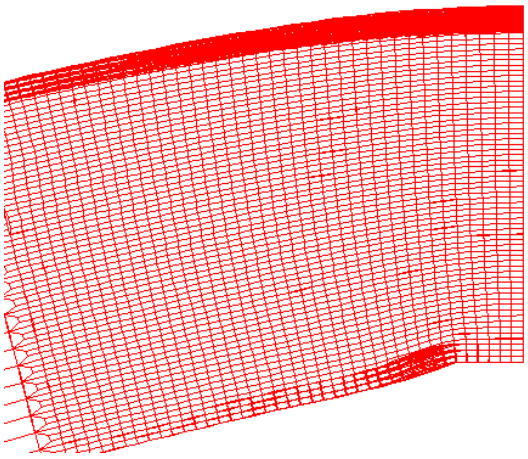

Figure 93: Deformation of the beam at u = 0.40 m (bi-linear law)

As for the u-P curves we observe that the F_H – P curves (figure 94) fit rather well, especially for the IPE 100 beam. For the curve of the IPE 160 beam, once a again a gap between the

numerical and analytical solution is noticeable. This can also be explained by the higher resistance of the numerical simulations due to strain hardening.

Furthermore, we notice, as for the u-P curves, that the transition from phase 1 to phase 3 is abrupt for the analytical model. On the other hand, the transition is more curved for the numerical model.

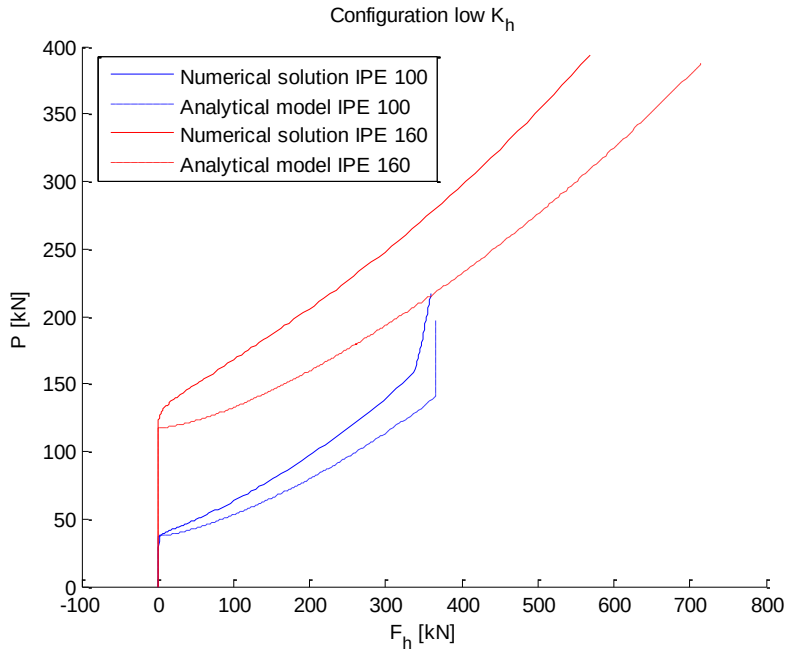

Figure 94: FH – P curve for configuration high K_H

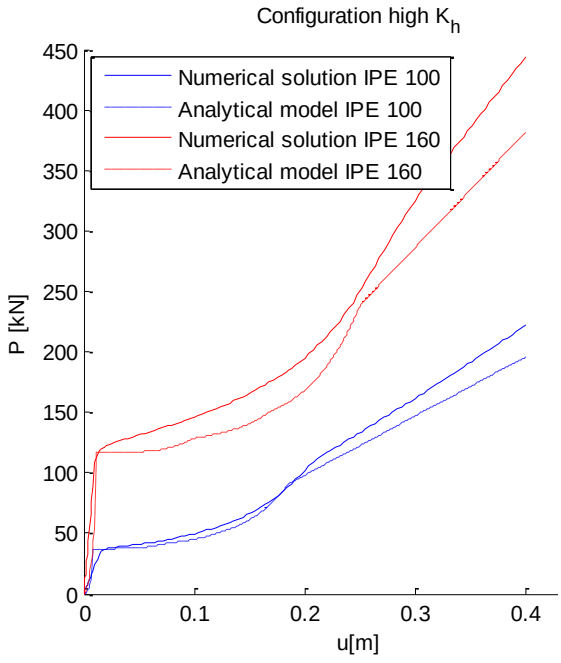

Figure 95: u – P curve for configuration high K_H

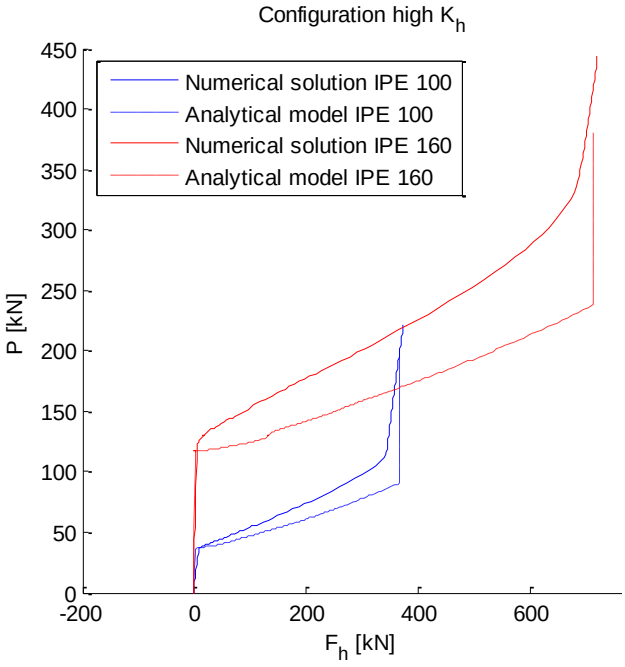

Figure 96: F_H – P curve for configuration high K_H

V.5.2. δ_H - F_H CURVE

In order to verify if the stiffness of the indirectly affected part is well taken into account, we trace the horizontal force acting on the spring F_H in function of the horizontal elongation of the spring δ_H (figure 97). We observe that the results superpose well for both configurations. Not only do the numerical simulations for both beam types, IPE 100 and IPE 160 fit well, they also correspond well to the numerical curves. When calculating the slope of the curve, we find the values given in table 17.

Configuration low $\mathbf{K_H}$	25000 kN/m
Configuration high $\mathbf{K_H}$	300000 kN/m

Table 17: Slopes of the curves

We notice that these values correspond to the imposed stiffness values. We can conclude that the numerical simulations and the analytical model take well into account the stiffness of the indirectly affected part.

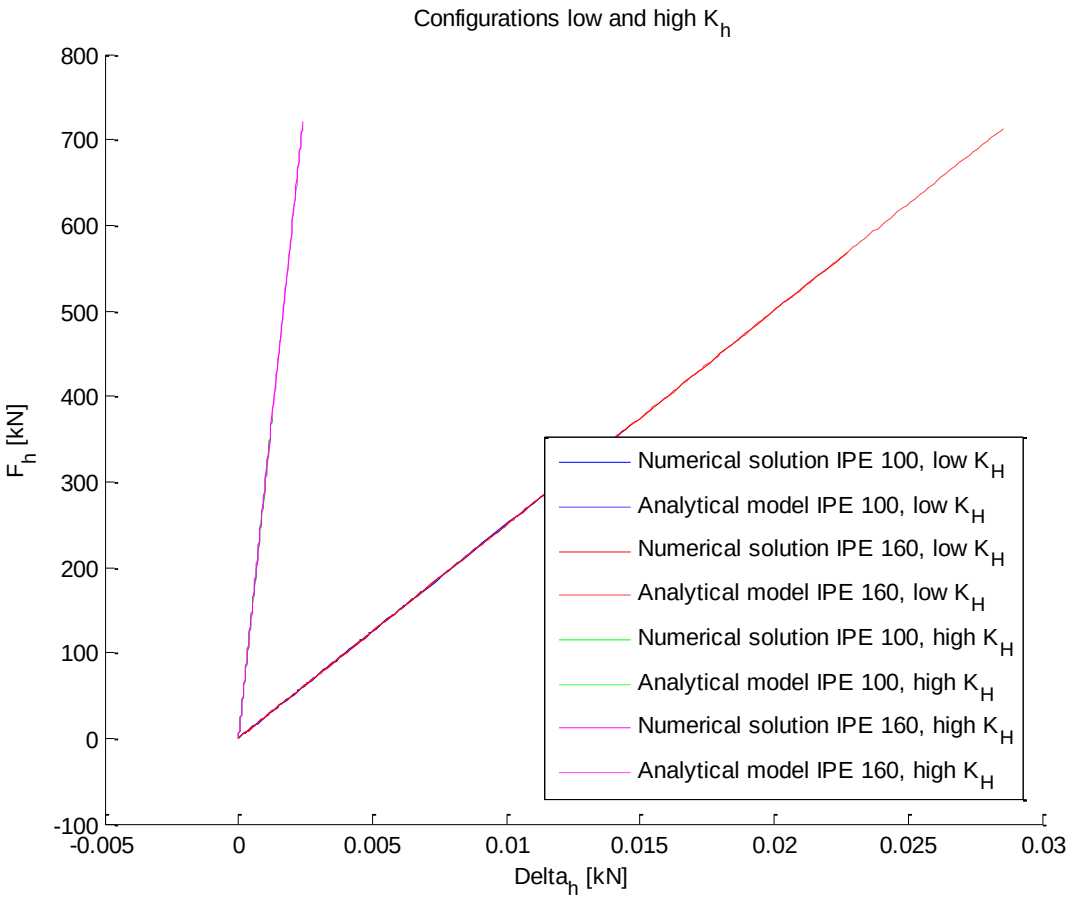

Figure 97: δ_H - F_H curve for both configurations

V.5.3. δ_N - N CURVE

In figures 98 and 99 the evolution of the axial force according to the elongation of the plastic hinges under M and N is showed. As explained earlier, the K_N parameter is represented by the slope of the δ_N - N curve. These values can be found in table 18.

In both figures, we observe that the analytical and numerical curves fit rather well. However, when looking at the values (table 18), we note that the K_N parameter is smaller for the numerical simulations, but they are in the same order of magnitude.

We can also remark the same points as we did for the analytical simulations. The K_H parameter plays an important role for the K_N parameter. We observe that for the same configurations we obtain similar values for K_N. Furthermore, the influence of the beam section is also noticeable. The values for the IPE 100 beam are slightly lower than those for the IPE 160 beam.

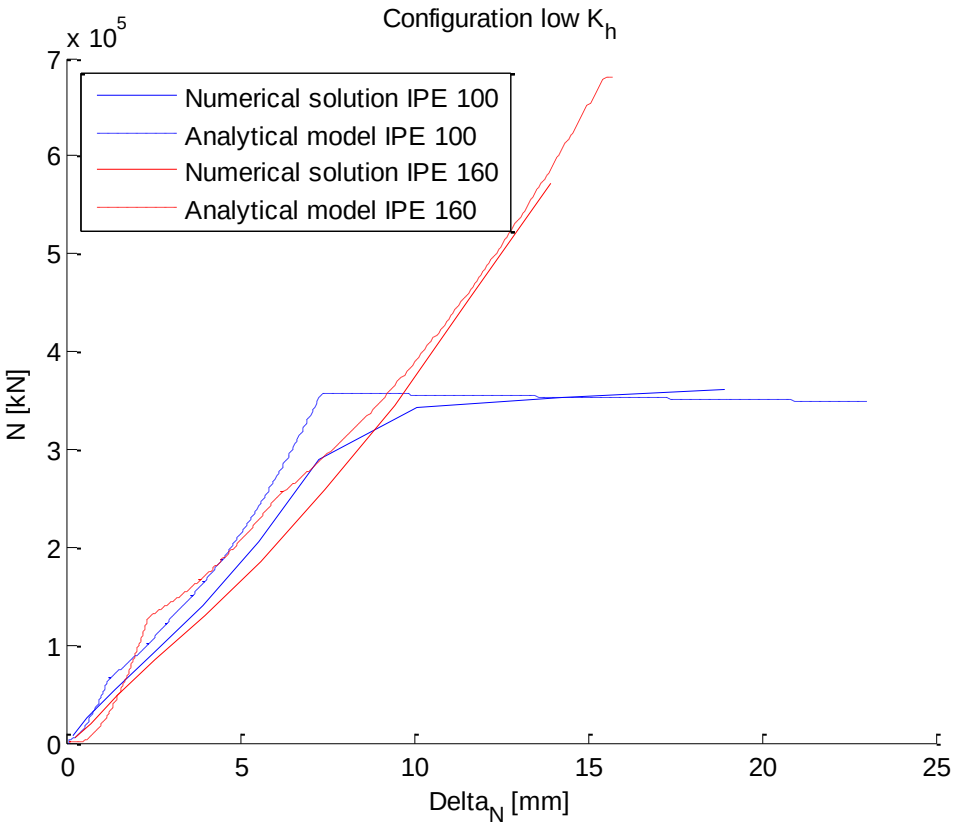

Figure 98: δ_N –N curves for the low K_H configurations

	Analytical model	Numerical simulations
Configuration low K_H – IPE 100	39622 kN/m	34548 kN/m
Configuration low K_H – IPE 160	42086 kN/m	34697 kN/m
Configuration high K_H – IPE 100	52980 kN/m	49672 kN/m
Configuration high K_H – IPE 160	57907 kN/m	54105 kN/m

Table 18: K_N value for the different configurations

Furthermore we observe that, as for the analytical results, a plateau is formed. This plateau corresponds to the point when N_{pl} of the cross section is reached in tension. We can see that this occurs at approximately the same moment for the analytical and numerical curves. However, for the numerical solutions we observe that the plateau has a very small slope. This may be due to the strain hardening, taken into account for the numerical model and not for the analytical one.

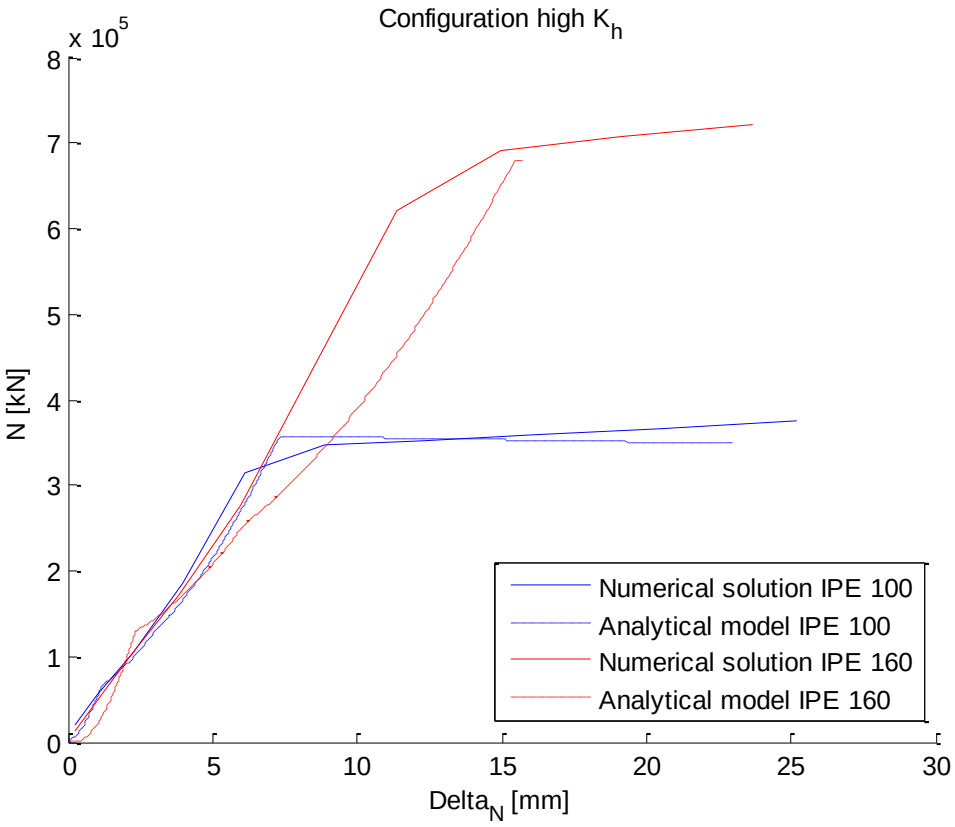

Figure 99: δ_N –N curves for the high K_H configurations

V.5.4. STRESSES

In the Lagamine program, it is also possible to show the distribution of stresses. In figure 100 and 101, the distribution of the Von Mises stresses at two different moments is shown.

Firstly we observe the stress distribution for a vertical displacement u of 0.04 m (figure 100). This point corresponds approximately to when the plastic hinges form in the beam. We can distinct the yielded zone, corresponding to a stress of 355 MPa (red in figure 100). We can observe that this form resembles the form of the plastic hinges considered for the analytical model (figure 102).

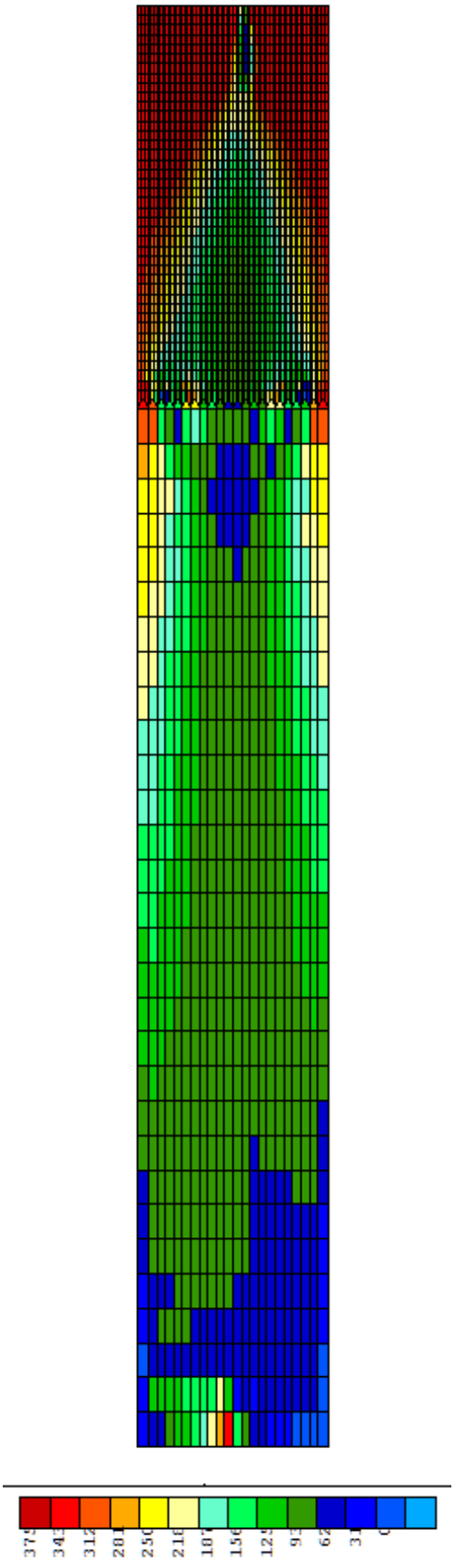

Figure 100: Von mises stresses at u = 0.04 m (in MPa)

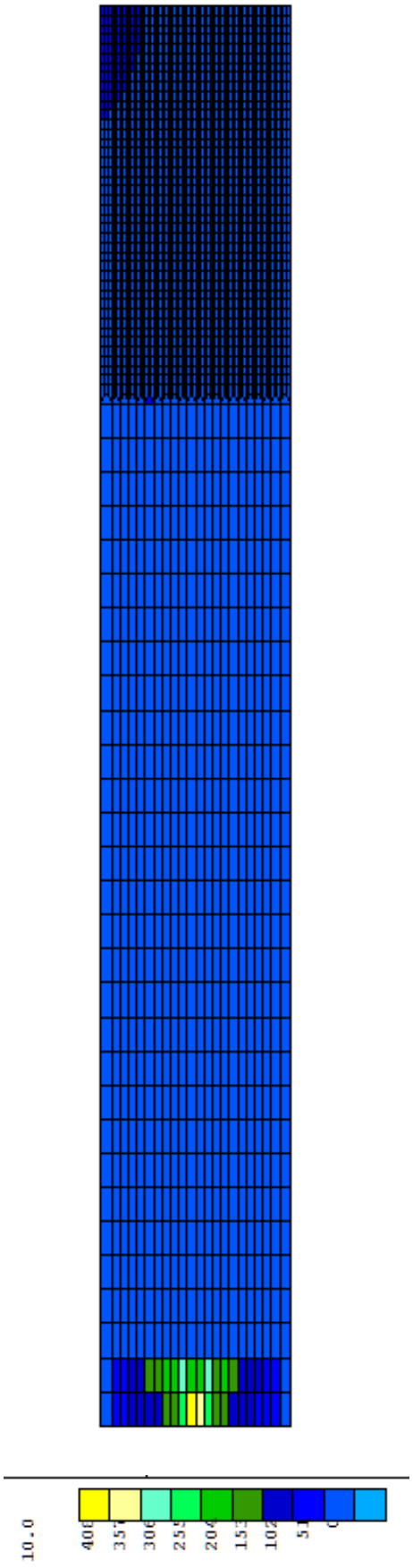

Figure 101: Von mises stresses at u = 0.24 m (in MPa)

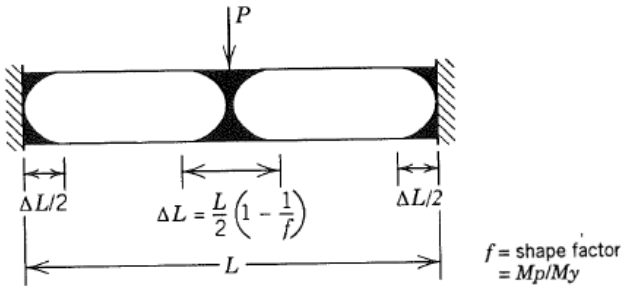

Figure 102: Hinge length (source: [4])

In figure 101 and 103, we can observe that we have reached 510 MPa, i.e. the ultimate stress. This occurs for a displacement of 0.24 m. We can consider that after having reached this value, the experimental test is finished.

Tough, the results that we have analysed above are still valid, as we did not program the simulations to take into account the ultimate stress for this constitutional law.

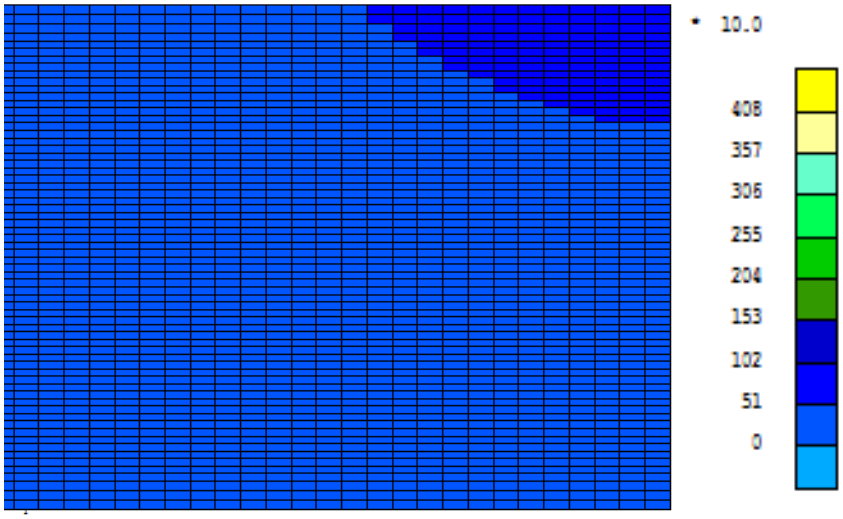

Figure 103: Zoom of figure 101 (in MPa)

V.6. RESULTS: QUAD-LINEAR LAW

The constitutional representing in a good way the behaviour of the material is the quad-linear law. This law and its parameters is presented in §IV.5.1.3.

As can be observed in figure 104, the numerical solution and the analytical model fit rather well. The curves for the IPE 100 cross section are even almost superposed. For the IPE 160 cross section, the gap between the two curves is much smaller than for the bilinear constitutional law. This is because, for this law, strain hardening will occur for greater values of the deformations. The increase in rigidity will thus not be immediately remarkable.

Furthermore we observe that for a vertical displacement u of 0.3 m, the analytical curve passes the numerical curve.

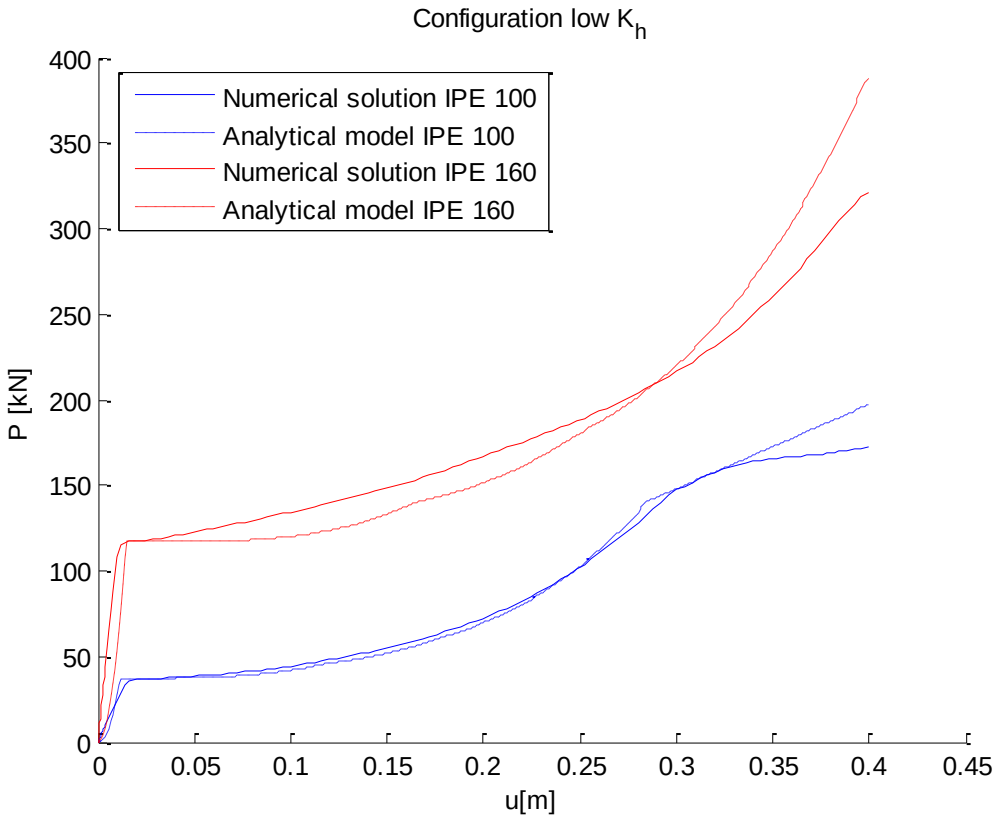

Figure 104: u – P curves for configuration low K_H

Furthermore, we observe that the F_H – P and the δ_N –N curves also fit rather well. The influence of strain hardening is present in the beginning as it is for the bilinear law.

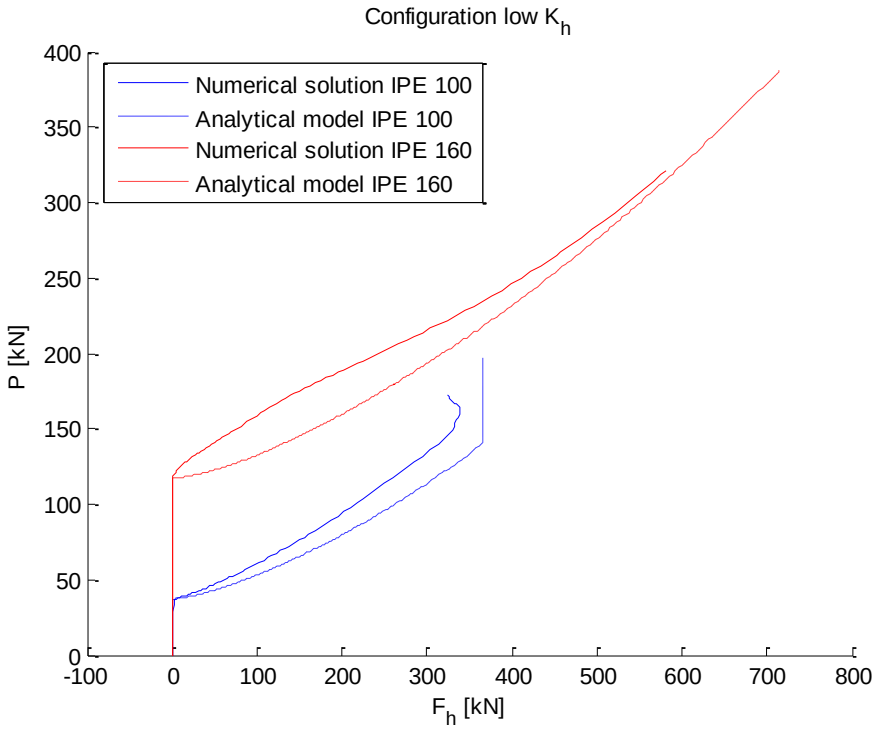

Figure 105: F_H – P curves for configuration low K_H

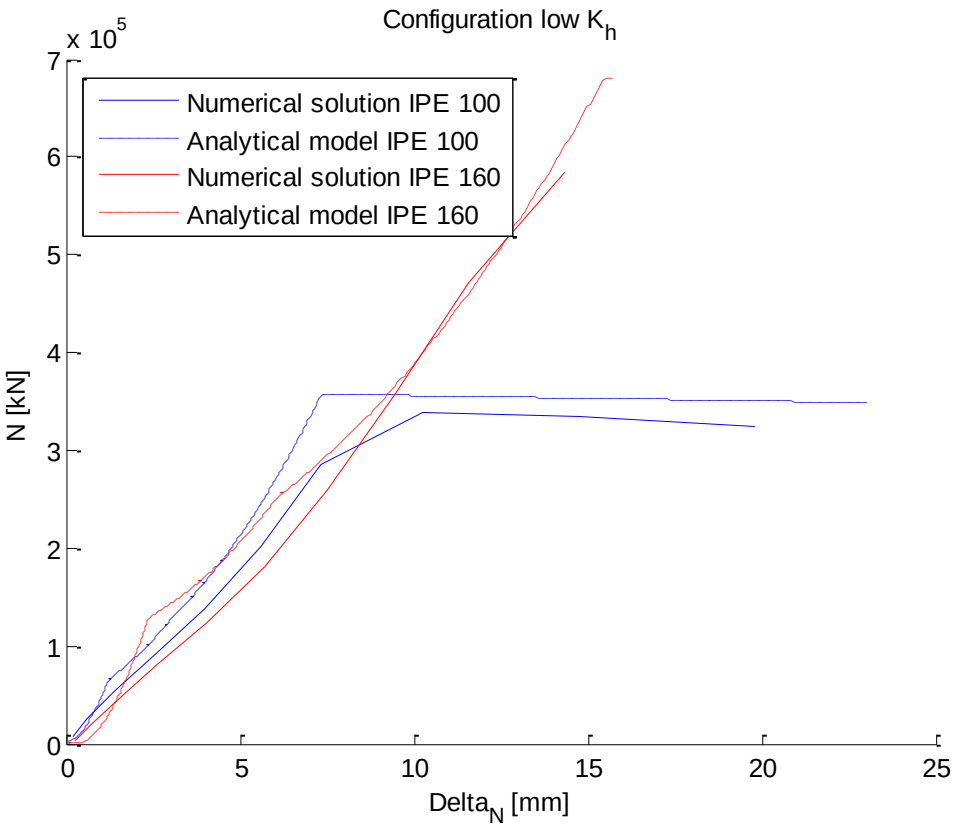

Figure 106: δ_N –N curves for configuration low K_H

V.7. INFLUENCE OF THE TANGENT MODULUS

As we noticed that the influence of the tangent modulus was significant in the results presented above, this aspect will be studied.

In order to have an idea about the influence of the tangent modulus, different values were tested. These vary from E/500 to E/100. In figure 107, the different possibilities are presented for the IPE 160 beam in the low K_H configuration.

Firstly, we can notice that the different curves superpose in the elastic domain. Obviously, the tangent modulus has no influence in this phase.

However, after this phase the influence of the tangent modulus is clearly noticeable. The higher its value, the higher the vertical force P needs to be to impose a certain displacement u. This is due to the strain hardening.

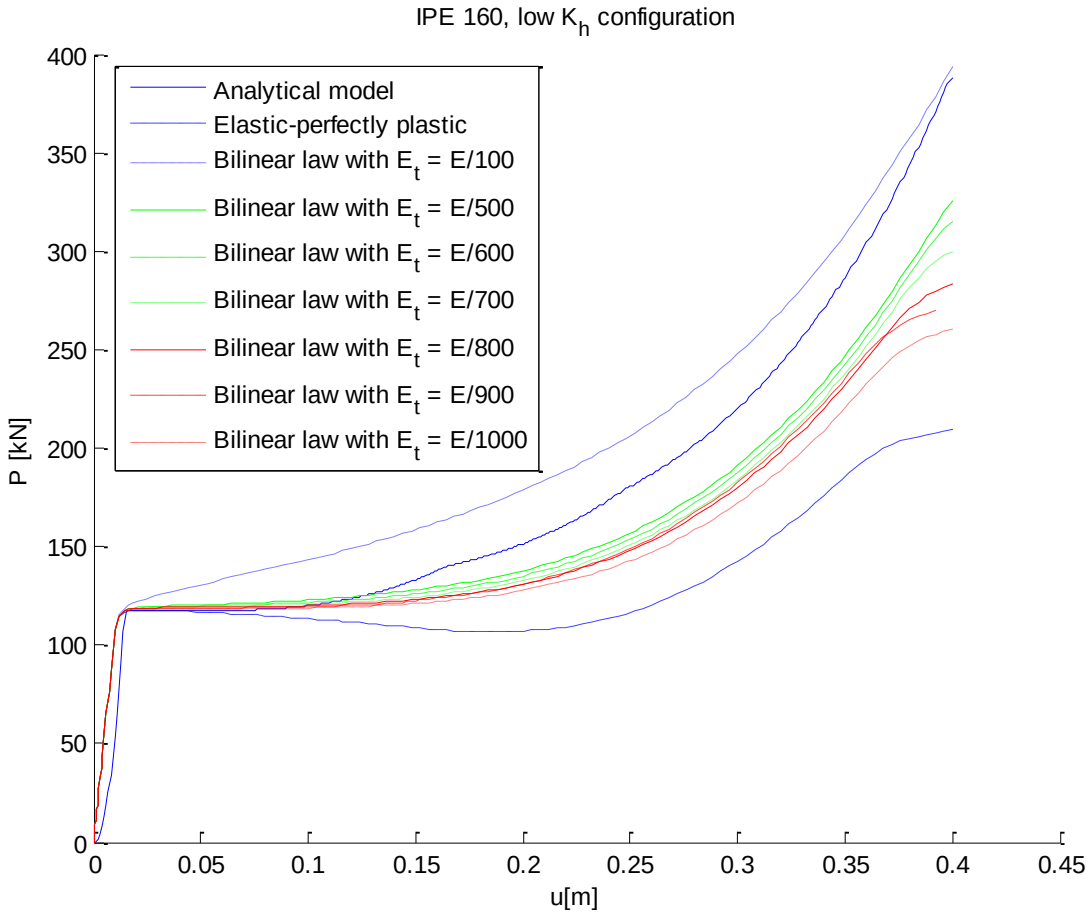

Figure 107: u-P curve for different constitutional laws

Even though the strain hardening has an influence on the results, the global allure of the curve is approximately the same for the different curves. The curves for the tangent modulus' values varying from E/500 to E/1000 are even very close. The analytical curve is situated in between the lower values of the tangent modulus and the value E/100, but seems to tend more towards the E/100 curve. It thus seems justified to have considered this value for the bilinear constitutional law as was proposed in [13].

It would be interesting to experimentally test a small sample of the constitutional material of the beams that will be tested. This way we will be able to determine the real tangent modulus.

V.8. INFLUENCE OF THE SHEAR FORCE

In the analytical model the shear force has always been considered negligible. Its influence on the resistant bending moment has thus not been taken into account. However, if the shear force is important enough, the resistant bending moment will be reduced as we follow the M-V interaction curve. The shear force is considered as negligible if:

$$\tau < \frac{f_y}{2} = \frac{355\ MPa}{2} = 177.5\ MPa$$

As can be observed in figure 108, the shear stress remains small in the beam. Its order of magnitude is 80 MPa. It can also be remarked that at the left extremity high values of the shear stress appear. However, this is in the artificial "rigid" zone. This zone should thus be not considered when investigating the shear force.

We can conclude that it is justified to not take into account the shear force for the calculation of the resistant bending moment.

Note that figure 108 represents the low K_H simulation for the section IPE 100. Nevertheless, for the other simulations we obtain similar results.

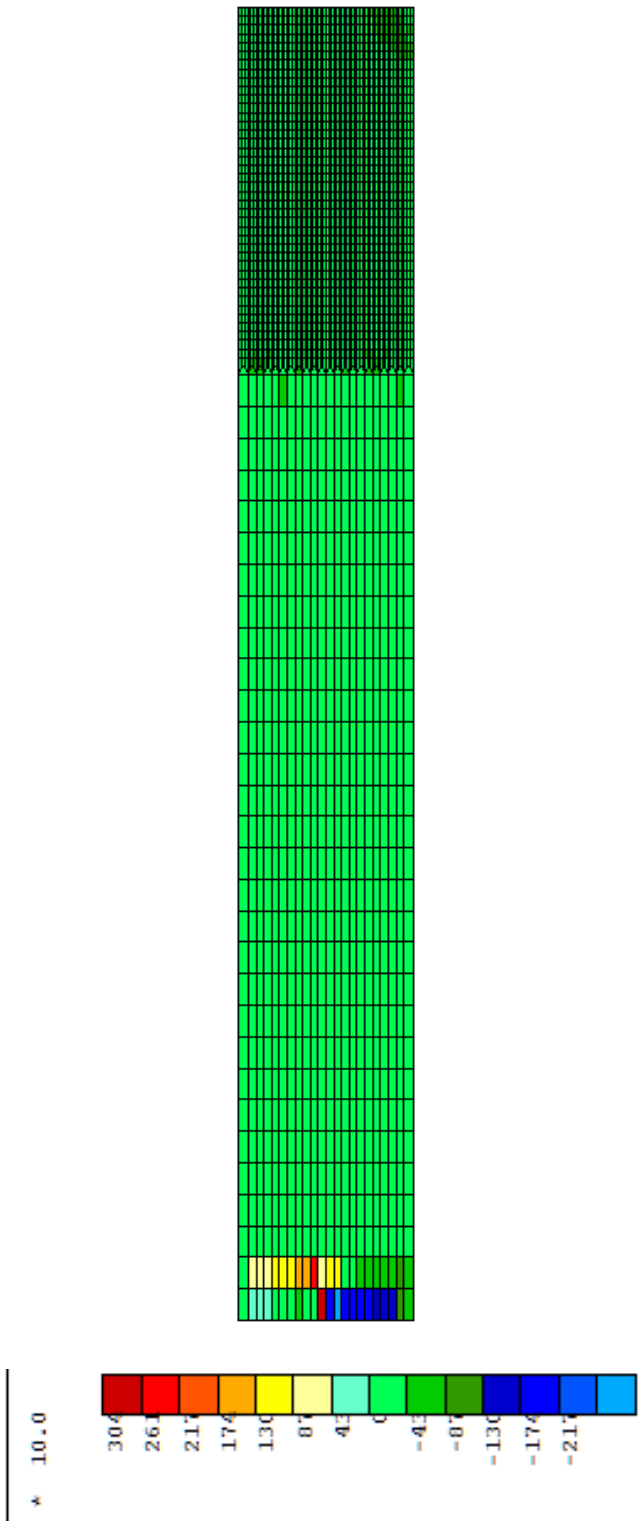

Figure 108: Shear stress (in MPa) at u = 0.4 m

V.9. INFLUENCE OF THE PLATE WIDTH

As has been explained in the paragraph detailing the numerical simulations, we consider that the imposed displacement is applied to a certain zone. This zone corresponds to the metallic plate that will be used in order to distribute the forces on a larger surface during the real experimental tests.

Furthermore we noted that this could affect the symmetry assumption. One of the explanations why it is justified to only consider one fourth of the beam length is the symmetrical moment diagram. However, as we have pointed out, this moment diagram is symmetrical for a punctual force being applied to the centre of the beam. The force being in the numerical solutions applied to a certain plateau, could thus influence the results. That is why the same configuration (low K_H – IPE160) is tested for two different plateau widths: a width of 30 mm, as is considered for all the numerical simulations in this master thesis, and a width of 60 mm (figure 109 and 110). Comparing the results of these two simulations will allow us to study if the influence of the plateau-width is negligible, as is assumed for the in .

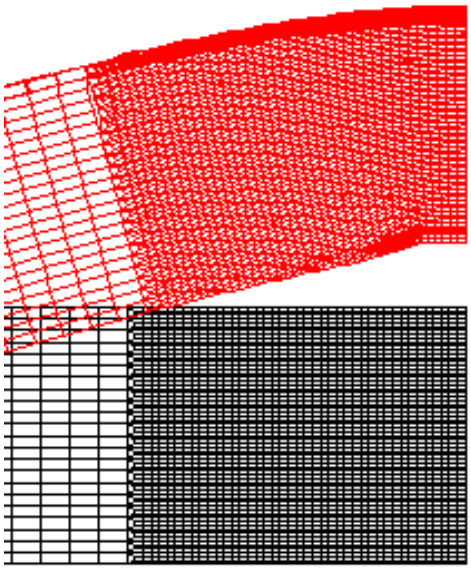

Figure 109: Plateau with width of 30 mm

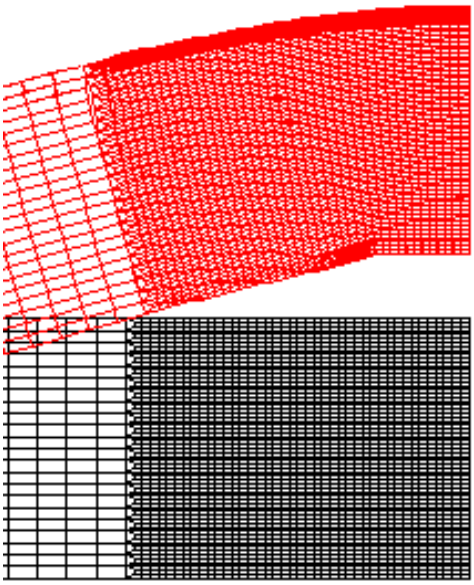

Figure 110: Plateau with width of 60 mm

As we can observe in figures 111 and 112, the two curves fit rather well. Especially for smaller values of the vertical displacement u, the two curves almost superpose. However for higher vertical displacements there is a gap in between the two curves. This gap remains small. It so seems that the width of the metallic plate, considered during the simulations, does not have a major influence on the results. The symmetry assumption is thus still justified.

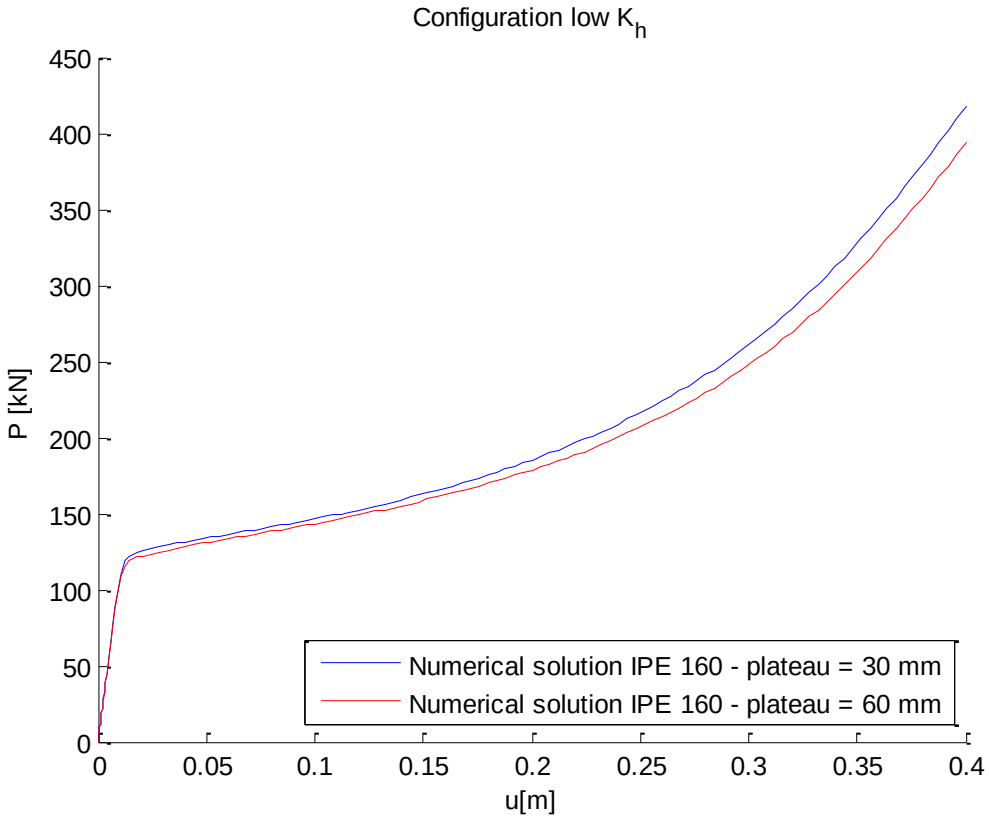

Figure 111: u – P curve

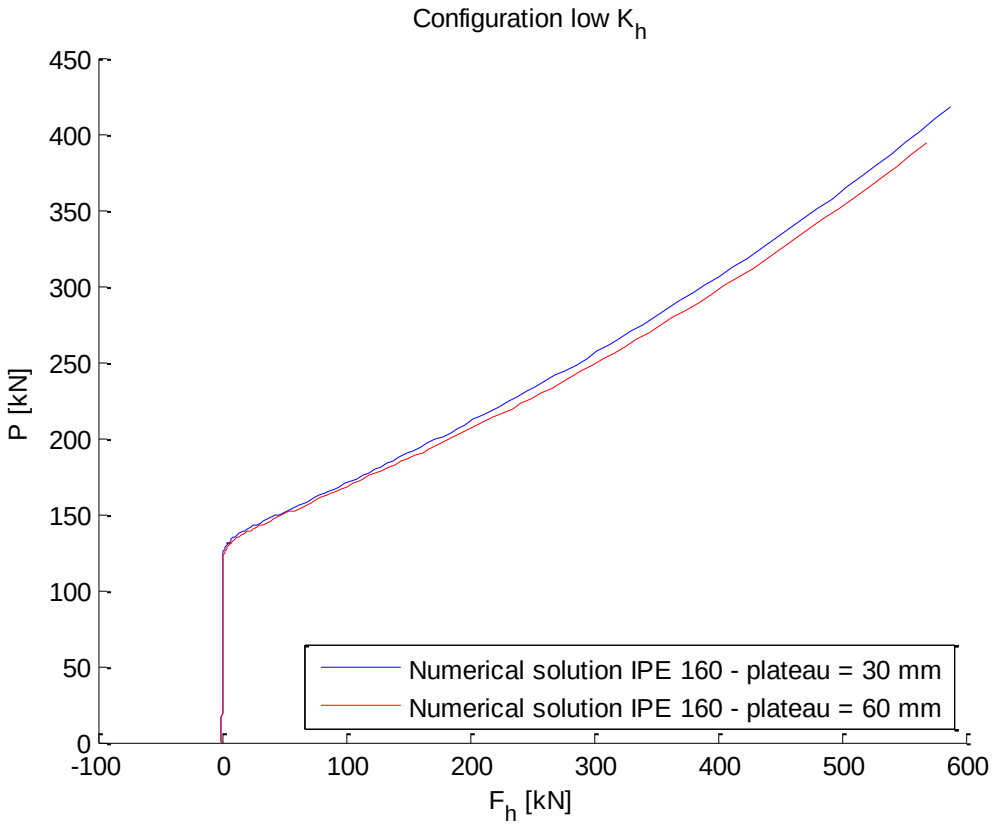

Figure 112: F_H – P curve

VI. CONCLUSIONS

VI.1. FOLLOWED APPROACH AND CONCLUSIONS

VI.1.1. EXPERIMENTAL TESTS

As a first part of this thesis, the experimental set-up for the tests, that will conducted at the University of Liège, was detailed. Two main configurations are presented: configuration low Kh (Kh = 25000 kN/m) and configuration high Kh (Kh = 300000 kN/m). This will allow us to study the influence of the stiffness of the indirectly affected part on the development of loads in the frame.

This was followed by a pre-design of the substructures. The main objective of the pre-design was to verify if the capacity of the jacks is big enough to reach phase 3 and to check whether the beam will not collapse due to other phenomena. Also was verified if the rest of the structure could sustain the loads during the whole experimental tests.

After pre-designing the frame, it can be concluded that the tested beam, as well as the rest of the substructure can sustain the applied loads.

VI.1.2. NUMERICAL SIMULATIONS

In second place, the approach followed for the numerical simulations in the finite element code Lagamine was detailed. The beam is modelled using 8-node block elements. Attention was brought to refine this meshing where needed, i.e. in the zone where we expect the plastic hinge to form. In the rest of the beam, the meshing is more coarse, as we are not so much interested in the information of this zone. Refining the meshing here, would increase the calculation time, but would not be a big gain in terms of interesting results. Note that the fillet radius is not modelled.

Furthermore, the adopted model is presented (figures 113 and 114). For the numerical model, only half the cross section and only one fourth of the beam length is modelled, in order to limit the calculation time of the program. This was permitted thanks to the symmetry of the problem. This is justified if the moment diagram is symmetrical and the rotation at the clamped extremities is zero. These assumptions were detailed and investigated. It was concluded that it is justified to consider this symmetry. The rotation at the clamped extremities is negligible and the influence of the distributed load remains very small. When comparing the results for a plateau of 30 mm and 60 mm, we observed that they fitted well. The influence of the width of the plateau is thus small.

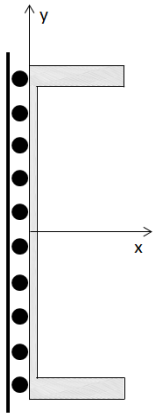

Figure 113: cross section model

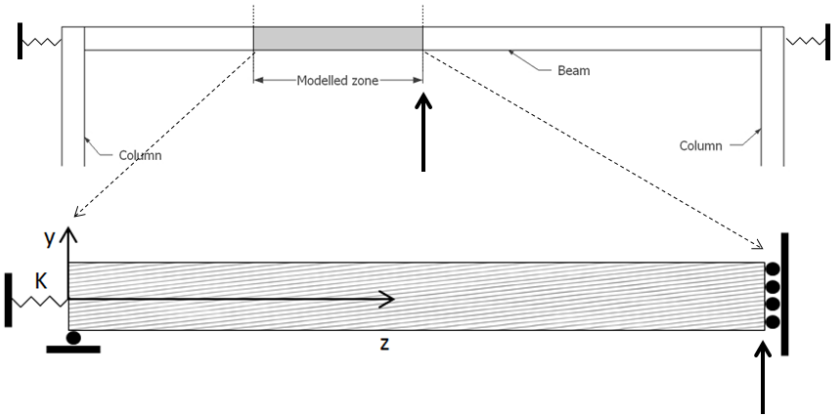

Figure 114: Longitudinal model

The influence of these symmetry considerations is explained hereafter. In order reflect the real behaviour of the beam, several degrees of freedom need to be blocked. To begin, the two symmetry plans need to remain straight during the simulations as the beam is continuous and symmetrical about these sections.

The lateral restraint coming from the indirectly affected part is modelled with the help of STIFF elements. These elements are applied to the left extremity of the beam as shown in figure 114. Here we made sure that the these elements are only applied to the middle nodes of the cross section as we do not want to create an restraint in this point because the bending moment values zero. The influence of the symmetry on the K value, representing the stiffness of the indirectly affected part, is also studied.

Next, attention has been brought to the simulation of the vertical displacement u in the numerical model. In fact, we impose that the displacement varies linearly with the time. The time does not correspond to the real calculation time, but varies from 0 (start of the simulation) to 1 (end of the simulation).

Hereafter, the constitutional laws used during the simulations are presented. The different laws are: an elastic-perfectly plastic law, a bilinear law and a quad-linear law. Also, during the first simulations, very large local deformations could be observed at the point where the spring was applied. In order to avoid these deformations, a rigid zone was introduced.

VI.1.3. RESULTS

To begin, the responses of the frame, obtained with the analytical model are established and discussed. These results correspond well to the theories detailed in the state of the art.

Afterwards, the numerical results for the elastic-perfectly plastic constitutional law are presented. Initially, the results would be used for comparison with the analytical model as they make use of the same law. However, high deformations were observed for these simulations. The cross section reduced drastically, which caused a decrease of the resistance

of the beam. Two possible causes for these large deformations are presented. On the one hand, not modelling the fillet radius, makes of the flange - web junction a likely place for deformations. On the other hand, we observe that the necking phenomena appears. Nevertheless, the results of these simulations are briefly commented.

Furthermore, the numerical simulations for a bilinear constitutional law are presented. These results are used to validate the analytical model, as they reflect better the real behaviour of the frame. Tough, we have to keep in mind that the hypothesis for the numerical and analytical model are not the same. Comparing both is thus not that evident. Nevertheless, we observe that the results of both models fit well. The strain hardening influences the results, but not in an out of proportion way. The K_N parameter, a parameter that is complex to determine, is approximately the same for the numerical and analytical solutions. Even tough, the hypothesis are not the same as mentioned above, we can still conclude that the analytical model gives produces a response similar to the one of the numerical model. The model gives also a very good estimation of the K_N parameter.

Hereafter, the results for a quad-linear constitutional law are presented. We observe once again that the numerical and analytical model fit well. The results fit even better for this constitutional law.

As we observed that the strain hardening plays an important role in the obtained results, its influence was studied. Different values of the tangent modulus were tested. When analysing the results, we noticed that the results had the same allure. However, the results for a tangent modulus of E/100 fit the best the analytical model.

Furthermore, the influence of the shear force is investigated. One of the hypothesis of the analytical model being that the influence of this force on the resistant bending moment is negligible. The results of the numerical simulations have confirmed this hypothesis.

Finally, the hypothesis of the symmetry of the moment diagram has been confirmed. The influence of the plateau-width when applying the displacement remains very small.

In conclusion, the analytical model gives a good estimation of the response of the frame during the exceptional event “loss of a column”. Under reservation of the different hypothesis of the two models, we can say that the analytical and numerical model fit well. The K_N parameter seems to be estimated well in the analytical model.

VI.2. PERSPECTIVES

To begin, it would be interesting to experimentally test a small sample of the constitutional material of the beams that will be tested. This way we will be able to determine the real tangent modulus. First of all, we could verify if the value of E/100 that is considered in the numerical model corresponds well to this value. If not, simulations with the tangent modulus, determined experimentally, could be conducted in order to obtain a more realistic response of the frame.

More so, the stress – strain curves of the tested sample can be determined. In order to obtain an even more realistic response of the frame, a similar constitutional law could be defined for the numerical simulations.

Afterwards, the numerical model and the experimental results could be compared. Also it will be possible to validate the analytical model again, but this time with the experimental results.

As for the modelling, it would be interesting to also model the filet radius. This would give more realistic results as we observed that the flange - web joints were often largely deformed.

APPENDIX

APPENDIX 1

The assumed plastic mechanism is shown in figure 115. The calculations for obtaining the value of the force P for which this mechanism is formed, goes as followed:

$$4\,\theta\,M_{pl} = P_{pl}\,\frac{\Delta}{\theta}\,\theta$$

$$\Rightarrow P_{pl} = \frac{4\,M_{pl}}{\Delta/_{\theta}} = \frac{4\,M_{pl}}{1.5} = 2.666\,M_{pl}$$

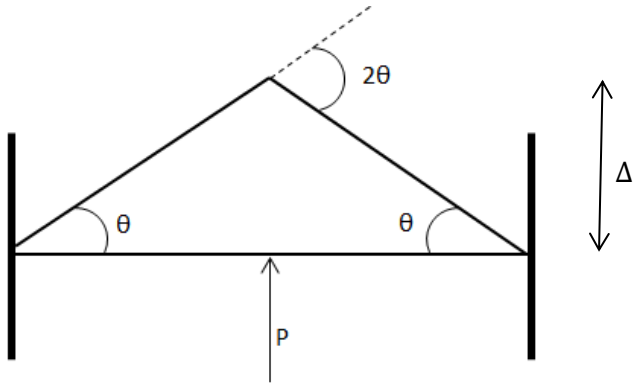

Figure 115: Plastic mechanism

We obtain the following results:

	IPE 100	***IPE 160***
N_{pl} [kN]	452.98	1427.1
N_{pl} [to]	45.298	142.71
N_u [kN]	325.38	1025.1
N_u [to]	32.538	102.51
M_u [kNm]	22.10901	69.564
M_{pl} [kNm]	13.99055	44.02
P_{pl} [kN]	37.30813333	117.3866667
P_u [kN]	58.95736	185.504

Table 19: Results for the IPE 100 and IPE 160 beams

APPENDIX 2

The moment diagrams for both structures are showed in figure 116 and 117.

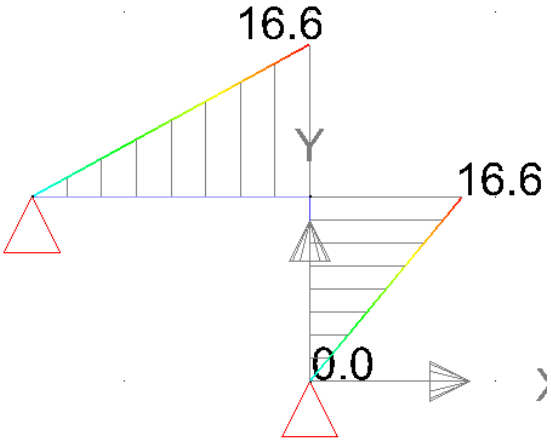

Figure 116: load case 1

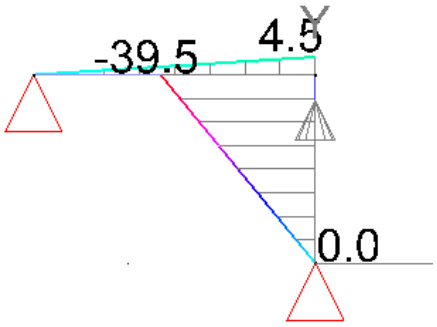

Figure 117: load case 2

The resistance and stability of the column is verified. The results are given in table 20.

k_z	0.5
k_w	0.5
C_1	1.86
C_2	0.48
z_g [mm]	0
C_3	1
z_j [mm]	0
M_{pl} [kN.m]	228.0875
M_{cr} [kN.m]	13160.43578
λ_{LT}	0.131648407
α_{LT}	0.21
Φ_{LT}	0.501488734
χ_{LT}	1
$M_{Rd,pl}$ [kN.m]	231.4694571
	> M_{Ed}=39.5 kN m

Table 20: Results for the IPE 200 beam

APPENDIX 3

The diagrams of the normal force and the bending moment are showed in figure 118-121.

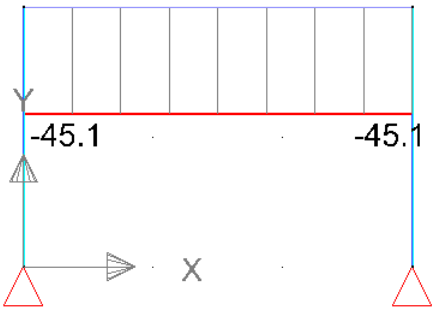

Figure 118: Load case 1: N

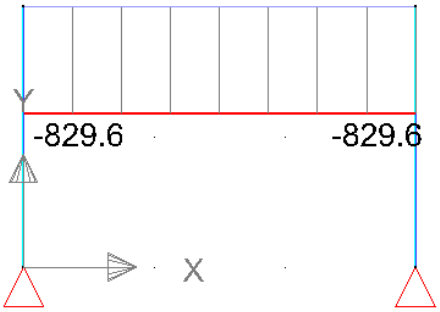

Figure 119: Load case 2: N

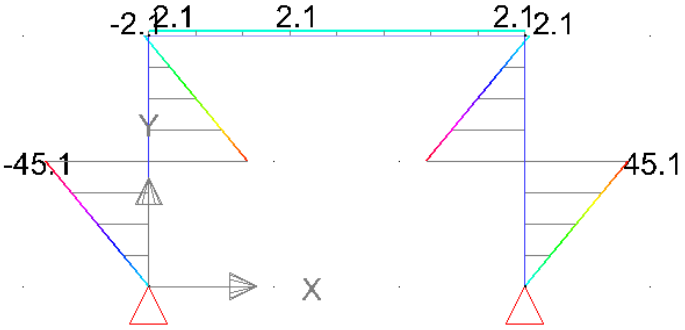

Figure 120: Load case 1: M

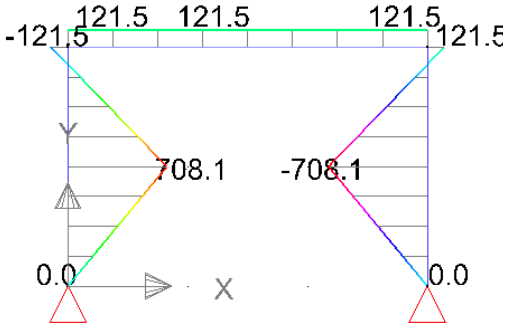

Figure 121: Load case 2: M

COLUMN HEB300 IN S460

First of all, it has to be checked that the elastic resistance of the cross section of the columns is high enough:

$$M_{elastic,HEB\ 300} = 771\ kNm > M_{Ed} = 708.1\ kNm$$

Next, the column will be checked for instability phenomena.

k_z	0.5
k_w	0.5
C_1	1.05
C_2	0.48
z_g [mm]	0
C_3	0.338
z_j [mm]	0
M_{pl} [kN.m]	859.74
M_{cr} [kN.m]	4292.149
λ_{LT}	0.447555
α_{LT}	0.21

Φ_{LT}	0.626146
χ_{LT}	1
$M_{Rd,pl}$ [kN.m]	807.9941
	> M_{Ed}=708.1 kN m

Table 21: Results for the HEB 300 beam

BEAM IPE360 IN S355

First of all, it has to be checked that the elastic resistance of the cross section of the beam is high enough:

$$M_{elastic,IPE\ 360} = 320.9\ kNm > M_{Ed} = 121.5 kNm$$

Furthermore the stability of the beam and the interaction of the bending moment and normal forces have to be checked. This verification was already made by Clara Huvelle. Her calculations can be found here after.

Profilé		
Type	IPE 360	
Autre type ?		
h [mm]	360	
b [mm]	170	
t_w [mm]	8	
t_f [mm]	12.7	
r [mm]	18	
A [cm^2]	72.73	
d [mm]	298.6	
I_y [cm^4]	16270	v
$W_{el,y}$ [cm^3]	903.6	v
$W_{pl,y}$ [cm^3]	1019	v
A_{vz} [cm^2]	35.14	
I_z [cm^4]	1043	v
$W_{el,z}$ [cm^3]	122.8	v
$W_{pl,z}$ [cm^3]	191.1	v
I_t [cm^4]	37.32	v
I_ω *10^{-3} [cm^6]	313.6	v

Classe de section	
Classe	1

Matériau et sécurité	
f_y [N/mm^2]	355
γ_{M1}	1.0

Longueurs	
L [m]	3.000
$L_{fl,y}$ [m]	3.000
$L_{fl,z}$ [m]	3.000

Efforts internes	
N_{Ed} [kN]	829.600
$M_{y,Ed}$ [kN.m]	121.500
$M_{z,Ed}$ [kN.m]	0.000
Coefficients d'équivalence	
$C_{my,0}$	0.787
C_{mz}	0.749

Si M_y linéaire :	ψ_y	0.000
Si M_z linéaire :	ψ_z	0.000
Si M_y linéaire :	$C_{my,0}$	0.787
Si M_z linéaire :	C_{mz}	0.749

Courbes de flambement		
y-y	a	a0, a, b, c, d
z-z	b	a0, a, b, c, d

Calcul $L_{fl,y}$		Calcul $L_{fl,z}$	
R_c		R_c	834.400
R_i		R_i	834.400
$\Sigma R_{p,i}$		$\Sigma R_{p,i}$	792.000
R_s		R_s	834.400
$\Sigma R_{p,s}$		$\Sigma R_{p,s}$	792.000
k_i		k_i	0.678
k_s		k_s	0.678
$k_{i(s)} = (R_c + R_{i(s)}) / (R_c + R_{i(s)} + \Sigma R_{p,i(s)})$			
$K_{y,noeuds\ fixes}$		$K_{z,noeuds\ fixes}$	0.772
$K_{y,noeuds\ mobiles}$		$K_{z,noeuds\ mobiles}$	1.878

Param. de déversement					
Courbe	a	a, b, c, d			
k_z	0.500				
k_w	0.500				
C_1	1.050	Si M_y linéaire et $k_z = 1$:	C_1	1.770	
C_2	0.480				
z_g [mm]	0.000	zg > 0 : effet défavorable			
C_3	0.338				
z_j [mm]	0.000				
k_c	0.752	Si M_y linéaire :	k_c	0.752	

Efforts résistants		Flambement d'axe fort		Flambement d'axe faible		Déversement			
$N_{pl,Rk}$ [kN]	2581.9	$N_{cr,y}$ [kN]	37468.3	$N_{cr,z}$ [kN]	2401.9	$M_{cr,0}$ [kN.m]	495.9	M_{cr} [kN.m]	1838.3
$M_{y,Rk}$ [kN.m]	361.7	λ_y	0.263	λ_z	1.037	$\lambda_{LT,0}$	0.854	λ_{LT}	0.444
$M_{z,Rk}$ [kN.m]	67.8	α_y	0.21	α_z	0.34	$N_{cr,T}$ [kN]	4300.1	α_{LT}	0.21
		ϕ_y	0.541	ϕ_z	1.180	λ_{limite}	0.175	ϕ_{LT}	0.624
		χ_y	0.986	χ_z	0.574	LTB ?	OUI	χ_{LT}	0.941
		μ_y	1.000	μ_z	0.816			f	0.907
								$\chi_{LT,mod}$	1.000

Corrections déversement		Coefficients d'interaction	
ε_y	1.179	w_y	1.128
a_{LT}	0.998	w_z	1.500
C_{my}	0.898	α	0.692
k_{LT}	1.107	β	0.520
b_{LT}	0.000	k_{yy}	0.983
c_{LT}	0.442	k_{yz}	0.922
d_{LT}	0.000	k_{zy}	0.809
e_{LT}	0.432	k_{zz}	1.049

Stabilité ?		
Axe fort y-y	0.673	OK
Axe faible z-z	0.739	OK

REFERENCES

[1] J.F. Demonceau, course notes of « Bâtiments sous actions accidentelles et exceptionnelles – partie robustesse » , course followed at Ulg in 2013

[2] J.-F. Demonceau, Steel and composite building frames: sway response under conventional loading and development of membrane effects in beams further to an exceptional action, PhD thesis submitted at ULg in 2008

[3] J.F. Demonceau, L. Comeliau, J.-P. Jaspart, Robustness of building structures, Recent developments and adopted strategy, EUROSTEEL 2011

[4] C. Huvelle, J.F. Demonceau, J.-P. Jaspart, Simplified Equivalent Static approach – Contribution from Liege University, Internal report, 2014

[5] Article currently in development at Ulg

[6] W.F. Chen, Yoshiaki Goto, J.Y. Richard Liew, "Stability Design of Semi-Rigid Frames", 1996, JOHN WILEY & SONS, INC, p. 162-163

[7] A.-F. Cambron, La prédiction de fissures, master thesis submitted at Ulg in 1997

[8] Course notes of « Méthodes numériques non-linéaires », course followed at Ulg in 2013

[9] Lagamine User's manuel

[10] L. Duchêne, P. de Montleau, A.M. Habraken, Development and performance assessment of an improved 8-node mixed type FEM element

[11] L. Duchêne, F. El Houdaigui, A.M. Habraken, Length changes and texture prediction during free end torsion test of copper bars with FEM and remeshing techniques, International journal of Plasticity 23, 2007, p. 1417-1438

[12] C. Lequesne, Modeling of fracture in heavy steel welded beam-to-column connection submitted to cyclic loading by finite elements, PhD thesis submitted at ULg in 2009

[13] Y. Li, Extension of the direct strength method to hot-rolled and welded H profiles, PhD thesis submitted at ULg in 2014